Title

Using Isotopes to Explore Global Peat Carbon Dynamics

Author

Hedgpeth, Alexandra

Publication Date

2024

Peer reviewed|Thesis/dissertation

UNIVERSITY OF CALIFORNIA

Los Angeles

Using Isotopes to Explore Global Peat Carbon Dynamics

A dissertation submitted in partial satisfaction of the requirements for the degree of Doctor of Philosophy in Geography

By

Alexandra Hedgpeth

2024

ABSTRACT OF THE DISSERTATION

Using Isotopes to Explore Global Peat Carbon Dynamics

by

Alexandra Hedgpeth

Doctor of Philosophy in Geography

University of California, Los Angeles, 2024

Professor Kyle C. Cavanaugh, Chair

This dissertation investigates the role of peatlands as critical carbon (C) reservoirs that sequester approximately 600 gigatons of C globally, effectively acting as a significant buffer against climate change. Despite their limited geographic extent—covering only 3% of the Earth's surface—peatlands store nearly twice the C of all global forests combined. This exceptional C storage potential is largely due to the waterlogged, anoxic conditions in these ecosystems that inhibit microbial decomposition and allow organic matter to accumulate over millennia. However, peatlands are highly vulnerable to both natural and anthropogenic pressures, including climate change, land-use modifications, and direct human disturbances, all of which threaten their capacity to serve as long-term C sinks.

This dissertation leverages isotopic analysis to examine peatland C dynamics across diverse regions and contexts by exploring the mechanisms driving C dynamics in tropical, boreal, and temperate peatlands, focusing on both surface-derived and deep peat C emissions and accumulation. Tropical peatlands, which differ from boreal and temperate peatlands due to consistently warm temperatures and seasonal rainfall, contain highly dense C deposits but are also at heightened risk of C release under changing rainfall patterns. One case study examines

tropical peatlands in Central America, where consistently warm temperatures and seasonal rainfall create dense C deposits. These tropical systems are especially susceptible to C loss with changing rainfall patterns, potentially releasing stored C from deep peat layers. In boreal regions, experimental warming simulates future climate conditions, assessing how elevated temperatures and CO_2 concentrations affect C storage across peat depths. Additionally, this dissertation uses global radiocarbon data to analyze peat accumulation and stability across climates, providing insights into regional differences in peatland resilience under environmental changes. These studies together highlight the significant impact of environmental variables such as precipitation, temperature, and proximity to coastlines on peatland C dynamics, as well as the potential influence of human activities like agriculture drainage and peat extraction on C loss. Findings underscore the importance of conserving and protecting pristine peatlands, which, as natural C sinks, are vital for mitigating greenhouse gas emissions.

Overall, this dissertation underscores the critical importance of peatlands in global C cycling and climate regulation. The research highlights the necessity of conservation efforts to protect these ecosystems from degradation, as their disruption could lead to substantial greenhouse gas emissions and further accelerate climate change. By examining the complex interactions between environmental conditions, C sequestration, and human impacts, this dissertation contributes to a deeper understanding of peatlands' vulnerability and resilience, informing strategies for their preservation in a rapidly changing world.

The dissertation of Alexandra Hedgpeth is approved.

Daniela Cusack

Alison Hoyt

Thomas W. Gillespie

Glen Michael MacDonald

Kyle C. Cavanaugh, Committee Chair

University of California, Los Angeles
2024

For those who keep going when it feels impossible.

Table of Contents

List of Figures

List of Tables

List of Appendix Figures

List of Appendix Tables

Acknowledgements

This dissertation would not have been possible without the guidance and support of my family, my chosen family, friends, and advisors. First, I want to express my deepest gratitude to Karis McFarlane, who, although not formally on my committee, has been an invaluable mentor throughout this process. Thank you for the countless hours of editing, the spontaneous emergency zoom calls, and the gut checks when I needed an extra set of eyes to reassure me. Your support and encouragement have been instrumental in getting me to this point and will continue to guide me throughout my career. I am also grateful to Daniela Cusack, a core member of my committee, whose mentorship was crucial in my development as a research scientist. Your feedback and perspective have shaped both my writing and my confidence, pushing me to produce thoughtful and rigorous science. My thanks also go to Alison Hoyt, whose efforts made difficult field logistics possible. Spending this last year mostly behind a computer made me miss the swamps, and you always reminded me of my love for fieldwork—mud and all. Each of these remarkable women has celebrated with me after successes, provided care after setbacks, and shown me, by example, that I can achieve my goals. Thank you. I consider myself incredibly fortunate that Kyle Cavanaugh agreed to take me on as a student and serve as chair of my dissertation committee. Your calm, reassuring presence has been a constant source of stability throughout this process, helping me stay grounded and keeping every anxiety attack at bay. Next, I'd like to thank my academic and soil science family: Kimber Morland, Lauren Deem, Clarice Perryman, and Lee Dietterich. Thank you all for indulging in passionate discussions about our work and for providing feedback that was informal yet deeply impactful. I'd also like to thank everyone who contributed to this work in the lab, in the field, and throughout the writing process. My sincere gratitude to Eric Brown, Dayana Agudo, Mackenna Brown, and Antonia L.

Herwig for their invaluable support with sample collection at the San San Pond Sak wetland. I'm also grateful to Paul Hanson, Jana Phillips, and the SPRUCE data collection team, as well as Ágatha Kuhnen and the entire ISRAD stewardship team. Your collective efforts and dedication have played an essential role in making this research possible.

I am deeply grateful to the many labs I have had the privilege of working with throughout this journey. My sincere thanks to the Smithsonian Tropical Research Institute, especially the team at the Bocas Field Station, for providing access to the project sites and for sharing their knowledge and expertise. I would also like to thank Sarah Burton and the staff at the Environmental Molecular Sciences Laboratory, who graciously hosted me during sample analysis at PNNL. A special thanks goes to my LLNL community—a unique group of physicists, chemists, ecologists, and administrators with whom I've worked for nearly a decade. Despite my attempts to move on more than once, each time I return to CAMS, I gain invaluable experience, joy, and inspiration to pursue great science. Thank you to my flamingo family for all the support and motivation along the way.

Chapter 1 of this dissertation is a version of "From the Top: Surface-derived Carbon Fuels Greenhouse Gas Production at Depth in a Neotropical Peatland" in preprint in 2022 in Biogeosciences with co-authors Alison Hoyt, Kyle Cavanaugh, Karis McFarlane, and Daniela Cusack. I would like to acknowledge Alison Hoyt for her help with methodology; resources; formal analysis; visualization; supervision; and preparation of the manuscript. I would like to acknowledge Kyle Cavanaugh for his supervision; writing – review and editing. I would like to acknowledge Karis McFarlane for her assistance with funding acquisition; resources; methodology; supervision; and preparation of the manuscript. I would like to acknowledge Daniela Cusack for her help with conceptualization; funding acquisition; methodology;

supervision; visualization; writing – review and editing. This project was supported in part by a University of California-National Lab In-Residence Graduate Fellowship (#L21GF3629) to A. Hedgpeth, which was hosted by Lawrence Livermore National Laboratory. Part of the analysis for this work was supported under a U.S. Department of Energy User Award (#60514) to D. Cusack and A. Hedgpeth, which was conducted at the Environmental Molecular Sciences Laboratory. Access to field and lab sites in Panama was supported by DOE Office of Science Early Career Award DE-SC0015898 and NSF Geography & Spatial Studies Grant #BCS-1437591 to D. Cusack. A portion of this work was performed under the auspices of the U.S. Department of Energy by Lawrence Livermore National Laboratory under Contract DE-AC52-07NA27344 and funded by the U.S. Department of Energy Office of Science Early Career Program Award (#SCW1572) to K. McFarlane.

I would like to thank the UCLA Geography Department staff who have made my PhD experience better in many ways. A special thanks to Kasi McMurray for being the biggest support system throughout my experience. You have the biggest heart and were there for me in the darkest moment after my dad's passing. I truly can't thank you enough for your kindness and understanding. Thanks to Jenee Misraje, for keeping track of literally everything and keeping things running smoothly.

Finally, I'd like to thank my family, whose unwavering support has been foundational to my journey. To my parents, I owe so much of my motivation and resilience. Joe, I wish you were here. You were the reason I chose to become a scientist—you gave me something to push against and, in doing so, helped me discover how to forge my own path, even when it frustrated you. Claudia, you always told me I could do anything, and I believed you. Your endless love and trust in me to find my own way have shaped who I am today. Thank you both for everything. To my

older siblings, Kathy, Joey, and Ben—I'm endlessly grateful for each of you and for all the ways you've supported me along the way. Thank you for always being there. To my little sister Marisa. Your humor and steady support have been a lifeline during this journey. You've taken on so much, from helping care for our parents and handling every family catastrophe with grace to validating me when our family quirks get intense. I truly couldn't have done this without you by my side, reminding me that I'm not alone in all of this. I love you more than words can say, and I'm endlessly grateful for everything you've done.

To my partner David, who had no idea what he was getting into three years ago when he chose to dive into life with me. I'm incredibly proud of all you've achieved while working on your own degrees. Your dedication and work ethic have inspired me more than you realize. I'm so thankful for all the experiences and adventures we've shared, and I can't wait to make more memories with you. I look forward to reminiscing about these chaotic and wild days in the years ahead when we have free time that actually means rest.

VITA

EDUCATION

2015	University of Hawaii at Manoa	M.A. in Geography
2013	McMaster University	B.Sc. in School of Geography and Earth Science

PEER-REVIEWED PUBLICATIONS

McFarlane K., Cusack D., Dietterich L., Hedgpeth A., Nottingham A.: Experimental Warming and Drying Increase the Age of Soil Respired Carbon in Lowland Tropical Forests, 24 October 2023, [preprint] [https://doi.org/10.21203/rs.3.rs-3409233/v1]

Hedgpeth, A. L., Hoyt, A. M., Cavanaugh, K., McFarlane, K. J., and Cusack, D. F.: From the Top: Surface-derived Carbon Fuels Greenhouse Gas Production at Depth in a Neotropical Peatland, EGUsphere [preprint], https://doi.org/10.5194/egusphere-2024-1279, 2024.

Capooci, M., Seyfferth, A. L., Tobias, C., Wozniak, A.
S., Hedgpeth, A., Bowen, M., Biddle, J. F., McFarlane, K. J., & Vargas, R. (2023). High methane concentrations in tidal salt marsh soils: Where does the methane go? *Global Change Biology*, 30, e17050. https://doi.org/10.1111/gcb.17050

Dietterich, L. H., Bouskill, N. J., Brown, M., Castro, B., Chacon, S. S., Colburn, L., Cordeiro, A. L., García, E. H., Gordon, A. A., Gordon, E., Hedgpeth, A., Konwent, W., Oppler, G., Reu, J., Tsiames, C., Valdes, E., Zeko, A., and Cusack, D. F.: Effects of experimental and seasonal drying on soil microbial biomass and nutrient cycling in four lowland tropical forests, Biogeochemistry, 161, 227–250, https://doi.org/10.1007/s10533-022-00980-2, 2022.

McFarlane, K. J., Throckmorton, H. M., Heikoop, J. M., Newman, B. D., Hedgpeth, A. L., Repasch, M. N., Guilderson, T. P., and Wilson, C. J.: Age and chemistry of dissolved organic carbon reveal enhanced leaching of ancient labile carbon at the permafrost thaw zone, Biogeosciences, 19, 1211–1223, https://doi.org/10.5194/bg-19-1211-2022, 2022.

Loisel, J., Gallego-Sala, A. V., Amesbury, M. J., Magnan, G., Anshari, G., Beilman, D. W., Benavides, J. C., Blewett, J., Camill, P., Charman, D. J., Chawchai, S., Hedgpeth, A., Kleinen, T., Korhola, A., Large, D., Mansilla, C. A., Müller, J., Van Bellen, S., West, J. B., Yu, Z., Bubier, J. L., Garneau, M., Moore, T., Sannel, A. B. K., Page, S., Väliranta, M., Bechtold, M., Brovkin, V., Cole, L. E. S., Chanton, J. P., Christensen, T. R., Davies, M. A., De Vleeschouwer, F., Finkelstein, S. A., Frolking, S., Gałka, M., Gandois, L., Girkin, N., Harris, L. I., Heinemeyer, A., Hoyt, A. M., Jones, M. C., Joos, F., Juutinen, S., Kaiser, K., Lacourse, T., Lamentowicz, M., Larmola, T., Leifeld, J., Lohila, A., Milner, A. M., Minkkinen, K., Moss, P., Naafs, B. D. A., Nichols, J., O'Donnell, J., Payne, R., Philben, M., Piilo, S., Quillet, A., Ratnayake, A. S., Roland, T. P., Sjögersten, S., Sonnentag, O., Swindles, G. T., Swinnen, W., Talbot, J., Treat, C., Valach, A. C., and Wu, J.: Expert assessment of

future vulnerability of the global peatland carbon sink, Nat. Clim. Chang., 11, 70–77, https://doi.org/10.1038/s41558-020-00944-0, 2021.

Cusack, D. F., Kazanski, C. E., Hedgpeth, A., Chow, K., Cordeiro, A. L., Karpman, J., and Ryals, R.: Reducing climate impacts of beef production: A synthesis of life cycle assessments across management systems and global regions, Global Change Biology, 27, 1721–1736, https://doi.org/10.1111/gcb.15509, 2021.

IN PREP

Hedgpeth, A., Hanson, P., Phillips, J., McFarlane K., Changes in peat stocks and characteristics following 5 years of warming and CO_2, Target journal: Global Change Biology

Hedgpeth A., Loisel, J., Winton, S., Kuhnen, A., Dommain, R., Hoyt, A., Tropical Peat Initiation and Development: A Pantropical Peat Synthesis using the ISRAD dataset, Target journal: Quaternary Science Reviews

FELLOWSHIPS, AWARDS AND GRANTS

2022	EMSL User Fee Award
2021	UC Lab Fees In-Residence Graduate Fellowship
2019	UCLA Travel Grant
2019	Smithsonian Tropical Research Institute Short Term Fellowship

ORAL AND POSTER PRESENTATIONS

Hedgpeth, A., McFarlane K, Phillips J, Schwaner G, Hanson P (May 3, 2023). Peat Organic Matter Characteristics following 5years of warming and eCO2 as described by Radiocarbon and 13CNMR Spectroscopy [SPRUCE All Hands Meeting], Minneapolis, MN, USA

Hedgpeth, A., McFarlane, K.J., Hoyt, A., Cusack, D., Cavanaugh, K., (2022, December 12-16). *Peatland formation and Accumulation: A Pantropical Synthesis* [American Geophysical Union], Chicago, IL, USA

Hedgpeth, A., McFarlane, K.J., Hoyt, A., Cusack, D., Cavanaugh, K., (2021, December 13-19). *Measuring the Radiocarbon Offset Between Soil Greenhouse Gases and Peat Help Determine Sources of Carbon Emissions from a Neotropical Peatland* [American Geophysical Union], New Orleans, LA, USA

Hedgpeth, A., McFarlane, K.J., Hoyt, A., Cusack, D., Cavanaugh, K., (2021, March 22-25). *Measuring the Radiocarbon Offset Between Respiration Products and Peat to Determine Sources of Carbon Gas Flux from a Neotropical Peatland* [13th International Symposium on Biogeochemistry of Wetlands], Virtual Meetin

1. Introduction

1.1. Peatlands and their place in the Global Carbon Cycle

Peatlands are among Earth's most critical long-term carbon (C) reservoirs, capable of sequestering vast amounts of atmospheric carbon dioxide (CO_2) in organic material over millennia. Although they cover just 3% of the global land surface, peatlands store an estimated 600 gigatons (Gt) of C—roughly double the amount stored in all the world's forests (Harenda et al., 2018; Yu et al., 2010). This stored C plays an essential role in regulating atmospheric greenhouse gases and mitigating climate change, as the waterlogged, anoxic conditions in peatlands inhibit microbial decomposition, enabling C-rich organic matter to accumulate over thousands of years (Clymo et al., 1998; Page et al., 2011). However, both natural and human pressures make peatlands highly vulnerable, posing risks to their C storage capacity and underscoring their importance in climate science and conservation efforts (Gumbricht et al., 2017).

Tropical peatlands, which are found in regions such as Southeast Asia, Africa, Central and South America, and Hawaii, differ significantly from boreal and temperate peatlands in terms of climatic conditions, including high temperatures and often seasonal rainfall. These climatic differences affect both the accumulation rates, and the stability of stored C. Tropical peatlands contain the most C-dense deposits but are especially vulnerable to C loss due to changing rainfall patterns, which can lead to rapid mineralization and release of stored C (Girkin et al., 2022; Loisel et al., 2021). Despite this importance, our understanding of tropical peatlands' long-term C dynamics remains limited by both the logistical challenges of studying these ecosystems and their underrepresentation in global C inventories (Ribeiro et al., 2021). For instance, tropical regions with consistent year-round rainfall can support rapid peat accumulation

by keeping water levels stable, while regions like the Amazon, with marked seasonal rainfall, tend to accumulate peat more slowly due to fluctuating water tables, which can affect both organic inputs and decomposition rates (Dommain et al., 2011; Draper et al., 2014). This variation highlights the importance of understanding how tropical peatlands respond to environmental factors like precipitation, temperature, and proximity to coastlines, as these can impact both their C storage potential and vulnerability to climate change (Gandois et al., 2014).

Peatlands form through the accumulation of partially decomposed plant material in waterlogged, oxygen-poor environments, where slowed microbial decomposition allows organic matter to build up over long periods. This C sequestration capacity makes peatlands invaluable in the global C cycle, as they act as both C sinks and, under certain conditions, C sources. Peatlands' ability to store C over thousands of years is due to unique environmental characteristics, such as low oxygen levels, high acidity, and sustained water saturation (Clymo et al., 1998).

Peatlands exist across various climate zones and can be classified into three main types: tropical, boreal, and temperate. Boreal peatlands, primarily located in northern regions like Canada, Russia, and Scandinavia, hold the largest share of peatland C globally. Cold temperatures in these high-latitude regions reduce microbial activity, which helps preserve organic matter, and nutrient-poor soils further inhibit decomposition, enhancing long-term C storage. In contrast, temperate peatlands, found in the British Isles, parts of Europe, and the northeastern United States, experience more moderate temperatures but still have high water tables and anoxic conditions favorable for peat accumulation.

Tropical peatlands, found in areas like Southeast Asia, Central and South America, and Africa, differ greatly from boreal and temperate types in terms of climate and vegetation

productivity. These ecosystems thrive in consistently warm and often humid conditions, with dense vegetation providing abundant organic material. While decomposition rates are higher due to the warmer climate, rapid plant growth and year-round productivity enable effective C accumulation. However, tropical peatlands are highly sensitive to environmental disturbances, such as agricultural drainage and deforestation, which can quickly lead to rapid oxidation and release of stored C as greenhouse gases (Yu et al., 2010).

The same conditions that enable peatlands to serve as long-term C sinks also render them vulnerable to climate change and human activity. Rising temperatures, altered precipitation patterns, and direct disturbances like drainage and agriculture can destabilize the waterlogged, anoxic conditions necessary for peat formation. When these ecosystems are disturbed, they can shift rapidly from C sinks to C sources, releasing CO_2 and methane (CH_4) into the atmosphere and amplifying global warming. This dual role as both vital carbon reservoirs and potential greenhouse gas sources highlights the urgent need to conserve peatlands. Their protection and sustainable management are essential for maintaining their climate-regulating functions and mitigating greenhouse gas emissions on a global scale.

1.2. Global Threats to Peatlands and Climate Change Implications

Peatlands, as vital global C sinks, face mounting threats from climate change, which jeopardize their stability and potential to continue sequestering C. Warming temperatures are a major concern, particularly for boreal peatlands, where cold conditions have historically slowed decomposition rates and supported long-term C storage (Davidson & Janssens, 2006; Schuur et al., 2015). As temperatures rise, microbial activity increases, accelerating the breakdown of stored organic matter and leading to the release of CO_2 and CH_4—both potent greenhouse gases—back into the atmosphere. This warming-induced release of C compounds creates a feedback loop, further amplifying global warming. Additionally, altered precipitation patterns,

including shifts in seasonal rainfall and prolonged droughts, can lower water tables, causing peatlands to dry out. This exposure to oxygen allows previously stable peat layers to decompose more rapidly, releasing stored C and diminishing the peatland's role as a C sink (Page et al., 2011; Turetsky et al., 2002).

Beyond climate change, peatlands are increasingly threatened by land-use changes and direct human activities, particularly in tropical regions. Agricultural expansion is a leading driver of peatland degradation, as forests and native vegetation are cleared to create farmland or palm oil plantations (Miettinen et al., 2016; Hirano et al., 2012). This process typically involves draining the peat, which not only reduces the waterlogged conditions required to maintain peat stability but also exposes the organic-rich soil to oxygen. Drained peatlands decompose at accelerated rates, often releasing vast amounts of CO_2 into the atmosphere. Palm oil plantations, especially in Southeast Asia, have transformed millions of hectares of tropical peatland, leading to substantial greenhouse gas emissions and biodiversity loss. In Central and South America, the expansion of cattle ranching and crop farming similarly threatens peatlands, as land conversion and drainage dry out these ecosystems, making them vulnerable to fire and further accelerating C loss (Draper et al., 2014).

Direct human activities such as drainage for infrastructure development, peat extraction for horticultural use, and mining further exacerbate the vulnerability of peatlands. Peat extraction, for example, directly removes stored C, destroying ecosystems that took thousands of years to form (Joosten & Clarke, 2002; Parish et al., 2008). The drainage required for extraction and development causes the water table to drop, leading to oxygenation and degradation of the peat. Infrastructure development, including road construction and urban expansion, often fragments peatlands, disrupting their hydrology and reducing their ability to retain water. These

disruptions not only release stored C but also increase the susceptibility of peatlands to fire, which can lead to catastrophic C emissions and loss of habitat (Hergoualc'h & Verchot, 2011). Together, these threats highlight the urgent need for conservation and restoration efforts to preserve peatlands' critical role in the global C cycle and climate regulation.

This dissertation addresses these challenges by investigating peatland C dynamics across three contexts: (1) tropical peatlands in Central America, where surface-derived C inputs may impact deep C emissions in undisturbed peatland ecosystems; (2) boreal peatlands subjected to experimental warming and elevated CO_2 to simulate future climate conditions; and (3) a global synthesis of peatland radiocarbon data to assess regional differences in peatland development and stability. Together, these studies aim to clarify how environmental and climate variables influence C storage and emissions in peatlands across spatial and temporal scales.

2. Surface-derived Carbon Fuels Greenhouse Gas Production at Depth in a Neotropical Peatland

2.1. Abstract

Tropical peatlands play an important role in global carbon (C) cycling but little is known about factors driving carbon dioxide (CO_2) and methane (CH_4) emissions from these ecosystems, especially production below the surface. This study aimed to identify source material and processes regulating C emissions from deep in a Neotropical peatland on the Caribbean coast of Panama. We hypothesized that: 1) surface derived organic matter transported down the soil profile is the primary C source for respiration products at depth and 2) high lignin content results in hydrogenotrophic methanogenesis as the dominant CH_4 production pathway throughout the profile. We used radiocarbon isotopes to determine whether CO_2 and CH_4 at depth (measured to 2m) are produced from modern substrates or ancient deep peat, and we used stable C isotopes to identify the dominant CH_4 production pathway. Peat organic chemistry was characterized using ^{13}C solid state nuclear magnetic resonance spectroscopy (^{13}C-NMR). We found that deep peat respiration products had radiocarbon signatures that were more similar to surface dissolved organic C (DOC) than deep solid peat. Radiocarbon ages for deep peat ranged from 1200 – 1800 yrBP at the sites measured. These results indicate that surface derived C was the dominant source for gas production at depth in this peatland, likely because of vertical transport of DOC from the surface to depth. Carbohydrates did not vary with depth across these sites, whereas lignin, which was the most abundant compound (55-70% of C), tended to increase with depth. These results suggest that there is no preferential decomposition of carbohydrates, but preferential retention of lignin. Stable isotope signatures of respiration products indicated that hydrogenotrophic rather than acetoclastic methanogenesis was the dominant production pathway of CH_4 throughout the peat profile. These results suggest, even C compounds that are typically considered vulnerable to

decomposition (i.e., carbohydrates) are preserved deep in these tropical peats, highlighting the importance of anaerobic, waterlogged conditions for preserving tropical peatland C.

2.2. Introduction

Climate change is expected to disturb hydrological cycles in the tropics, with changes in rainfall regimes already observed for many tropical regions (Kharin et al. 2007, Feng et al. 2013, Magrin et al. 2014, Duffy et al. 2015, Chadwick et al. 2016, Barkhordarian et al. 2019). Changes in rainfall are of particular relevance to the storage of the 70 – 130 Gt of carbon (C) stored in tropical peatland soils under anaerobic conditions, which could be under threat of rapid mineralization if rainfall declines and aerobic conditions emerge (Girkin et al., 2022; Loisel et al., 2021). Tropical peatlands store the largest pool of vulnerable and irrecoverable C of any ecosystem type, and this pool is sequestered over thousands of years (Goldstein et al., 2020; Noon et al., 2021). Despite their importance, tropical peatlands are logistically challenging environments to work in and are understudied compared to their northern counterparts, making tropical peatlands underrepresented in global C inventories (Ribeiro et al., 2021).

Peatlands sequester C as they build vertically with the oldest deposits at the base and less decomposed younger material accumulating at the surface (Clymo et al., 1998; Ingram, 1987). Despite temperatures ideal for microbial activity, the buildup of organic matter is possible because rates of primary production in the tropics exceed decomposition rates, which are low because peatland water tables are high (Nottingham et al., 2019; S. E. Page et al., 2011). Thus, deep peat is comprised of minimally processed plant material from the surface that accumulates due to anaerobic conditions, creating a globally significant buildup of C over time that could be metabolized if conditions became more favorable for decomposition (Hoyos-Santillan et al., 2019; Kettridge et al., 2015; Wilson, Griffiths, et al., 2021). However, this age-depth relationship is not as straightforward in the tropics as in northern peatlands, because tropical peatland

microtopography shows higher variability due to increased vegetation diversity and size, and forest disturbance can have dramatic effects on peat accumulation patterns (Dommain et al., 2015; Girkin et al., 2019). The dominant vegetation that acts as the stabilizing structure in early peat development, as well as the vegetation that serves as the biological origin of the peat itself, is also different in northern and tropical peatlands, leading to differences in peatland development, organic chemistry, and accumulation patterns between these two regions (United Nations Environment Programme et al., 2008).

Under current conditions, there is considerable variation in C emissions across tropical wetland systems (Farmer et al., 2011; Fritts, 2022), but some relationships have been generally characterized. It is mostly accepted that water table depth (Cobb et al., 2017; Hoyos-Santillan et al., 2019; A. M. Hoyt et al., 2019), temperature (Girkin et al., 2020; Hirano et al., 2009), substrate availability, and associated links with the dominant vegetation type (Upton et al., 2018; Wright et al., 2011, 2013), are strong controls on atmospheric emissions from tropical peatlands. Furthermore, surface vegetation plays an important role in the release of C by several processes, including being the biological origin of the peat matrix, which is composed primarily of lignin rich fibrous material in woody tropical peatlands, and determining labile C inputs in the form of decomposing plant tissues or root exudates (Girkin, Turner, Ostle, Craigon, et al., 2018; Lampela et al., 2014; Osaki et al., 2021). The majority of studies conducted in tropical peatlands have focused on the top 30 cm of the peat column; these depths are not only more accessible and easier to measure, but they are assumed to contribute the majority of emissions (Dhandapani et al., 2022; Jauhiainen et al., 2005; Sjögersten et al., 2011). However, it is not known if the above drivers are mainly restricted to the surface, or if these processes influence CO_2 and CH_4 production deeper within the peat profile.

In many peatlands, microbial respiration across the soil profile can be supported by multiple C sources, and it is possible to use the radiocarbon signature of C respired from peatlands to partition sources into modern/surface dissolved organic C (DOC) transported down the soil profile, versus older/buried solid C (Chanton et al., 2008; Hoyos-Santillan et al., 2016). Modern DOC, derived from surface vegetation, root exudates, and other recently photosynthesized organic matter, has a signature that is enriched in ^{14}C. The existing peat and DOC from *in situ* decomposition of that deep peat, would have depleted radiocarbon signatures compared to the modern DOC (Girkin, Turner, Ostle, Craigon, et al., 2018; Wilson et al., 2016).

There have been several studies exploring the source of DOC used by microbes for respiration within peat soils. Most studies were from northern peatlands, and determined that respiration products were intermediate in their radiocarbon activity between newer surface DOC and *in situ* older C in peat (Aravena et al., 1993; Chanton et al., 1995, 2008; Charman et al., 1999; Clymo & Bryant, 2008; Elizabeth Corbett et al., 2013). Fewer studies have reported that respiration products are more similar to modern DOC radiocarbon signatures, demonstrating dominant use of surface DOC in deep peat gas production (Wilson et al., 2021). There is limited data from tropical peatlands, but two previous studies from the tropics have contrasting results; one shows intermediate respiration products (i.e., produced by mixed sources) in a tropical peatland in Borneo (A. Hoyt, 2014), and another shows modern, surface-derived inputs are the dominant source in sites across the Pastaza-Marañon basin in Peru (A. Hoyt et al., 2020). Potential explanations for this variable source contribution in tropical peatlands include differences in hydrology across sites, as well as the difference in dominant vegetation across the tropics. Biological origin can influence the chemistry and bioavailability of both modern DOC inputs and the resulting older peat (Dhandapani et al., 2023; Gandois et al., 2014), which could

contribute to the different results reported for these two tropical peatlands with distinct surface vegetation.

Methanogenesis is an important pathway of decomposition in wetland systems. Acetoclastic methanogenesis is associated with acetate fermentation and the production of CH_4 from more relatively labile organic compounds such as in fresh DOC, while hydrogenotrophic methanogenesis is associated with CO_2 reduction and is supported by the decomposition of more complex organic matter, such as that which accumulates at depth (Kotsyurbenko et al., 2004; Sugimoto & Wada, 1993). Metabolically, acetoclastic methanogenesis is more efficient in CH_4 production and generally results in higher rates of CH_4 production compared to hydrogenotrophic methanogenesis (Kotsyurbenko et al., 2004; Liebner et al., 2015). Shifts in CH_4 production pathways between acetoclastic methanogenesis and hydrogenotrophic methanogenesis can occur, as have been seen with depth in northern wetlands (Chanton et al., 2008; Corbett et al., 2013; Hornibrook et al., 2000). Therefore, changes in the availability of labile material throughout the peat profile may play an important role in not only supplying the source for CO_2 and CH_4 production but also dictating how and how much CH_4 is produced (Sun et al., 2012).

This study explored sources of C emissions, CH_4 production pathways, and organic carbon chemistry of peat in three sites in a Neotropical peatland in Panama. Previous work suggested that subsurface peat may contribute substantially to net CO_2 and CH_4 flux from this peatland, but the source of C for these emissions was unclear (Wright et al., 2011). We used a combination of stable and radioisotope signatures of CO_2 and CH_4, and ^{13}C solid state nuclear magnetic resonance spectroscopy (^{13}C-NMR) characterization of peat soils to identify the sources of the C emitted from subsurface (>30 cm) peat. We hypothesized that: 1) surface-

derived DOC is the primary C source for microbial respiration products at depth where peat is more chemically complex, reflecting more advanced decomposition at depth, and 2) hydrogenotrophic methanogenesis is the dominant CH_4 production pathway at depth, resulting from the high lignin content typical of tropical peatlands. We report and discuss radiocarbon analyses of subsurface DOC, CH_4, and CO_2 as well as peat molecular characterization assessed via solid state ^{13}C-NMR spectroscopy in a tropical peatland to address the hypotheses.

2.3. Methods

2.3.1. Field Site Description

The Bocas Del Toro Province on the Caribbean coast of Panama is home to an internationally recognized wetland (Ramsar site #611), encompassing the 80 km^2 Changuinola peat deposit, an ombrotrophic domed peatland to the southeast of the Changuinola river (Fig. 2.1). Located 10 km east from the peatland is the town of Bocas del Toro, Isla Colon, where the average annual rainfall and temperature are 4000 mm and 30°C respectively (Isla Colon, STRI Environmental Monitoring Station). There is continuous rainfall throughout the year with no pronounced dry season, although there are two distinct periods of lower rainfall (February–April and September–October). The water table was consistently at the surface of the peatland throughout the sampling period, but has been reported to fluctuate +20 cm to -0.4 m during high or low rainfall (Hoyos-Santillan, 2014). Mean peat temperature 10 cm below the surface is 25 °C and shows little intra-annual variation (Wright et al., 2011). The oldest deposits in the peatland are in the centre of the dome, are estimated to have been formed 4000–4500 years ago, and are roughly 8 m deep (Phillips et al., 1997).

The Changuinola peat deposit developed from *Raphia taedigera* palm swamp, unlike southeast Asia coastal peatlands that begin as sediment trapping mangrove stands (Anderson & Muller, 1975; S. Phillips et al., 1997). The vegetation communities that formed the Changuinola

peat deposits have shifted spatially over time, reflecting variations in environmental conditions, and resulting in spatial heterogeneities in C inputs across the peatland (Cohen et al., 1989; S. Phillips & Bustin, 1996). At present, there are seven distinct phasic plant communities that form concentric rings within the peat dome. From the periphery and moving to the interior they are as follows: (i) *Rhizophora mangle* mangrove swamp, (ii) mixed back mangrove swamp, (iii) *Raphia taedigera* palm swamp, (iv) mixed forest swamp, (v) stunted *Campnosperma panamensis* forest swamp, (vi) sawgrass/stunted forest swamp and (vii) *Myrica-Cyrilla* bog-plain (S. Phillips et al., 1997). Previous work showed that nutrient content in the peat was generally higher near the edge (1200 µg-phosphorus (P)g^{-1}, 27mg-nitrogen (N)g^{-1}) and lower in the interior of the peatland (377 µg-Pg^{-1}, 22mg-Ng^{-1}) (Sjögersten et al., 2011; Troxler, 2007; Troxler et al., 2012).

For this study we selected sites in three of the representative plant communities, with dominant vegetation and nutrient patterns described previously. These include Outer (*Raphia taedigera* palm swamp), Intermediate (mixed forest swamp), and Inner (stunted *Campnosperma panamensis* forest swamp) peatland sites (Fig. 2.1). Previous studies conducted within the Changuinola deposit have reported differences in peat properties, root exudate characteristics, and *ex situ* experimental response in lab studies tied to vegetation community (Girkin, Turner, Ostle, Craigon, et al., 2018; Girkin et al., 2019; Sjögersten et al., 2011; Upton et al., 2018; Wright et al., 2013). Previously reported surface (<30 cm) CO_2 flux rates for the outer and inner sites used here varied from 320-500 mg CO2 m^{-2} hr^{-1} with no significant variation between sites (Wright et al., 2011), and subsurface peat across the vegetation gradient (>30 cm) appeared to have similar carbohydrate to aromatic C ratios following initial phases of decomposition occurring at the surface (Upton et al., 2018).

2.3.2. Sample Collection

Bulk peat, pore water samples, and greenhouse gases (CO_2 and CH_4) were collected in October of 2019. We sampled from 30 cm to basal depths that were identified by a marine clay boundary at the base of the peat, and did not sample surface samples (0–30 cm) that we understand might have stronger surface vegetation influence on peat chemistry compared to deeper layers that are further along in the decomposition process (Barreto & Lindo, 2020). This study aimed to compare bulk peat and pore water components of deep peat with gas produced at the same depth, and for that reason only those deeper samples were collected. Peat cores from were collected using a 5.2 cm diameter and 51 cm long Russian peat corer (Eijkelkamp, Product code 04.09). Bulk peat, pore water samples, and greenhouse gases (CO_2 and CH_4) were collected in October of 2019 from depths of 30 ± 5 and 60 ± 5 cm, as well as 100 ± 5, 200 ± 5, 300 ± 5, and 400 ± 5 cm depending on total peat depth at each site. Porewater was collected using a peristaltic pump with Teflon tubing from 1.25 cm diameter PVC pipe piezometers to measure DOC from the same depths as the peat collection. Porewater was filtered with 45 um particle retention using plastic syringes fitted with stopcocks and filters and deposited into 50 ml falcon tubes for transport. Following collection, peat cores were subsampled to coordinate with gas well depths and sealed in plastic bags to avoid oxidation during transport to the Smithsonian Tropical Research Institute soils lab in Panama City, Panama.

Diffusion gas wells were deployed at the intermediate and outer site at the same depths as pore water and peat collection to ensure robust comparison between the two source materials (bulk peat and DOC) and respiration products. There was insufficient time to include the inner site in gas collection at time of sampling. These diffusion wells consisted of PVC pipe with mesh coverings positioned within the peat to allow water to be sampled from the desired depth without contamination of bulk peat or water pulled from other depths. Water was taken from the desired

depth using a peristaltic pump and cycled into a 1L glass container. The headspace within the glass container was allowed to equilibrate over several hours while the water was pumped through the container at a rate of 1.5–1.8 L/min. Air samples from the equilibrated headspace were taken using a syringe fitted with a stopcock and needle and deposited into evacuated 125 ml serum bottles fitted with heavy butyl rubber septa.

2.3.3. Elemental and Isotopic Analyses

Elemental composition of solid homogenized airdried peat was analysed using an elemental analyser 205 (CHNOS) coupled to an IsoPrime 100 isotope ratio mass spectrometer at the Center for Stable Isotope Biogeochemistry (CSIB) 206 at the University of California, Berkeley. This analysis produced measurements for percent C and N content, ^{13}C, and ^{15}N. The ash content of bulk peat was determined by ignition of aliquots (~1.0 g) at 460°C for 5 hr.

Sample preparation and analysis for ^{14}C was completed at the Center for Accelerator Mass Spectrometry (CAMS) at Lawrence Livermore National Laboratory. To ensure that peat samples were handled appropriately for both biogeochemistry and chronology, following homogenization with a ball and mill grinder we measured two subsamples; one that underwent acid-base-acid (ABA) pre-treatment to remove possible interfering carbonates and modern C derived humic acids, and a second with no pre-treatment (Norris et al., 2020). Samples were immersed in 1N hydrochloric acid (HCl) to remove carbohydrates. Humic acids were then removed from the sample with 0.25M sodium hydroxide (NaOH) and treated with a 1N HCL immersion before they were rinsed with deionized water until neutral. The pre-treated samples were then placed on a heating block until dried. The two sets of peat samples had identical ^{14}C results and the no pre-treatment values were used in this study (Appendix Table 2.1). The porewater DOC samples were acidified with 1N HCl at 70 ∘C to remove dissolved inorganic C

and freeze dried. Both sets of peat samples and the residual DOC were loaded into quartz tubes with excess CuO and combusted at 900∘C to ensure complete combustion to CO_2.

Gas samples for CH_4 and CO_2 were extracted following the protocol outlined by (McNicol et al., 2020). For $^{14}CO_2$ samples, a series of cryogenic traps were used to purify and isolate the CO_2. For $^{14}CH_4$ samples, the mixed composition field samples were cryogenically purified to remove water and CO_2, and the remaining CH_4 was converted to CO_2 by combustion (Petrenko et al., 2008). Resulting CO_2 from samples was split to measure both a $\delta^{13}C$ and ^{14}C. Extracted CO_2 and CH_4 were analyzed for ^{14}C and ^{13}C when possible, but some sample masses were too small for both analyses (minimum 20 ug C needed for ^{14}C analysis and for the purpose of this study, we prioritized measurements for ^{14}C). The $\delta^{13}C$ values were analyzed at the Stable Isotope Geosciences Facility at Texas 210 A&M University on a Thermo Scientific MAT 253 Dual Inlet Stable Isotope Ratio Mass Spectrometer. To obtain a ^{14}C measurement, the CO_2 was reduced to graphite onto Fe powder in the presence of H2 (Vogel et al., 1984) and analysed on the HVEC 10 MV Model FN Tandem Van de Graaff Accelerator or the NEC 1 MV Pelletron Tandem Accelerator at CAMS (Broek et al., 2021). ^{14}C values are reported as $\Delta^{14}C$ (‰) corrected to the year of measurement (2019) and for mass-dependent fractionation using $\delta^{13}C$ values, and age is reported in years before present (yBP) within two standard deviations using the Libby half-life of 5568 years following the conventions outlined by Stuiver and Polach, 1977. Age-depth models were generated for each site in R v.4.2.2 (The R Foundation for Statistical Computing, 2022) using the “rbacon” package v2.3.9.1. BACON (Bayesian accumulation), is based on Bayesian theory, and simulates the sediment deposition process while accounting for both variable deposition rates and spatial autocorrelation of deposition from one layer to another within the core. Long-term peat accumulation rates were estimated by fitting

linear regressions to age-depth model outputs. The calibrated ages showed timing of peat development and accumulation between the three sites, and the conventional radiocarbon values were used to compare and identify the sources of material used to generate CO_2 and CH_4 at depth.

Differences in stable isotopic ($\delta^{13}C$) composition between $\delta^{13}CO_2$ and $\delta^{13}CH_4$ can identify the dominant pathway that produces methane, because hydrogenotrophic methanogenesis fractionate against heavy C isotopes more than acetoclastic methanogenesis (Wilson et al., 2016). Values of this apparent fractionation factor ($\alpha app = [(\delta^{13}CO_2 + 1000)/(\delta^{13}CH_4 + 1000)]$) that are greater than 1.065 are characteristic of environments dominated by hydrogenotrophic methanogenesis, while values lower than 1.055 are characteristic of environments dominated by acetoclastic methanogenesis (Zhang et al., 2019).

2.3.4. ^{13}C-NMR Spectroscopy and Mixing Model

Solid State ^{13}C NMR spectra of untreated peat samples were obtained at the Pacific Northwest National Laboratory in Washington state at the Environmental Molecular Science Laboratory facility using cross-polarization under magic angle spinning conditions (CP/MAS) with a Varian Direct Drive NMR spectrometer equipped with a Varian 4-mm probe. These bulk peat samples were free of charcoal. Approximately 30 mg of peat were packed in 4 mm zirconia rotors sealed with Kel-F caps. The CP spectra were acquired after 14k scans with a MAS rate of 14 kHz resulting in no interference from sidebands as they were outside the range of the spectrum, and a ramp-CP contact time on proton of 1 ms and a 1 or 2 s recycle delay depending on the sample with 62.5 kHz tppm proton decoupling (Aliev, 2020). The one-dimensional 1H NMR spectra of all samples were processed and analysed relative to the external standard adamantine. All spectra were corrected against a KBr background, and signals arising from C in the NMR probe and rotor were accounted for by subtracting the spectra of an empty rotor from

the sample. Spectra were digitally processed with exponential apodization (100 Hz line broadening with the first point set to 0.50), phase correction, and baseline correction using a Bernstein polynomial fit with Mnova software (v. 14.3.3; Mestrelab Research). Peak areas were integrated within seven chemical shift regions for input to the molecular mixing model corresponding to: alkyl C (0–45 ppm), N-alkyl/methoxyl C (45–60 ppm), O-alkyl C (60–95 ppm), di-O-alkyl (95–110), aromatic C (110–145 ppm), phenolic C (145–165 ppm), and carboxyl C (165–215 ppm). Example spectra output available as an overlay of all depths in Appendix Figure 2.1 and as separated depth profiles Appendix Figure 2.2.

We used a mixing model which incorporates six components to describe the molecular composition of samples based on ^{13}C NMR outputs (Baldock et al., 2004). This peatland soil has no visual evidence of char, so that component was removed from the model. The five remaining components (carbohydrate, protein, lipid, lignin, and carbonyl) have each been assigned a discrete percent of different regions of the ^{13}C NMR signal intensity based on knowledge of molar elemental contents and C content of terrestrial soil ecosystems. The measured C:N ratio of each sample was used to constrain the protein concentration of each ^{13}C NMR spectrum in the molecular mixing model. The optimisation process of the molecular mixing model compares fits for all five biomolecules to models eliminating one, two, and three components; in all cases the model fit was best when all five components were included in the model (sum of squares of deviation < 6%). The mixing model outputs are available in Appendix Table 2.2.

2.3.5. Statistics

We assessed our data at two scales: 1) among-site comparisons of the three sites, considering overall differences in peat characteristics and isotopic signatures and 2) peatland-wide patterns in soil profile characteristics and relationships among peat chemistry and isotopic signatures. Relationships between peat physical properties (C and N concentrations, C:N,

^{13}C,^{15}N, and radiocarbon) and the five biomolecules identified with the molecular mixing model were assessed using Pearson correlation analysis. We also conducted separate analyses of the ^{13}C-NMR data using raw data for spectral regions. The three sites were pooled to get peatland scale relationships between the peat physical properties and the five biomolecules versus depth. Due to the limited size of this dataset, the spearman method was used to measure covariance, and the coefficients are reported in the full correlation matrix results, including r^2 values and significance, in supplementary materials (Appendix Fig. 3 & 4). We assessed differences among the three sites using Principal Component Analysis (PCA) based on all factors included in the correlation matrices (all peat physical properties, chemistry, and isotopes for each site). Significant trends in biomolecule abundance across depth were identified by linear regression. To identify differences between mean radiocarbon values of the sources and respiration products we utilized two-sample t-tests. Bulk peat and gas products were determined by Welch two-sample t-test to account for lack of homogeneity of variance, and differences between mean radiocarbon values of DOC and gas products were assessed by student two sample t-test (Appendix Table 2.3). All relationships explored were considered significant at the 0.1 alpha level. Statistical analyses were conducted in R v.4.2.2 (The R Foundation for Statistical Computing, 2022). Reported means in the text are shown with standard errors in parentheses.

2.4. Results

2.4.1. Isotopic composition of source material and respiration products

Across all sites and depths, dissolved CH_4 and CO_2 were relatively modern, ^{14}C-enriched relative to peat, and had similar ^{14}C values to DOC, indicating the use of DOC as a preferential substrate over solid peat for microbial respiration (Fig. 2.2). Overall, the respiration products had statistically similar values to the DOC ($t(23)=0.534$ $p= 0.60$) compared to the bulk peat ($t(16)=|8.67|$, $p= <0.05$) (Appendix Table 2.3). The radiocarbon values for the bulk peat are

consistent with constant accumulation over time. The calibrated basal ages for outer, intermediate, and inner sites were 1215 ± 35, 1060 ± 30, and 1750 ± 35 yrBP respectively.

2.4.2. Peat Properties and Chemistry

The percent C across the sites was consistently 40–55% down to basal depths, which had lower C contents and higher ash content, reflecting the influence of underlying mineral sediments (Fig. 2.3). The negative correlation between both C and N concentrations with depth was not significant, however the negative correlations between ash content and depth ($r(16) = -0.62$, $p \leq 0.1$) and age and depth ($r(16) = -0.93$, $p \leq 0.1$, Fig. 2.3) were strongly significant (Appendix Fig. 2.3). Bulk peat stable isotopes, $\delta^{13}C$ and $\delta^{15}N$, showed no strong relationship with depth or site. Linear slopes across the age-depth profiles suggested consistent peat accumulation rates across the peatland over time (Fig. 2.3f). Estimates of long-term peat accumulation rates were calculated using the calibrated ages, and were 0.192 cm yr^{-1}, 0.473 cm yr^{-1}, and 0.275 cm yr^{-1} for the outer, intermediate, and inner sites respectfully.

Example spectra from surface (30 cm) and deep (basal depths; Outer 200 cm, Intermediate 248 cm, and Inner 431cm) can be seen in Figure 2.4, and complete spectra datasets can be seen in supplemental material (Appendix Fig 2.1 & 2.2). The ^{13}C-NMR molecular mixing model results showed that depth was positively correlated with lignin ($r(16) = 0.70$, $p \leq 0.1$) and negatively correlated with lipid abundance ($r(16) = -0.54$, $p \leq 0.1$) (Fig 2.5.A–C; Appendix Fig 2.4). To further explore patterns in peat chemistry across depth, we pooled the three sites for linear regression. We found significant decreases in lipid abundance ($R^2 = 0.25$, $F(1,14) = 5.88$, $p < 0.029$) and increases in lignin abundance ($R^2 = 0.46$, $F(1,14) = 13.7$, $p < 0.002$) with increasing depth (Appendix Fig 2.6).

Compared to the other four molecular components (protein, lipid, carbonyl, and carbohydrate), lignin was the most abundant biomarker making up an average 64% ± 1.1 of peat

organic matter across the sites (Fig 2.5.D). Carbohydrate was the second most abundant compound and averaged 17% ± 0.2 across the sites. There was almost no carbonyl-C present (all sites averaged < 2%), except for deep peat at the outer site and 60 and 200 cm layers of the inner site, which had 0.4% ± 0.9 and 2% ± 2 carbonyl-C respectively (Fig 2.5. A&C). Overall, the organic chemistry of peat was very similar across the sites explored here, and the main patterns that emerged were trends with depth.

We used PCA to explore differences in peat properties among the three sites. The scores and loadings of the first and second principal components accounted for the majority of variance (74%) with the first principal component accounting for 54.93% (Fig 2.6). Separation along the first principal component axis showed stratigraphic effects related to depth and peat accumulation over time, with strong separation between the 30 and 60 cm layers versus the underlying peat. The clustering of the 30 and 60 cm peat layers was primarily driven by C and N concentration, age, ash content, and lipid, alkyl-C, and protein contributions to soil organic C (Fig 2.6, Appendix Table 2.2). By contrast, the second principal component was mainly driven by site differences, with the inner site being relatively more distinct than the outer and intermediate sites while still showing some overlap (Fig 2.6). This separation appeared to be tied to the small amount of carbonyl present at this site (Fig 2.6, Appendix Table 2.2, Appendix Table 2.4).

2.4.3. Using $\delta^{13}C$ to identify CH_4 Production Pathway

The α_{app} values overlap between the outer and intermediate sites and averaged 1.078 (+/- 0.003) (Fig 2.7). These data demonstrate no shift in α_{app} with depth throughout the peat profile. The α_{app} is consistent with hydrogenotrophic methanogenesis being the dominant production pathway across all depths measured at the outer and intermediate sites.

2.5. Discussion

2.5.1. Source

The Changuinola peat deposit is important as an internationally protected wetland and is an example of a pristine undisturbed functioning tropical peatland. This is supported by the age-depth profiles that showed continuous undisturbed peat accumulation over time, and similarities in C and N concentrations and C:N ratios to other ombrotrophic peat domes across the tropics (Beilman et al., 2019; Dargie et al., 2017; Lähteenoja et al., 2012; Omar et al., 2022). This paper contributes a novel characterization of the organic components contributing to surface CO_2 fluxes (bulk peat, respiration products, peat chemical composition) to identify the dominant source of C for a tropical peatland. Across all sites and depths, DOC was enriched in radiocarbon relative to the bulk peat indicating that it is largely derived from recent photosynthate as opposed to the solid peat, which became progressively older solid peat at depth. Similar behaviour has been reported in other tropical peatlands that preferentially use modern DOC as the source for microbial respiration (Hoyt et al., 2020), while one site in Borneo reported respiration products from mixed sources (A. Hoyt, 2014). These contrasting results suggest either the Borneo peatland site is an exception to this behavior or there is need to explore more tropical peatland sites to characterize source selection behavior in the tropics. While the microbial utilization of surface DOC deep in the soil profile was seen at our sites, which have contrasting surface vegetation (*Raphia taedigera* vs. mixed hard wood), it is important to note that the preference of surface derived DOC may be related to these being two wood dominated locations. Tropical peatlands with higher abundance of sedge or shrub species may display different source selection preference compared to woody peats based on DOC, root exudate, and peat composition differences (Girkin, Turner, Ostle, & Sjögersten, 2018; Waldron et al., 2019).

2.5.2. Peat Chemistry and Stabilization

The dominant biomolecule making up this peat C was lignin, which generally represented >60% of the C in our samples. Despite the lack of a depth difference in the aromaticity index, we saw an accumulation of lignin with depth, indicating preferential preservation of this biomolecule and microbial discrimination against its decomposition through time. This selective preservation of lignin has been reported for this wetland (Hoyos-Santillan et al., 2016) and other tropical peatlands (Gandois et al., 2014) previously, and supports a paradigm of selective preservation of aromatic compounds under anaerobic conditions. Coarse woody material from fallen trees, branches, and dead roots contribute a large yet relatively sporadic portion of C inputs to tropical peat, in addition to the more constant inputs from leaf litter and fine root turnover (Hodgkins et al., 2018), and our data together with the previous studies indicate that this large-scale treen mortality and branch shedding is crucial for peat C accumulation. The waterlogged conditions in tropical peatlands can particularly reduce the decomposition of lignin by inhibiting ligninolytic microbes (Hoyos-Santillan et al., 2015; Thormann, 2006). There was little change in the carbohydrate portion of peat C with depth, even though carbohydrates typically represent the most labile compounds in plant tissues for decomposition (Bader et al., 2018). This lack of change in carbohydrate abundance with depth below 30 cm may indicate consistent preservation of this molecule after any initial decomposition in the top 30 cm, and contrasts with the preferential preservation of lignin. Interestingly, we see a significant decline in lipids with depth, even though other tropical and temperate forest studies have indicated preferential preservation of lipids in upland soils (Cusack et al., 2018; Jastrow et al., 2007; Wiesenberg et al., 2010). Our data suggest that under anaerobic conditions, lipids are decomposed more than other compounds, and/or microbial biomass production of lipids declines, or changes in carbon inputs over time. Taken together, our data support different decomposition rates and preservation processes of

individual biomarkers that contribute to the accumulation of organic C within tropical peatlands (Girkin, Turner, Ostle, & Sjögersten, 2018; Hoyos-Santillan et al., 2015, 2016).

Our outer site is closest to the edge of the peatland in an area in the peatland that is dominated by *Raphia taedigera* palm swamp and with relatively high nutrient availability, while the intermediate site dominated by mixed forest swamp species, and the inner site closest to the centre of the peatland dominated by stunted *Campnosperma panamensis* forest and has relatively low nutrient availability (S. Phillips & Bustin, 1996; Sjögersten et al., 2011; Troxler, 2007). Despite these documented differences, we found strong similarity across sites in peat characteristics as well as the radiocarbon content of porewater DOC, CO_2, and CH_4. Our results demonstrate that the peat at or below 2 m is relatively carbohydrate- and lignin-rich and potentially less decomposed than expected, making these soils vulnerable to rapid decomposition if exposed to aerobic conditions.

Based on the ^{14}C and age of peat collected across these sites, the dome shape of the peatland has built up with older layers closer to the surface at the margins (Fig 2.8). This shape and accumulation pattern has been described and modelled across other tropical peat domes that have the similar ombrotrophic characteristics as Changuinola (Cobb et al., 2017). Our results suggest age was not a driver of peat chemical characteristics or properties that describe decomposability, and that older peat that accumulated over 1000 years ago is closer to the surface at the margins and would be the first layers to experience aerobic conditions with changes in water table draw down or disturbance (Dommain et al., 2011).

2.5.3. Using $\delta^{13}C$ to understand CH_4 Production

Peat organic matter quality influences not only decomposition rates but also the CH_4 production pathway (Holmes et al., 2015). When easily degradable inputs are decomposed, acetate is produced by fermentative bacteria, increasing the importance of acetoclastic

methanogenesis (Mobilian & Craft, 2022). After the labile material is depleted, the decomposition of more resistant material and related CO_2 production leads to an increase in importance of hydrogenotrophic methanogenesis (Conrad, 2020). The high αapp (1.078 ± 0.003) observed here indicates that hydrogenotrophic methanogenesis is the dominant production pathway with no signs of depth distribution. While this study is unable to map the exact progression of the fermentation process from original plant material to CH_4, we know hydrogenotrophic methanogenesis is only possible with the availability of CO_2 for reduction to CH, and that CO_2 produced in the initial steps of decomposition is a strong potential supply of CO_2 to support hydrogenotrophic methanogenesis (Gruca-Rokosz & Koszelnik, 2018; Kotsyurbenko et al., 2004). This cooperation between microbial communities, where initial degraders provide necessary precursors (in this case CO_2 from decomposition) for further microbial metabolism by other communities, has been observed in soils and could be a mechanism regulating the release of CO_2 in this peatland (Chen et al., 2023; D. Li et al., 2021). Further work is needed to explore the methanogen community composition and stratigraphy that might affect net CH_4 flux from this wetland and determine potential surface processes that would cause a shift in CH_4 production pathway in surface (0-30cm) peat.

2.5.4. Future Implications

Tropical peatlands are important C rich ecosystems that are vulnerable to future change. Here, we described how sites within a peatland with varied surface vegetation and nutrient status all preferentially support deep peat respiration with surface derived DOC, produce CH_4 via hydrogenotrophic methanogenesis, and continue to accumulate C dense bulk peat. We found that the bulk peat currently saturated in the Changuinola peatland is primarily comprised of lignin, with accumulation of lignin at depth, presumably because of microbial discrimination against its

decomposition in anaerobic conditions. It is unclear how resistant to decomposition this lignin would be if exposed to aerobic conditions. Changes in climate and drying of peatlands will expose C that has been preserved under anaerobic conditions to rapid microbial decomposition. Vegetation shifts and drops in water table depth that can also disconnect the surface from deep peat layers and expose peat previously preserved by anoxic conditions to rapid, aerobic decomposition (Kettridge et al., 2015; Ofiti et al., 2023). Shifts in composition, availability or amounts of inputs from the surface will influence greenhouse gas production in ways that are not straightforward or direct, and there is a need and plenty of room to further study these relationships. Taken together, these results make it clear that this peatland is storing and protecting peat C under current conditions. However, based on the importance of DOC transport and deep peat preservation and decay dynamics, changes in precipitation and evapotranspiration that influence transport and connectivity between surface and deep peat could greatly impact the C storage capacity of this ecosystem.

2.6. Figures

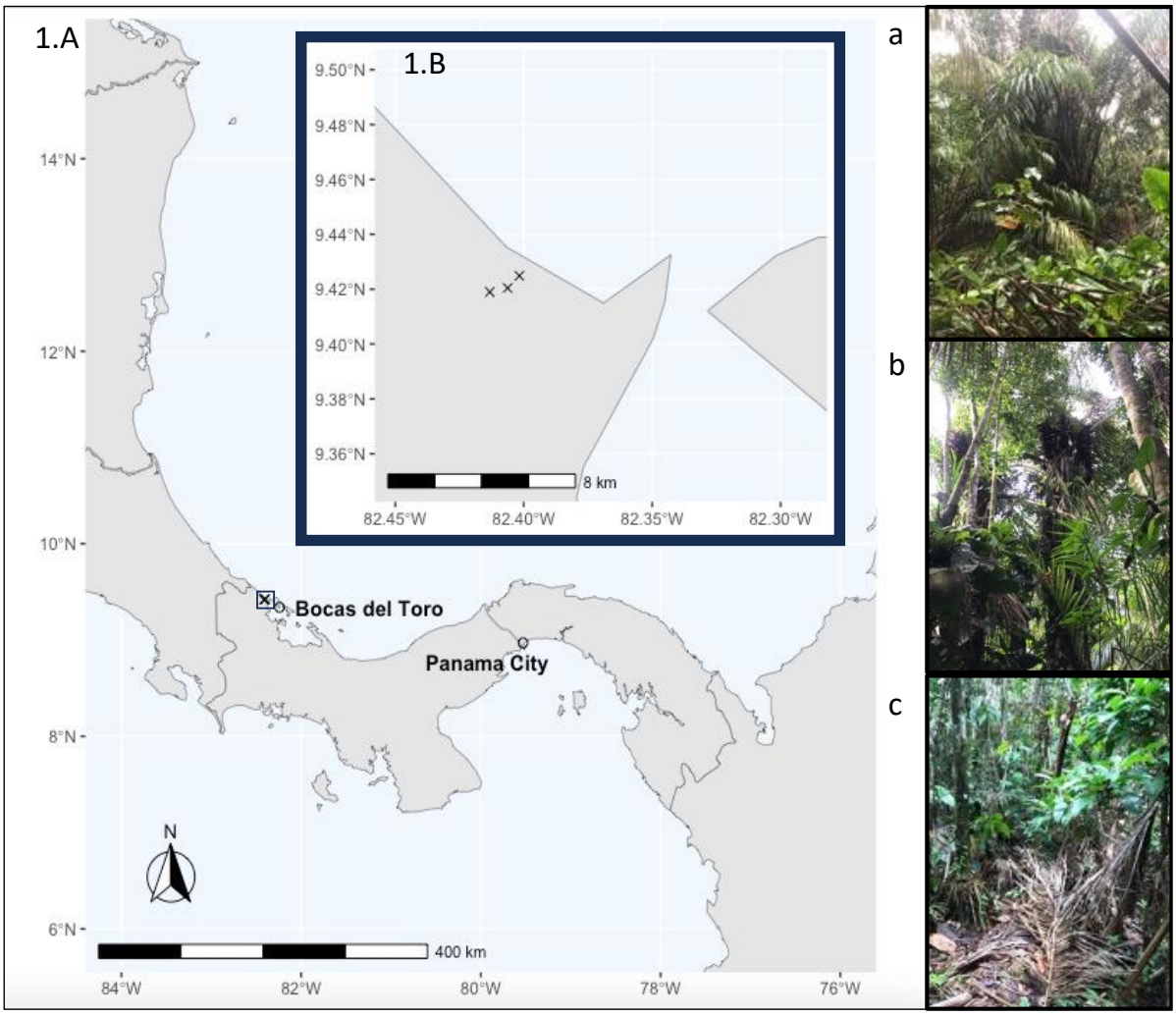

Figure 2.1 Map of sites included in this study from the Changuinola peat deposit. A. Location of study site identified by square in relation to the city of Bocas Del Toro and Panama City. B. Inset showing the location of the sites along the transect. The sites follow a vegetation gradient with a) the outer site closest to the channel *Raphia taedigera* palm swamp b) the intermediate site mixed forest swamp and c) the inner site closest to the centre of the peatland composed of stunted *Campnosperma panamensis* forest swamp. The nutrient gradient decreases from outer site to inner site.

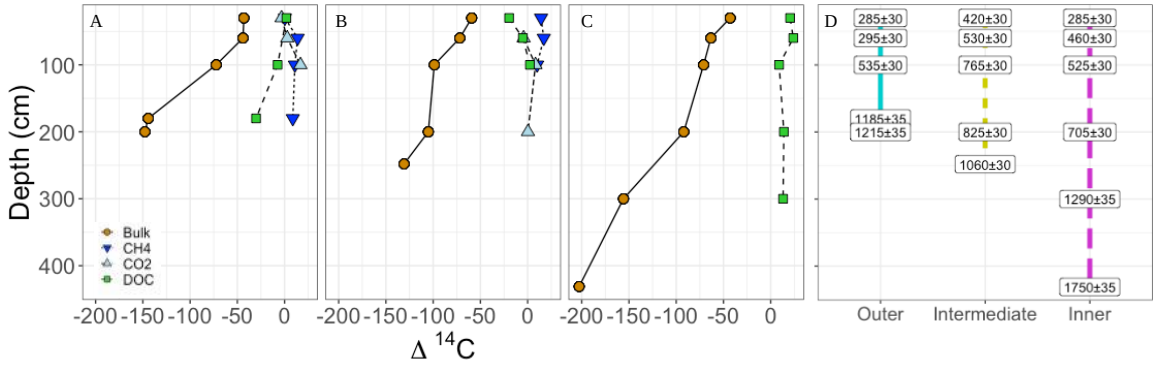

Figure 2.2 Isotopic composition of respiration products and substrates. Bulk peat, DOC, and respiration products (CH_4 = methane, CO_2 = carbon dioxide) plotted by depth across all three sites; A) Outer, B) Intermediate and C) Inner. Brown circles and solid lines represent bulk peat and green squares with dashed lines represent DOC; these are the two measured sources available for gas production. The gas products are denoted by inverted dark blue triangles and dotted lines for methane, and the light blue triangles and dashed lines for dissolved carbon dioxide. Note the age difference between solid peat and all DOC and gas values; this offset indicates that gas production is driven by modern DOC throughout the peat profile. D. Calibrated ages for all bulk peat measured in yBP within two standard deviations for the outer, intermediate, and inner sites denoted by solid blue, dashed yellow, and dashed pink respectively.

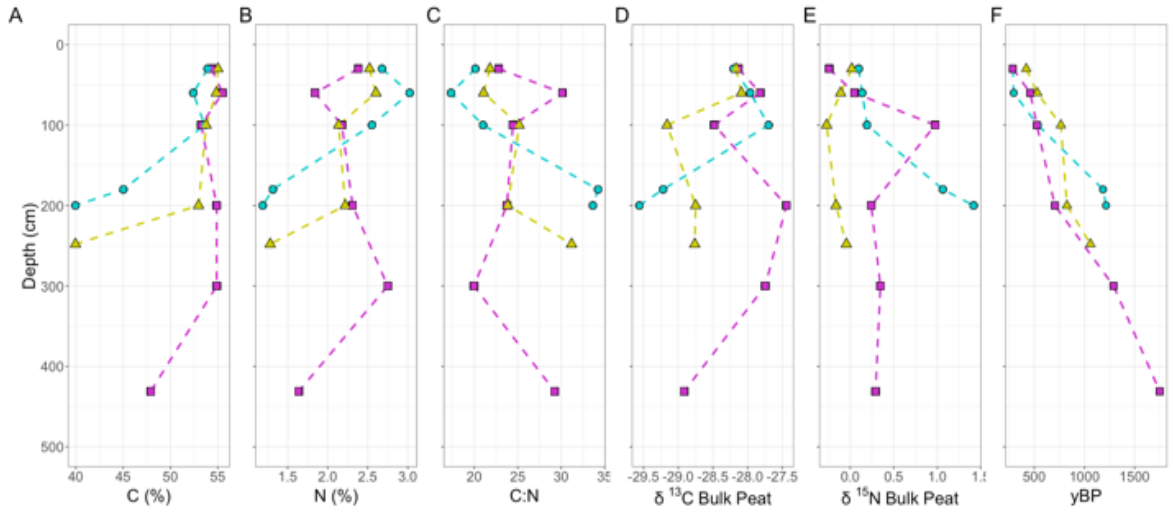

Figure 2.3 Bulk Peat Properties and Characteristics. Depth profiles for A. percent carbon, B. percent nitrogen, C. the ratio of carbon to nitrogen, D. stable carbon isotope, E. stable nitrogen isotope, and E. calibrated age for layers measured for the three sites. Sites are indicated by colour and shape with blue circles indicating the outer site, yellow triangles the intermediate site, and pink squares the inner site.

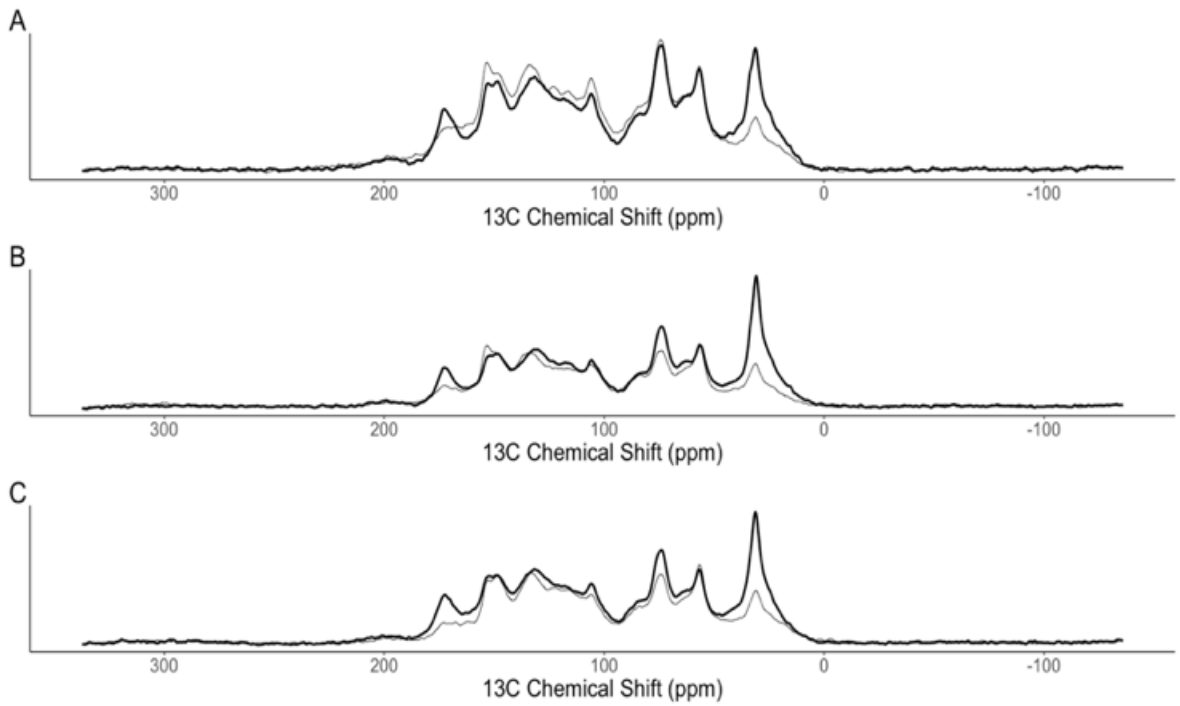

Figure 2.4 Example 13C NMR spectra. Bulk peat layers sampled from the A. outer, B. intermediate, and C. inner sites showing differences between the shallow (bold) and basal (thin) depths with stacked spectra; the complete spectra dataset can be found in additional data located in supplemental material. Spectra were digitally processed with Mnova software (v. 14.3.3; Mestrelab Research) with exponential apodization (100 Hz line broadening with the first point set to 0.50), phase correction, and baseline correction using a Bernstein polynomial fit.

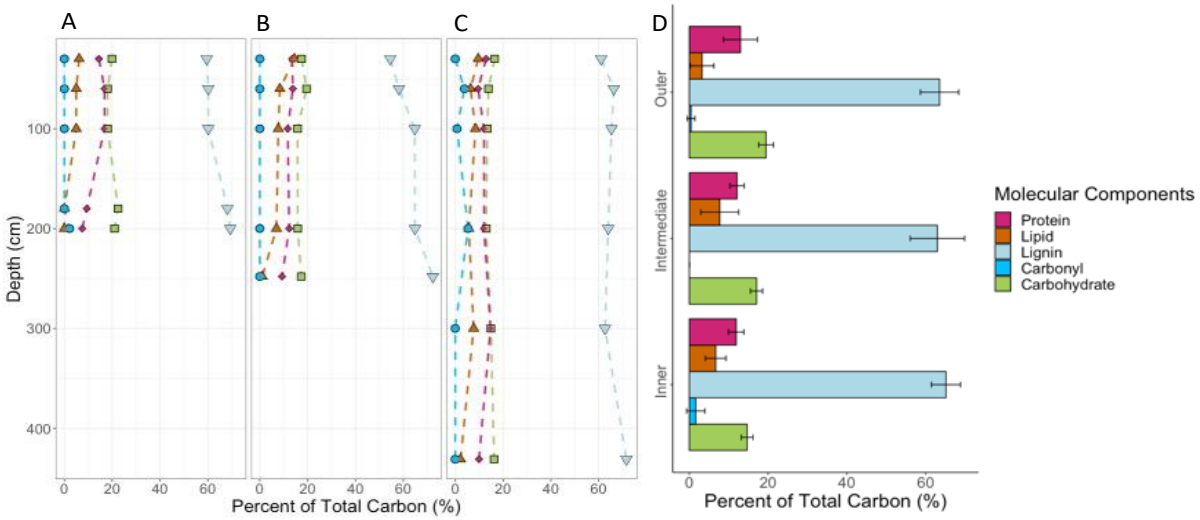

Figure 2.5 Proportion of total organic C attributed to each molecular component across sites and depths. Mixing model results showing little change in the five molecular components described by the model with depth for the A) outer site, B) intermediate site, and C) inner site. Colours and symbols represent the molecular components with proteins as pink diamonds, lipids as orange triangles, lignin as light blue inverted triangles, carbonyl as blue circles, and carbohydrates as green squares. D) Average proportion of total organic C attributed to each molecular component across sites with standard error.

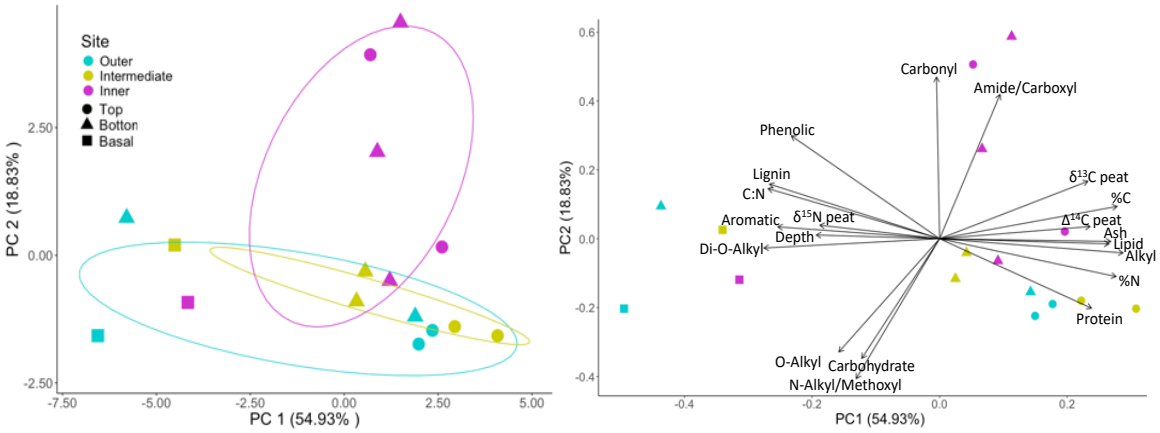

Figure 2.6 Scores and loadings from the PCA for all peat properties and chemistry and depth for the outer (blue), intermediate (yellow), and inner (pink) sites. Depths have been indicated by shape with the top (30-60 cm) as circles, the bottom (>1 m) as triangles, and the three basal depths as squares (basal depths; Outer 200 cm, Intermediate 248 cm, and Inner 431cm). Combined PC1 and PC2 account for 74% of variance.

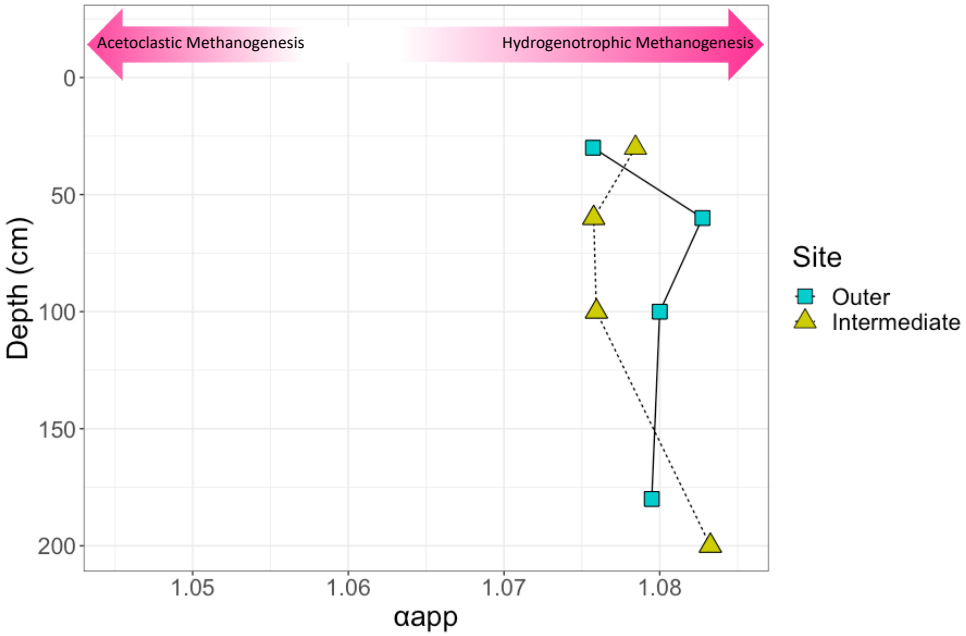

Figure 2.7 Differences in stable C isotopic composition between DIC and CH_4. Calculated estimates of apparent fractionation factor (αapp) across depth for gas collected from the outer (blue squares) and intermediate (green triangles) sites. The samples from the inner site did not have sufficient amounts of C for this analysis. Note the x-axis shows little variation in αapp between sites and soil layers; values of αapp higher than 1.065 is usually characteristic of environments dominated by hydrogenotrophic methanogenesis, while a value lower than 1.055 is characteristic of an environment dominated by acetoclastic methanogenesis (Corbett et al., 2013).

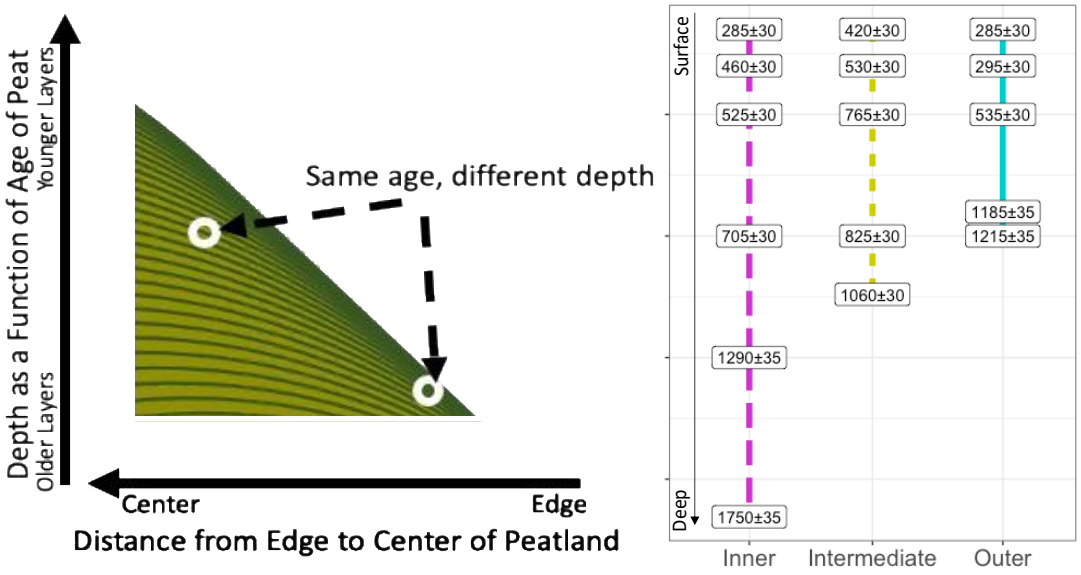

Figure 2.8 Schematic of peatland shape and layer accumulation pattern based on peat layer age and depth from surface. This concept was presented in model data from Cobb et al., 2017 and has been modified to create this schematic that is not to scale. Peat layers accumulate over time with the youngest layers at the surface and oldest layers at the base of the peat deposit. Based on this and ages collected from the sites within the Changuinola peat deposit, layers that correspond to the same age are located at different depths across the peat dome with older peat layers are closer to the surface at the margins.

2.7. Appendix

Appendix Table 2.1: Radiocarbon results for both untreated (No Acid-Base-Acid) and treated (Acid-Base-Acid) sets of peat samples. Radiocarbon concentration is expressed as $\Delta^{14}C$ within two standard deviations.

Site	Depth	$\Delta^{14}C$ (No ABA)	±	$\Delta^{14}C$ (ABA)	±
Outer	100	-72.4	3.1	-77.5	4.0
	180	-147.8	3.2	-157.6	3.6
	200	-144.3	3.2	-157.8	3.6
	30	-43.1	3.4	-54.9	4.1
	60	-44.0	3.4	-54.2	4.1
Intermediate	30	-59.2	3.4	-59.9	4.0
	60	-71.8	3.3	-70.2	4.0
	100	-98.8	3.3	-107.5	3.8
	200	-105.1	3.2	-110.8	3.8
	248	-130.8	3.2	-141.0	3.7
Inner	30	-42.9	3.3	-45.6	4.1
	60	-63.3	3.3	-68.5	4.0
	100	-71.0	3.2	-75.9	4.0
	200	-92.0	3.3	-93.6	3.9
	300	-155.8	3.2	-155.2	3.6
	431	-202.7	3.1	-203.1	3.4

Appendix Table 2.2: Mixing model outputs for all depths sampled from the three sites. Molecular component proportion of total C measured via ^{13}CNMR described by the mixing model output as weighted percent (Wt%) developed by Baldock et al., 2004, %C measured from bulk peat combustion via elemental analyser.

Site	**Depth**	**Molecular Component**	Wt%	**%C**
Inner	30	Carbohydrate	16.5	54.33
Inner	30	Protein	12.9	54.33
Inner	30	Lignin	61.0	54.33
Inner	30	Lipid	9.6	54.33
Inner	30	Carbonyl	0.0	54.33
Inner	60	Carbohydrate	13.9	55.49
Inner	60	Protein	9.6	55.49
Inner	60	Lignin	66.3	55.49
Inner	60	Lipid	6.4	55.49
Inner	60	Carbonyl	3.8	55.49
Inner	100	Carbohydrate	13.4	53.24
Inner	100	Protein	12.1	53.24
Inner	100	Lignin	65.3	53.24
Inner	100	Lipid	8.5	53.24
Inner	100	Carbonyl	0.7	53.24
Inner	200	Carbohydrate	13.0	54.87
Inner	200	Protein	12.1	54.87
Inner	200	Lignin	64.0	54.87
Inner	200	Lipid	5.7	54.87
Inner	200	Carbonyl	5.3	54.87
Inner	300	Carbohydrate	14.9	54.88
Inner	300	Protein	14.8	54.88
Inner	300	Lignin	62.6	54.88
Inner	300	Lipid	7.7	54.88
Inner	300	Carbonyl	0.0	54.88
Inner	431	Carbohydrate	16.3	47.91
Inner	431	Protein	9.9	47.91
Inner	431	Lignin	71.6	47.91
Inner	431	Lipid	2.2	47.91
Inner	431	Carbonyl	0.0	47.91
Intermediate	30	Carbohydrate	17.4	55.01

Intermediate	30	Protein	13.5	55.01
Intermediate	30	Lignin	54.5	55.01
Intermediate	30	Lipid	14.5	55.01
Intermediate	30	Carbonyl	0.0	55.01
Intermediate	60	Carbohydrate	19.6	54.84
Intermediate	60	Protein	13.8	54.84
Intermediate	60	Lignin	58.2	54.84
Intermediate	60	Lipid	8.4	54.84
Intermediate	60	Carbonyl	0.0	54.84
Intermediate	100	Carbohydrate	15.8	53.76
Intermediate	100	Protein	11.7	53.76
Intermediate	100	Lignin	64.8	53.76
Intermediate	100	Lipid	7.7	53.76
Intermediate	100	Carbonyl	0.0	53.76
Intermediate	200	Carbohydrate	15.9	52.96
Intermediate	200	Protein	12.3	52.96
Intermediate	200	Lignin	64.9	52.96
Intermediate	200	Lipid	7.0	52.96
Intermediate	200	Carbonyl	0.0	52.96
Intermediate	248	Carbohydrate	17.3	39.96
Intermediate	248	Protein	9.3	39.96
Intermediate	248	Lignin	72.4	39.96
Intermediate	248	Lipid	1.0	39.96
Intermediate	248	Carbonyl	0.0	39.96
Outer	30	Carbohydrate	19.9	53.92
Outer	30	Protein	14.4	53.92
Outer	30	Lignin	59.5	53.92
Outer	30	Lipid	6.2	53.92
Outer	30	Carbonyl	0.0	53.92
Outer	60	Carbohydrate	18.1	52.40
Outer	60	Protein	16.8	52.40
Outer	60	Lignin	60.2	52.40
Outer	60	Lipid	5.0	52.40
Outer	60	Carbonyl	0.0	52.40
Outer	100	Carbohydrate	18.1	53.60
Outer	100	Protein	16.8	53.60
Outer	100	Lignin	60.2	53.60
Outer	100	Lipid	5.0	53.60
Outer	100	Carbonyl	0.0	53.60

Outer	180	Carbohydrate	22.4	39.96
Outer	180	Protein	9.4	39.96
Outer	180	Lignin	68.2	39.96
Outer	180	Lipid	0.0	39.96
Outer	180	Carbonyl	0.0	39.96
Outer	200	Carbohydrate	21.0	45.03
Outer	200	Protein	7.5	45.03
Outer	200	Lignin	69.4	45.03
Outer	200	Lipid	0.0	45.03
Outer	200	Carbonyl	2.2	45.03

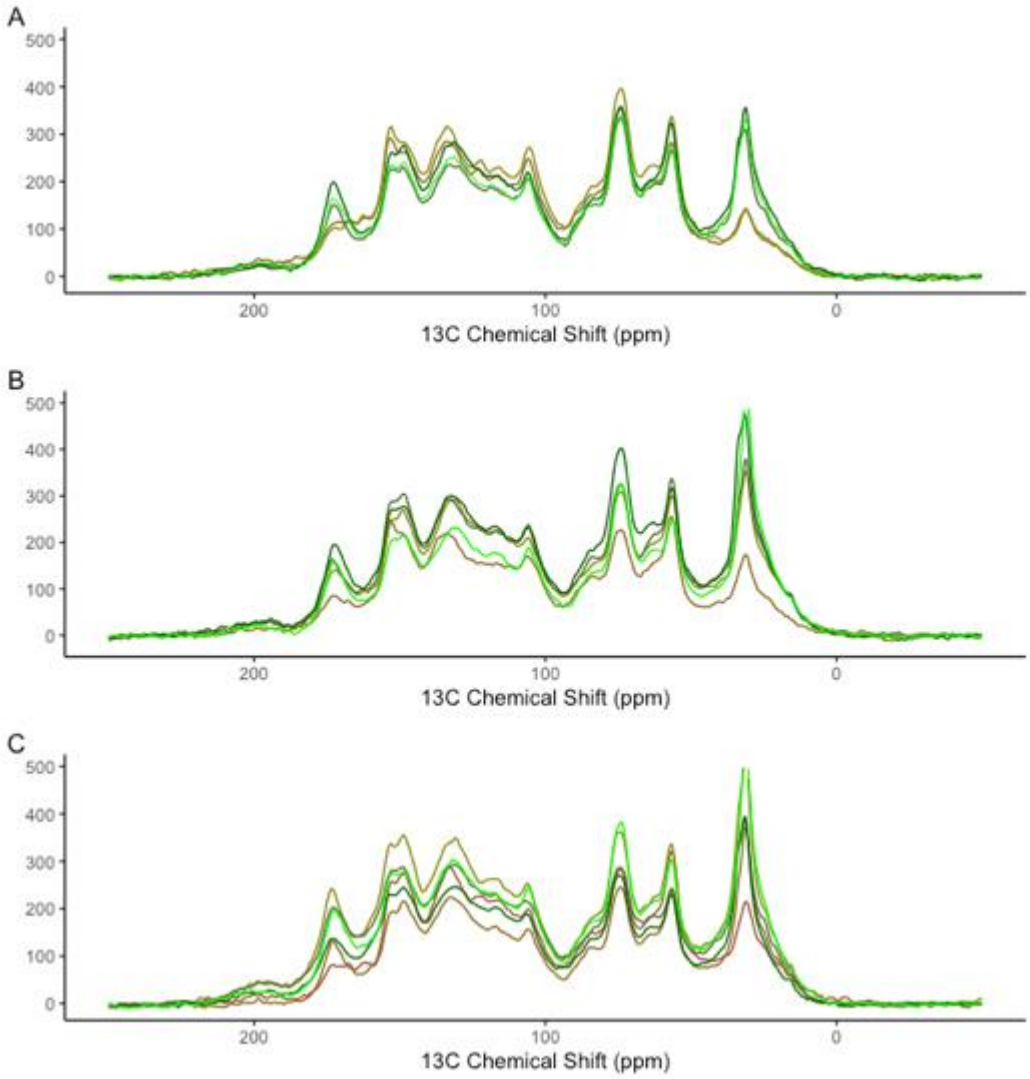

Appendix Figure 2-1 Stacked overlay of depth profiles of ^{13}C NMR spectra of the A) Outer, B) Intermediate, and C) Inner site. Colors increase in darkness representing an increase in depth with light green being the 30cm material and dark brown being the basal material. Spectra were digitally processed with Mnova software (v. 14.3.3; Mestrelab Research) with exponential apodization (100 Hz line broadening with the first point set to 0.50), phase correction, and baseline correction using a Bernstein polynomial fit. Peak areas were integrated corresponding to; alkyl C (0–45 ppm), N-alkyl/methoxyl C (45–60 ppm), O-alkyl C (60–95 ppm), di-O-alkyl (95–110), aromatic C (110–145 ppm), phenolic C (145-165 ppm), and carboxyl C (165–215 ppm).

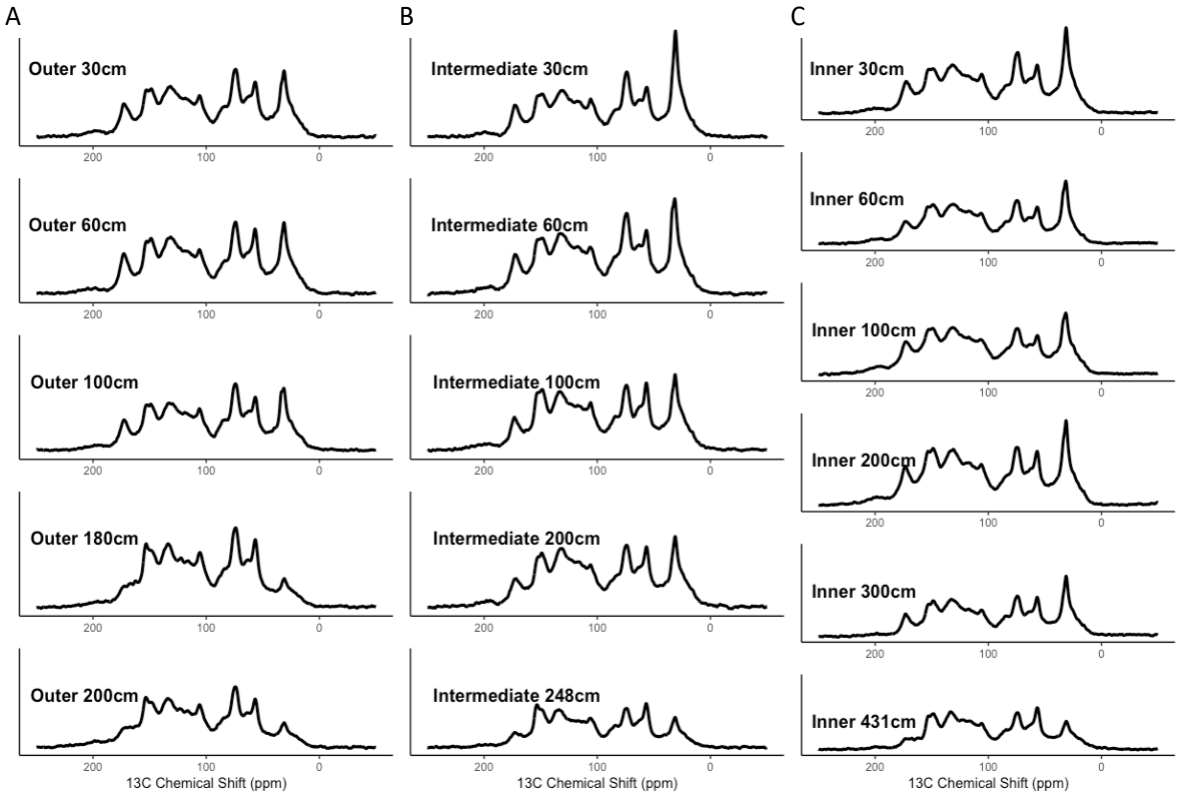

Appendix Figure 2-2 Depth profiles of 13C NMR spectra for the A) Outer, B) Intermediate, and C) Inner sites. Spectra were digitally processed with Mnova software (v. 14.3.3; Mestrelab Research) with exponential apodization (100 Hz line broadening with the first point set to 0.50), phase correction, and baseline correction using a Bernstein polynomial fit. Peak areas were integrated corresponding to; alkyl C (0–45 ppm), N-alkyl/methoxyl C (45–60 ppm), O-alkyl C (60–95 ppm), di-O-alkyl (95–110), aromatic C (110–145 ppm), phenolic C (145-165 ppm), and carboxyl C (165–215 ppm). The y-axis has been scaled equally across all plots to visually compare changes in peak heights and area across depth, however the additional depths at the Inner site need to be considered when comparing across sites.

Appendix Table 2.3 Results from two-sample t-tests comparing bulk peat radiocarbon vaues versus respiration product radiocarbon values, and DOC radiocarbon values versus respiration product radiocarbon values.

	Sample Type	Mean	t-value	df	p-value
Pair 1	Bulk Peat	-96.5625	-8.6657	15.974	1.96E-07
	Gases (CH4, CO2)	7.95			
Pair 2	DOC	2.027273	0.53811	23	0.5957
	Gases (CH4, CO2)	-3.878571			

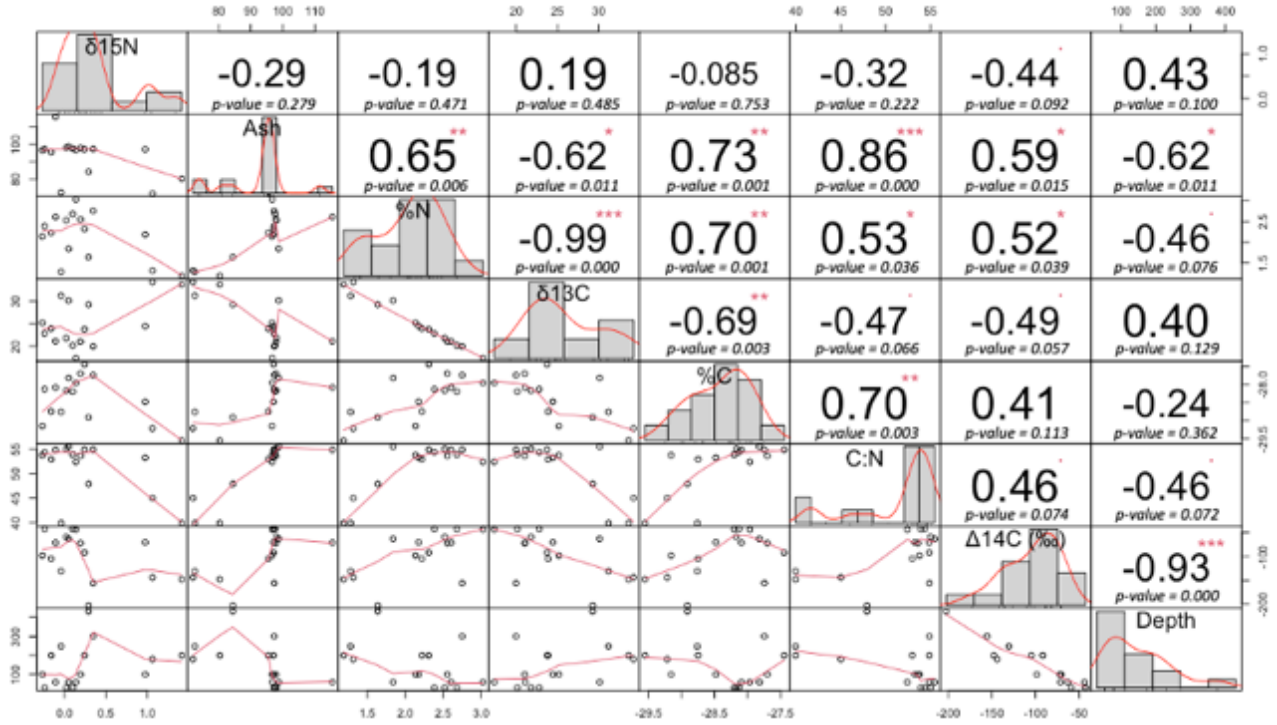

Appendix Figure 2-3 Correlation matrix for peat physical properties and depth. The numbers represent the value of the correlation coefficient (r) plus the result of the cor.test as stars. On the bottom of the matrix are the bivariate scatterplots with a fitted line. Significand codes: 0 '***' 0.001 '**' 0.01 '*' 0.1 ''.

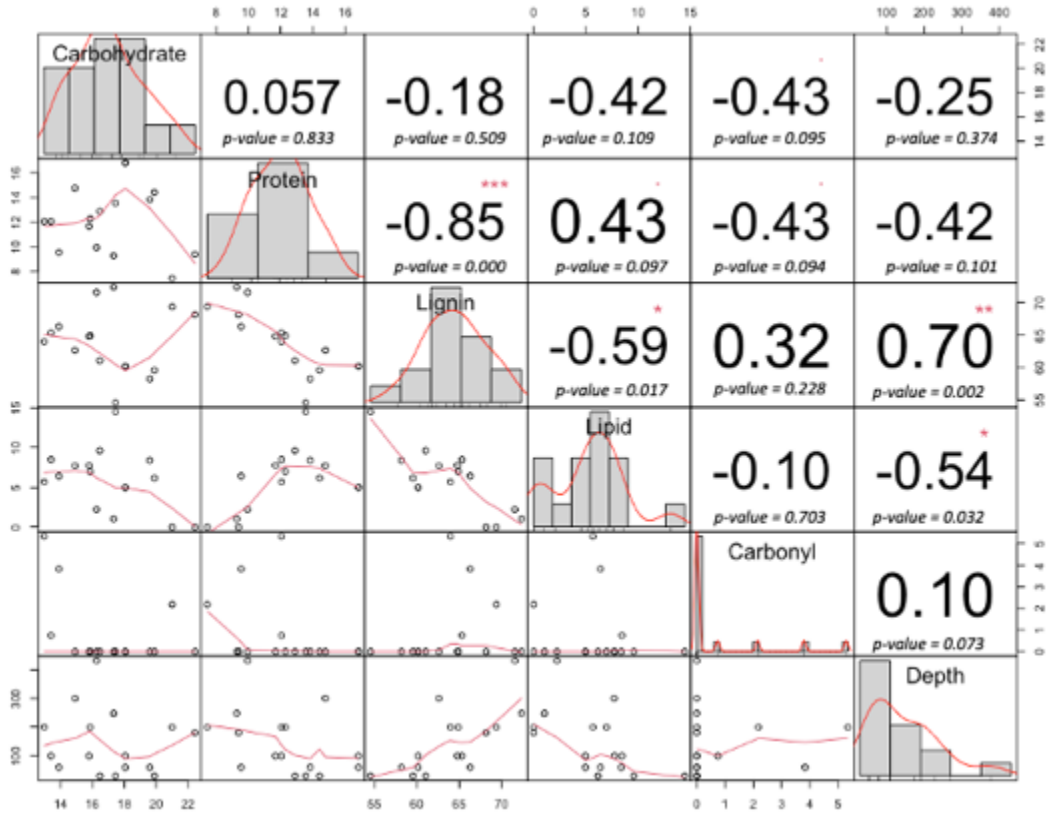

Appendix Figure 2-4 Correlation matrix for peat molecular components and depth. The numbers represent the value of the correlation (r^2) plus the result of the cor.test as stars. On the bottom of the matrix are the bivariate scatterplots with a fitted line. Significand codes: 0 '***' 0.001 '**' 0.01 '*' 0.1 ''.

Appendix Table 2.4 PCA eigenvalues and loadings for PC1 and PC2.

	PC1	PC2
Eigenvalues	**3.314e+00**	**1.941e+00**
Variable		
δ15N	-0.186	0.039
Ash	-0.386	-0.077
%N	0.274	-0.109
δ13C	0.230	0.165
%C	0.275	0.091
C:N	-0.266	0.144
Δ14C (‰)	0.233	0.035
Depth	-0.191	0.011
LOI	0.265	-0.008
Alkyl	0.284	-0.041
N-Alkyl/Methoxyl	-0.129	-0.402
O-Alkyl	-0.156	-0.325
Di_O_Alkyl	-0.273	-0.027
Aromatic	-0.251	0.034
Phenolic	-0.230	0.296
Amide/Carboxyl	0.094	0.414
Carbohydrate	-0.121	-0.344
Protein	0.236	-0.200
Lignin	-0.264	0.157
Lipid	0.263	-0.015
Carbonyl	-0.005	0.464

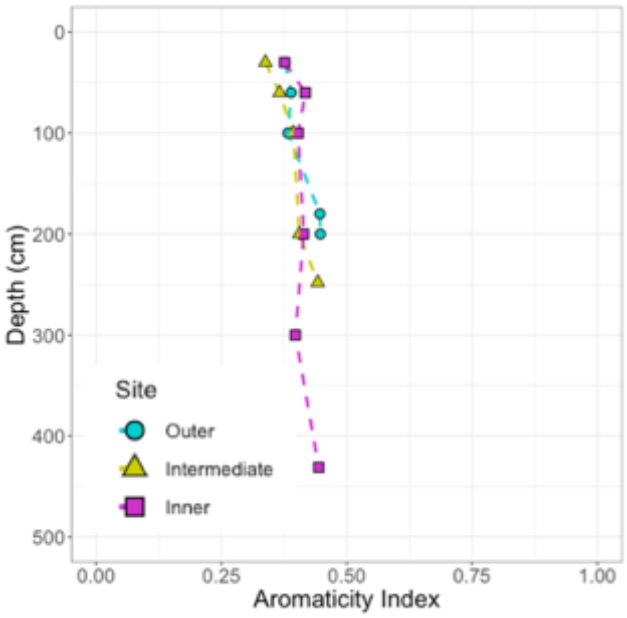

Appendix Figure 2-5 Aromaticity Index. The aromaticity index has been used to describe decomposition state of soils. This index is expressed as the ratio of Aromatic-C to Alkyl + O-Alkyl + Aromatic C and is calculated using the results from integration of the ^{13}C NMR spectra. As the aromaticity index approaches 1, the soil is considered more decomposed. The lack of change in aromaticity with depth, and the consistency across all three sites, suggests little decomposition has occurred over space and time. Sites are indicated by color and shape with blue circles indicating the outer site, yellow triangles the intermediate site, and pink squares the inner site.

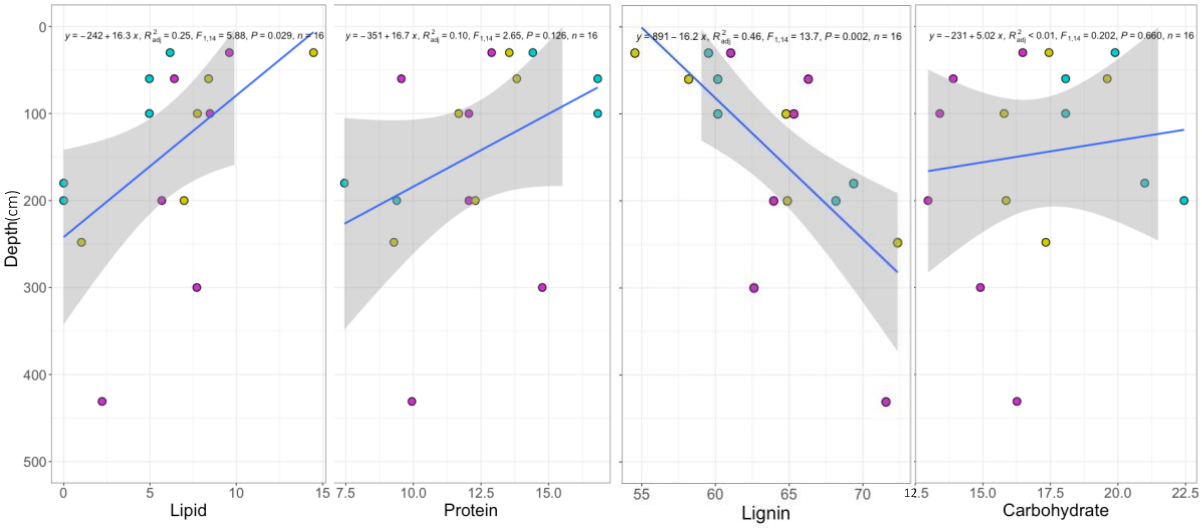

Appendix Figure 2-6 Linear regression of the four most abundant biomolecules from the mixing model versus depth. Sites have been pooled for this analysis but are indicated by color with blue indicating the outer site, yellow the intermediate site, and pink the inner site. Regressions show significant declines with depth for lipids, and significant increases with depth for lignin across sites.

3. Changes in Peat Stocks and Characteristics following Warming and Elevated CO2 of an Ombrotrophic Boreal Bog

3.1. Abstract

This study investigates peatland C dynamics at the Spruce and Peatland Responses Under Changing Environments (SPRUCE) site over five years of warming and elevated CO_2, revealing an increase in C stocks within deep peat layers, despite past reported overall net C losses at the ecosystem level. Previous research indicated that warming shifted the peatland from a net C sink to a source, primarily due to increased decomposition of surface layers and downward C transport. Our findings suggest that while surface layers experience significant C emissions due to enhanced decomposition, deep peat layers benefit from sustained waterlogged conditions that facilitate C storage.

Despite no significant changes in bulk peat chemistry between control and warming treatments, the increase in deep peat C stocks highlights the complexity of C sequestration processes in peatlands. The observed stability in peat chemistry suggests that fundamental properties may resist short-term environmental changes, indicating that significant alterations in peat characteristics might require longer durations or more intense stressors to become detectable.

The balance between C sequestration in deep peat and emissions from surface layers illustrates the nuanced dynamics of peatland ecosystems. Overall, this research underscores the importance of considering both short-term and long-term processes in understanding peatland C dynamics and highlights the need for continued long-term studies to better predict peatland responses to climate change and inform effective management strategies. Given the critical role of peatlands in the global C cycle, these insights are essential for developing conservation approaches in the face of ongoing environmental change.

3.2. Introduction

Despite covering only 3% of the Earth's land surface, peatlands are the most efficient terrestrial C sink, storing 600 Gt C in their soils – double the amount stored by all the world's forests combined (Harenda et al., 2018; Yu et al., 2010). Their ability to store tremendous amounts of C results from anaerobic waterlogged conditions combined with low temperatures and anoxic conditions, which slow decomposition and promote accumulation of organic matter (Barreto and Lindo 2020). Over time, dead plant material, primarily sphagnum mosses, accumulates and becomes compacted into peat. As the layer of peat thickens, it creates a distinctive, water-saturated, anaerobic environment that further inhibits decomposition, allowing peat to build up. This accumulation of partially decomposed plant material forms a carbon-rich substrate that can store large amounts of C over millennia (Clymo et al., 1998). Peatlands, therefore, play a crucial role in C sequestration and climate regulation. If these environmental constraints on organic matter decomposition are removed, there is the potential to alter the balance of these systems and reduce their ability to accumulate and store C.

Under the highest emissions no-policy baseline scenario, climate models project a 4–6°C increase in atmospheric and peat soil temperatures by 2100 (IPCC 2023). Rising temperatures are expected to enhance peatland heterotrophic respiration, potentially releasing substantial amounts of carbon dioxide (CO_2) and methane (CH_4) to the atmosphere (Hopple et al., 2020; Li, Gogo, et al., 2021; Wilson et al., 2016). Rising atmospheric CO_2 concentrations are expected to stimulate photosynthesis and increase plant litter production. This could lead to greater C uptake by plants, which might help offset some of the C losses from increased respiration and decomposition. To simplify, the C balance can be viewed as the difference between C inputs (like CO_2 absorbed through photosynthesis) and C losses (such as CO_2 and CH_4 emissions). However,

the combined effects of elevated temperatures and increased atmospheric CO_2 concentrations on peatland C cycles are still uncertain. Elevated temperatures can accelerate microbial activity and decomposition rates, potentially leading to increased CO_2 release from peat soils (Q. Li et al., 2021). At the same time, higher CO_2 levels might enhance plant growth and root biomass, which could sequester more C and offset some of the emissions (Thompson et al., 2017).

Water table depth is another important driver of peatland C stability and transport and imposes an additional control on peatland C balance. A higher water table might reduce decomposition rates and enhance C storage by promoting anaerobic conditions, whereas a lower water table could increase decomposition and C loss (Zhong et al., 2020). The water table also influences vertical transport of peat material throughout the profile, and changes in water table height can facilitate or cut off delivery of surface C to deeper peat (Elizabeth Corbett et al., 2013). Additionally, changes in water table depth can affect peat layers differently, with pronounced responses observed at various depths, particularly around the acrotelm/catotelm boundary (Szajdak et al., 2019). The acrotelm (the upper, more active, and aerobic layer) and the catotelm (the deeper, water-saturated, anaerobic layer) can exhibit significant changes in peat characteristics based on their decomposition conditions. Specifically, the acrotelm's characteristics can vary with its more aerobic decomposition environment, while the catotelm's traits are influenced by its anaerobic environment. This can affect the decomposition state of the peat found in each of these layers (Ingram, 1987). Changes in water table depth will have potential consequences for peat material residing at this boundary (Holden & Burt, 2003; Ofiti et al., 2022). Consequently, the influence of all the interacting factors on C storage and release remains uncertain and is a critical area of ongoing research (Blodau et al., 2004; Chanton et al., 2008; Elizabeth Corbett et al., 2013; Hoyos-Santillan et al., 2019; Sjögersten et al., 2018).

The Spruce and Peatland Responses Under Changing Environments (SPRUCE) experiment aims to provide insights into how climate change will affect peatland ecosystems and their role in the global C cycle. SPRUCE is a long-term study focused on warming and elevated CO_2 levels in a forested boreal peatland (Fig 3.1; https://mnspruce.ornl.gov/). Established in 2012, the experiment began applying whole-ecosystem warming up to +9°C above ambient temperatures in 2015, using a regression-based design. The +0, +2.25, +4.5, +6.75 and +9°C warming treatments are each conducted at ambient and elevated CO_2 (eCO_2) conditions. The eCO2 treatment are imposed as +500 ppm above ambient CO_2 concentrations of reference plots with actual concentrations ranging from 800 to 900 ppm. This experimental design allows researchers to investigate how different levels of warming, eCO_2 concentrations, and their interactions influence peatland C dynamics, microbial processes, and ecosystem responses over time.

Previous work at SPRUCE has reported changes in response to experimental treatments by vegetation communities, greenhouse gas fluxes, water table depth, and net C balance. These changes include shifts in species composition and growth patterns (McPartland et al., 2020). Some studies within SPRUCE have noted increased growth of certain plant species in warmed plots, which could potentially lead to higher rates of C sequestration if the new vegetation contributes to peat accumulation (McPartland et al., 2020). However, there is evidence that warming has led to increased C loss from the peatland, as indicated by higher emissions of CO_2, CH_4, and both dissolved organic and inorganic C (Gill et al., 2017; P. J. Hanson et al., 2020; Hopple et al., 2020; Wilson et al., 2016). Thus, experimental warming has shifted the balance between C input (through plant growth) and output (through decomposition and emissions),

leading to overall net C loss in the warmest plots (P. J. Hanson et al., 2020; Wilson, Griffiths, et al., 2021; Wilson, Tfaily, et al., 2021).

There is evidence that both warming and increased CO_2 concentrations significantly alter the sources of C in the SPRUCE peatland soils. Warming enhances microbial activity and decomposition rates, which can affect the types, amounts, and turnover times of C sources in the soil (Ofiti et al., 2023). However, analyzing the bulk peat from SPRUCE may provide critical additional data on C dynamics, potentially revealing complex patterns or alternative trends that current observations and measurements might not fully capture.

The water table at SPRUCE shows a notable response to experimental treatments (Wilson, Tfaily, et al., 2021). Increased temperatures have caused a decline in water table depth, which in turn has elevated oxygen levels in previously saturated peat layers (Ofiti et al., 2022; Schlesinger & Bernhardt, 2020). This increased oxygenation accelerates microbial decomposition of peat C and enhances the incorporation of various soil constituents through plant litter and root exudates. Consequently, this process speeds up the decomposition of fast-cycling C while diluting slowly-cycling C (Ofiti et al., 2022). Variations in water table depth are particularly pronounced near the boundary between the acrotelm and catotelm layers, where shifts in peat saturation can significantly affect peat properties and C dynamics (Wilson et al., 2016).

In this study, we investigated changes in bulk peat over the five-year period of warming and eCO_2 at SPRUCE. We quantified changes in C content (%C), nitrogen content (%N), bulk density, stable and radioactive C isotopes, and overall C stock to assess how peat characteristics and C stock have been affected by these experimental treatments. We expected one of two outcomes: 1) an increase in peat C stocks from 2012 to 2020, or 2) a decrease in peat C stocks

over the same period (Fig 3.2). An increase in C stock is expected if enhanced C deposition, driven by increased plant productivity, results in the preferential loss of newer, more labile surface material. This preferential use of newer additions to fuel C flux from the system could lead to the preservation of older and more stable organic matter accumulation under warming and eCO2 conditions (Fig 3.2 Outcome 1). A decrease in peat C stock would result from warming-induced aerobic conditions that accelerate both the decomposition of previously stabilized peat C and modern C inputs (Fig 3.2 Outcome 2). Additionally, we hypothesized that treatment effects would be most pronounced at intermediate depths around the acrotelm/catotelm boundary, where the water table is most dynamic and can expose stable anaerobic catotelm peat to an aerobic decomposition environment (Fig 3.2 Additional Hypothesis).

3.3. Methods

3.3.1. Study Site

The SPRUCE experiment takes place in the S1 Bog at the Marcell Experimental Forest in northern Minnesota (Lat. 47.503, Long. -93.483) (Kolka, 2011). S1 Bog spans 8.1 hectares and features a raised dome, ombrotrophic bog dominated by black spruce (Picea mariana) and Sphagnum mosses. It is weakly ombrotrophic with a perched water table and minimal regional groundwater influence. The bog's surface exhibits typical northern peatland hummock and hollow microtopography, with peat depths ranging from 2 to 3 meters in the central area, where peat accumulation began around 11,000 years ago (McFarlane et al., 2018). The perched water table separates the aerobic shallow peat (acrotelm) from the anaerobic deep peat (catotelm). This boundary usually lies 0–30 cm below the hollow surface but can drop to 140 cm below during historical dry periods (Sebestyen et al., 2011; Tfaily et al., 2014).

3.3.2. SPRUCE Experimental Treatments

Whole-ecosystem warming was accomplished by installing top open 12.8-m diameter × 7-m tall enclosures enabling both air and soil warming for a range of treatment levels: +0°C, +2.25°C, +4.5°C, +6.75°C, and +9°C. Belowground warming began in June 2015 and was achieved using an array of 67 low wattage 3 m long resistance heaters positioned throughout the plot and enclosed in coated pipes (P. J. Hanson et al., 2017). Whole ecosystem warming began August 2015 and was accomplished with propane furnaces that generated warm air from recirculated air drawn from within the enclosure. Each warming treatment was conducted at both ambient (approx. 400 ppm) and elevated CO_2 (800–900 ppm). The source of the additional CO_2 for enrichment is pure CO_2 from a commercial facility with radiocarbon dead (-999 ‰ $\Delta^{14}CO_2$) and depleted $\delta^{13}CO_2$ signature. Initiation of eCO_2 treatments was in July 2016. Warming treatments were run continuously, while eCO_2 treatments were restricted to the growing season and day light hours. Two plots without enclosures (Plots 7 and 21) were also fully instrumented and evaluated as "ambient control" reference plots, without enclosures, to allow assessment of the influence of the enclosures themselves.

3.3.3. Environmental Measurements

Aboveground vertical profile of air temperature was measured at +0.5, +1, +2, and +4 m at half-hour intervals (P. Hanson et al., 2016), and for this analysis the measurements at 1m above the peat were used to describe average annual air temperature within the experimental plots. Automated water table depth data was collected for 12 SPRUCE plots (4, 6, 7, 8, 10, 11, 13, 14, 16, 17, 19, 20, and 21) beginning during DPH in 2015 and continuing throughout the WEW manipulations for the SPRUCE Project (P. J. Hanson et al., 2017). Other data on surface moisture, radiation levels, and enclosure CO_2 concentrations were also recorded at half-hour intervals and are available from archived data sets (Hanson, Riggs, et al., 2016).

Changes in bog surface associated with peat mass and C losses from warming have been evaluated (P. Hanson et al., 2018) with a modified version of the Cahoon et al. (2002) surface elevation table instrument and a full description can be found in Hanson et al., 2020. Renamed the SPRUCE Elevation Transect instrument (SET) for SPRUCE purposes, these instruments were deployed two per plot to measure changes in bog surface elevation in mm every year. The SET instrument is bolted to a permanent platform on the day of measurement. Fiberglass rods are fitted into the SET transect arm and allowed to fall under their own mass. These rods are sometimes assisted in reaching the peat surface by tweaking the bypass shrub branches or large vegetation obstacles, but they are never pushed into the bog surface. Once the rods are settled on the surface, the length of the rod remaining above the SET transect arm is measured to the nearest mm. Realistically, there is a random variable associated with how the rods situate themselves once on the bog surface, and the accuracy of this measurement is therefore limited to ± 5mm.

Elevation changes over time may have impacted sampling depths between 2012 and 2020. In order to overcome this, depths have been binned into depth intervals that allow us to see changes in stock and characteristics across the surface acrotelm, middle average water table interface depth, and deep catotelm peat. These bins are as follows; surface (0–40cm), middle (40–60cm), and deep (60–100cm). Each variable measured for this analysis has been treated in this manner to allow for better comparison between the two years; even with the elevation change seen between 2012 and 2020 we are still capturing the differences between these expanded depth increments. The body of measurements being made by the project is available for use by project scientists and participants and can be found on the SPRUCE website (https://mnspruce.ornl.gov).

3.3.4. Peat Properties and Characteristics

In August 2012 (Iversen, 2014) and August 2020 (J. Phillips et al., 2022), SPRUCE researchers and collaborators participated in core sampling of peat from the experimental plots. The sampling and analytical methods were similar between the collection timepoints (following Iversen, 2014), with one key difference: the original 0-10 cm depth increment sampled from 2012 for hollows was divided into two separate increments, 0-5 cm and 5-10 cm in 2020 and 2021. This change allowed for a more detailed examination of the shallow peat layer (0-5 cm, representing mostly live Sphagnum tissues) and the upper layer of decomposing peat (5-10 cm). For the purpose of this study, this new depth separation facilitated a more precise spatial and temporal assessment of physical changes and the incorporation of new ^{13}C and ^{14}C isotopic signatures related to the SPRUCE eCO_2 treatments (P. J. Hanson et al., 2017). Pre- and post-treatment cores were collected from 10 experimental plots (Plots 4, 6, 8, 10, 11, 13, 16, 17, 19, and 20) and two ambient plots (Plots 7 and 21). Sampling was carried out from hollow surfaces (referenced at 0 cm) down to a depth of 200 cm in specific increments, and the coring locations within each plot were mapped (Iversen, 2014; J. Phillips et al., 2022).

Data included in this analysis includes %C, %N, bulk density, C/N ratio, ^{14}C, and ^{13}C, and are available from archived datasets on the SPRUCE website as well as related publications (Iversen, 2014; J. Phillips et al., 2022). Concentrations of C and N as % (g C/g dry peat *100; g N/g dry peat *100) were analyzed on 0.1g samples of oven dried finely ground peat on a LECO TruSpec elemental analyzer (LECO Corporation, St. Joseph, MI). Peat bulk density was calculated by dividing the peat sample dry mass by the peat sample volume. The C/N ratio was calculated by dividing the peat C by the peat N. The isotopic ratios of $^{13}C/^{12}C$, expressed as $\delta^{13}C$ (‰), were measured on the GVI Optima Stable Isotope Ratio Mass Spectrometer at the University of California Davis Department of Geological Sciences Stable Isotope Laboratory.

Radiocarbon values, expressed as $\Delta^{14}C$ (‰), were measured on the Van de Graaff FN accelerator mass spectrometer or the NEC 1 MV Pelletron Tandem Accelerator at the Center for Accelerator Mass Spectrometry at Lawrence Livermore National Laboratory (Broek et al., 2021; Stuiver & Polach, 1977). Radiocarbon values were corrected for mass dependent fractionation using measured delta ^{13}C values and for ^{14}C decay since 1950. Missing values of these variables (%C, %N, bulk density, C/N ratio, ^{14}C, and ^{13}C) were filled in with weighted means using above and below depth measurements.

3.3.5. End Member Mixing Model

The fraction of new tissue peat C that was derived from plant biomass input during the experimental period was calculated using a simple end member mixing model for each isotope (^{13}C and ^{14}C) measured in bulk peat and plant tissue.

$$F = \left[\frac{(\sigma_{2020} - \sigma_{2012})}{(\sigma_{tissue} - \sigma_{2012})}\right]$$

Where F is the absolute portion of C from new addition of plant material to the peat, σ_{2020} is the ^{13}C or ^{14}C value of the 2020 bulk peat, σ_{2012} is the ^{13}C or ^{14}C value of the 2012 bulk peat, and σ_{tissue} is the ^{13}C or ^{14}C value of the plant tissues at the surface. The average tissue value was used as it was considered the most representative average of the plant tissue incorporated into the peat as litter from all species. These average tissue values were -44.65 ‰ for $\delta^{13}C$ and -407.38 ‰ for $\Delta^{14}C$.

3.3.6. ^{13}C-NMR Spectroscopy and Mixing Model

Solid State ^{13}C NMR spectra of untreated peat samples were obtained at the Environmental Molecular Science Laboratory at the Pacific Northwest National Laboratory in

Richland, Washington using cross-polarization under magic angle spinning conditions (CP/MAS) with a Varian Direct Drive NMR spectrometer equipped with a Varian 4-mm probe. Approximately 30 mg of peat were packed in 4 mm zirconia rotors sealed with Kel-F caps. The CP spectra were acquired after 14k scans with a MAS rate of 14 kHz resulting in no interference from sidebands as they were outside the range of the spectrum, and a ramp-CP contact time on proton of 1 ms and a 1 or 2 s recycle delay depending on the sample with 62.5 kHz tppm proton decoupling (Aliev, 2020). The one-dimensional 1H NMR spectra of all samples were processed and analyzed relative to the external standard adamantine. All spectra were corrected against a KBr background, and signals arising from C in the NMR probe and rotor were accounted for by subtracting the spectra of an empty rotor from the sample. Spectra were digitally processed with exponential apodization (100 Hz line broadening with the first point set to 0.50), phase correction, and baseline correction using a Bernstein polynomial fit with Mnova software (v. 14.3.3; Mestrelab Research). Peak areas were integrated within seven chemical shift regions for input to the molecular mixing model corresponding to: alkyl C (0–45 ppm), N-alkyl/methoxyl C (45–60 ppm), O-alkyl C (60–95 ppm), di-O-alkyl (95–110), aromatic C (110–145 ppm), phenolic C (145–165 ppm), and carboxyl C (165–215 ppm).

We used a mixing model which incorporates six components to describe the molecular composition of samples based on ^{13}C NMR outputs (Baldock et al., 2004). This peatland soil has previously been analyzed for pyrogenic C, and therefore was processed with char included in the mixing model (Ofiti et al., 2022). The five remaining components (carbohydrate, protein, lipid, lignin, and carbonyl) have each been assigned a discrete percent of different regions of the ^{13}C NMR signal intensity based on knowledge of molar elemental contents and C content of terrestrial soil ecosystems. The measured C:N ratio of each sample was used to constrain the

protein concentration of each ^{13}C NMR spectrum in the molecular mixing model. The optimization process of the molecular mixing model compares fits for all five biomolecules to models eliminating one, two, and three components; in all cases the model fit was best when all five components were included in the model (sum of squares of deviation < 6%). The mixing model results can be found in Appendix Table 3.1.

3.3.7. Statistics

This dataset required non-parametric testing to compare differences between 2012 and 2020. The Kruskal-Wallis test was used to explore changes in peat C stock and content, as well as characteristics over time; i.e. between 2012 and 2020. Effect size was calculated as $(X^2\text{-}1)/(n\text{-}2)$, where X^2 is the Kruskal-Wallis test result and n is the number of samples included in each comparison.

Three regression models were built to assess possible effects of temperature, eCO_2, and depth interval on the calculated difference in soil C stock (stock difference = [stock 2020 - stock 2012]), $D^{14}C$ values measured in 2020, and ^{13}C values measured in 2020. The relationship between differences in soil C stock and temperature was determined to be a 3rd degree polynomial relationship, and experimental plot was treated as a random factor. The results from these regressions can be found in Appendix Table 3.2, 3.3, and 3.4.

Linear regression was used to evaluate several relationships: the association between mean annual temperature and water table depth in relation to mean hollow height (both across all experimental plots and at the peatland level); the correlation between temperature and the percentage of new tissue-derived carbon incorporated into bulk peat over time; and the relationship between relative peat elevation and time (2015-2020) for each temperature treatment.

All relationships explored were considered significant at the 0.05 alpha level. All statistics were executed in R v.4.2.2 (The R Foundation for Statistical Computing, 2022). Reported means in the text are shown with standard errors in parentheses.

3.4. Results

3.4.1. Environmental Measurements

Mean annual temperature (MAT) measured at +1m above the peat surface reached target differentials by 2015 (Fig 3.3). Subsurface heating started in 2014, and temperature measurements at depths of 10, 30, and 100 cm showed consistent differentials across treatments. However, the temperature differences were most significant below 30 cm and diminished closer to the peat surface, likely due to heat loss (Appendix Fig 3.1). This heat loss also contributed to increased variability in temperature measurements at shallower depths.

From 2012 To 2020, the water table depth relative to the mean hollow height decreased significantly across the peatland (R^2=0.1, F=1.541, df=14602, $p<0.001$; Fig. 3.4) This trend was evident in all experimental plots, though the decrease was more pronounced in plots with higher temperatures compared to the unwarmed plots, suggesting an effect of the temperature treatments (Fig. 3.4, Appendix Fig. 3.2).

During the five-year warming period, higher temperature treatments showed a decrease in peat elevation over time, with the most significant declines observed at +6.75 °C and +9 °C above ambient levels. Elevated CO_2 treatments introduce additional variability, sometimes reducing the loss of peat elevation in high-temperature conditions. Overall, this suggest that warming temperatures, especially extreme increases, can destabilize peatland elevation, potentially impacting carbon storage in these ecosystems (Fig. 3.5). Significant changes were observed in four of the six treatments, including one control plot, the +4.5°C ambient CO_2 treatment, and both the elevated CO_2 and ambient CO_2 +9°C plots ($p<0.05$; Appendix Fig 3.3).

3.4.2. Peat Carbon Stock and Characteristics

From 2012 to 2020, we observed an overall increase in total C stock in plots to a depth of 200 cm (Fig 3.6A). In 2012, the median C stock for shallow, middle, and deep peat layers was 1.87, 5.64, and 7.24 gC per depth increment, respectively. By 2020, these values had changed to 1.45, 6.42, and 8.62 gC per depth increment. This increase at the plot level was primarily due to a significant rise in C stock within the deep peat layer (100–200 cm) over time (Kruskal-Wallis X^2=11.172, $p < 0.05$; Fig 3.6B; Table 3.1). This increase in deep peat C stock was not driven by changes in bulk density or related to changes in ash content down the profile (Appendix Figure 3.4).

In contrast, C stocks in the shallow (0–40 cm; Kruskal-Wallis X^2=2.083, p =0.149; Fig 3.6B; Table 3.1) and middle (40–100 cm; Kruskal-Wallis X^2=3.797, p = 0.051; Fig 3.6B; Table 3.1) depth intervals did not show significant changes over time. Despite the notable increase in deep peat C stocks, this change was not affected by warming or eCO_2. When examining the differences in C stock from 2012 to 2020, the effects of depth increment, temperature, CO_2 treatment, and their interactions were not statistically significant (Appendix Table 3.2).

To further examine changes in %C, %N, bulk density, and C:N ratio between 2012 and 2020 peat, we combined the experimental treatments, as there was no treatment effect on changes in C stock (Fig. 3.6, Appendix Table 3.2). Peat %C in the shallow and middle depth increments remained consistent from 2012 to 2020. However, %C in the deep peat (100–200 cm) increased significantly during this period (Kruskal-Wallis X^2=20.278, $p<0.05$; Fig. 3.7A and Appendix Table 3.1). The %N increased with depth in both sampling years, with greater variability observed in the middle and deep layers in 2020 (Fig. 3.7B). All depth increments showed a rise in %N from 2012 to 2020 ($p<0.05$; Appendix Table 3.1). The C:N ratio and its variability decreased with depth in both sampling years (Fig. 3.7C). From 2012 to 2020, the C:N

ratio in the shallow depth increment dropped from 41 ± 10 to 37 ± 6, while in the middle depth increment, it rose from 25 ± 5 to 27 ± 6 ($p<0.05$; Fig. 3.7C and Appendix Table 3.1). Bulk density increased in the middle depth layer ($p < 0.05$), while the other layers remained unchanged between the sampling years (Fig. 3.7D and Appendix Table 3.1).

Radiocarbon profiles from all plots show similar trends in bulk peat from 2012, before treatments began (Fig. 3.8A), and from 2020, after five years of exposure to elevated temperature and CO_2 (Fig. 3.8B). The data suggest some influence of the CO_2 treatment on radiocarbon values of surface peat in the eCO_2 plots (Fig. 3.8B). However, the overall treatment effects were only moderately significant, with radiocarbon values for the peat layers remaining similar between 2012 and 2020. Depth had a notable effect on peat ^{14}C ($p < 0.01$; Appendix Table 3.3), reflecting peat formation processes, where older material is buried beneath younger more recent deposits.

Stable isotope results showed minimal variation between the sampling years and significant effects of CO_2 treatment ($p<0.05$; Fig. 3.9 and Appendix Table 3.4). Ambient plots displayed remarkable consistency over the five years, underscoring the stability of this isotope. However, analysis of the surface peat revealed a marked depletion of $\delta^{13}C$ within the top 30 cm in response to eCO_2. This isotopic shift was not associated with temperature treatments and likely reflects the incorporation of newly deposited plant material with a lower $\delta^{13}C$ signature compared to the existing peat.

3.4.3. Estimation of the incorporation of labelled C into peat

Evidence of new tissue incorporation was observed in both surface and deep peat layers (Fig. 3.10). The highest percentages of new tissue were found in the surface layers of the +9, +0, +4.5, and +6.75°C temperature treatments, with values of 26.4%, 24.7%, 24.1%, and 13.8%, respectively. In the deep peat layers, the +9°C and +6.75°C treatments showed notable new

tissue incorporation, with rates of 8.3% and 6.1%, respectively. Despite these variations, there was no statistically significant trend related to temperature or depth in new tissue incorporation. No significant trend was found between new C incorporation and temperature ($r^2<0.01$, F=0.0614, p=0.805, df=45; Appendix Fig. 3.5). The fraction of new litter-derived carbon varied with depth, with a greater percentage of new litter tissue incorporated into the surface peat (Fig 3.10).

3.4.4. ^{13}C-NMR Spectroscopy and Mixing Model

To assess the effects of warming on peat C chemistry, we compared the concentrations of molecular compounds measured in the 2020 peat samples with estimates from 2012. This comparison showed little to moderate changes across most molecular compounds, with the exception of carbohydrates and lipids in the middle depth increment. In both the warmed and +0°C plots, carbohydrates and lipids exhibited similar patterns of increase and decrease, respectively. At SPRUCE, bulk peat is predominantly composed of carbohydrates (22.8–50.5%) and lignin (25.8–35.6%), which remain the most dominant compounds measured by ^{13}C-NMR, regardless of the measurement year (Fig. 3.11). Carbohydrates decrease with depth, while lignin remained relatively constant throughout the peat profile. There is a general trend of increasing lipid, char, and protein content with depth. No clear pattern emerged linking changes in molecular compounds or aromatic index to temperature treatments (Appendix Fig 3.6).

3.5. Discussion

3.5.1. Deep Peat Carbon Remains Stable after 5 Years of Warming

This analysis revealed an increase in peat C stocks from 2012 to 2020, regardless of warming or eCO_2 treatments. Previous research at SPRUCE has indicated that warming has shifted this peatland from being a net C sink to a net C source, leading to significant net C loss at the ecosystem level (Hanson et al. 2020). This transition is attributed to increased deposition of

new surface material under warmer temperatures and eCO_2, as well as direct C release from the surface layers of peat, either as gas or dissolved C (Wilson et al. 2021b). Additionally, observed C losses have been linked to the downward movement of residual C, driven by vertical transport, compaction, and reduced pore space (Wilson et al. 2021a; Ofiti et al. 2022).

Our findings align with these earlier results, showing that the increase in C stocks we observed primarily stems from the deep peat layers. Despite surface losses, the persistent waterlogged conditions in the deep peat layers support ongoing C storage and incorporation.

Previous radiocarbon analyses have suggested that most C flux originates from recent surface inputs, significantly contributing to observed C losses, with some influence from older, previously deposited C (Wilson, Griffiths, et al., 2021). Warming accelerates the decomposition of readily degradable compounds, such as carbohydrates, which are less abundant in the warmed plots compared to the +0°C treatments (Fig. 3.11). While some newly added C may survive decomposition and move to intermediate layers (Fig. 3.10), we propose that the increase in deep peat C is primarily driven by the export of material from these shallow and intermediate layers. This process enhances deep peat C stocks, ultimately resulting from increased plant productivity and sustained vertical transport due to the continued saturation of the middle and deep peat.

3.5.2. Deep Incorporation of New Tissue and Chemical Transformation in Bulk Peat

Our findings indicate that the impacts of experimental warming and eCO_2 on peat C are relatively small, aligning with previous research that also found no significant trend in the contribution of experimentally derived plant C to bulk organic matter across the SPRUCE experiment (Ofiti et al., 2022). This stability may stem from the competing effects of warming and eCO_2, both of which increase the incorporation of new organic matter while also accelerating its degradation. These processes can counterbalance each other, resulting in no significant net

change in bulk organic matter, despite shifts in individual components like n-alkanes and long-chain n-fatty acids (Ofiti et al. 2022).

For all temperature treatments, the incorporation of new tissue was most pronounced in the surface layers of the peat profile; however, we also observed increased new tissue incorporation in deeper peat layers with warming. This suggests that new C is entering the system and being transported downward, supporting our conceptual model (Fig. 3.12) and highlighting the significant loss of new C at the surface, where 75% of the remaining peat is derived from old tissue.

After five years of warming, we found no differences in peat chemistry between the control and +9°C treatments. This stability may be attributed to several factors, including the gradual nature of peatland processes such as decay and accumulation (Clymo et al. 1998). Global long-term projections of peatland responses to climate change indicate a lag in the long-term effects of environmental shifts on these ecosystems (Müller and Joos 2021). Additionally, the inherent stability of peat chemistry, characterized by low nutrient availability and a high degree of decomposition resistance, may play a critical role. Depth-specific effects could also influence this stability, as different layers may respond variably to external stimuli. Peat chemistry is generally stable and resistant to short-term fluctuations, particularly concerning fundamental properties like nutrient content, organic matter composition, and decomposition products, which remain relatively constant even under varying climatic conditions (Freeman et al. 2001). This stability may result from the slow rate at which chemical changes manifest within the peat column over time.

Changes in peat characteristics, such as %C, %N, bulk density, C/N ratio, and isotopic ratios (^{14}C and ^{13}C), often require prolonged environmental shifts to become detectable. A

previous SPRUCE experiment indicated that the relative amounts of labile and recalcitrant chemical compounds in peat did not significantly change after four years of whole-ecosystem warming and five years of deep peat heating (Baysinger et al. 2022). This supports our finding that C stores remain largely stable, despite evidence of net C losses in other studies (Hopple et al. 2020; Hanson et al. 2020; Wilson et al. 2021a). Changes in peat chemistry may be occurring at a finer depth or chemical resolution, in either deeper or shallower layers, or in unmeasured aspects of peat chemistry (Ofiti et al. 2022; Serk et al. 2022). Finally, there may be a threshold of warming intensity or duration beyond which significant changes in bulk peat chemistry become detectable.

3.5.3. Implications

The increased C in deep peat, despite surface elevation loss, highlights the complex dynamics of C within peatlands throughout the SPRUCE experiment. While our findings align with the anticipated accumulation of C in deep peat, we did not identify a significant relationship between experimental treatments and the measured peat characteristics, suggesting that C dynamics are more intricate than initially expected. This emphasizes the need to consider both short-term and long-term processes, including environmental changes and the balance between C sequestration and emissions.

The rise in deep peat C stocks, despite stable bulk chemistry, indicates that enhanced decomposition rates are being counterbalanced by increased C accumulation in deeper layers. Factors such as greater plant growth, elevated rates of C transport, and sustained waterlogged conditions likely contribute to this trend (Fig. 3.12). Elevated plant productivity boosts the incorporation of new tissue and the abundance of bioavailable compounds in the surface layers (Fig. 10), resulting in higher decomposition rates and significant C emissions. Concurrently, C from shallower layers may be mobilized downward, contributing to gains in deep peat while

depleting the upper layers. Modern organic material is transported to deep peat more rapidly than it decomposes in shallower layers, with older C compounds moving downward through peat water or compaction.

Deep peat layers show less sensitivity to warming and eCO_2 than shallower layers and are less impacted by changes in surface conditions. Traditionally, the boundary between the acrotelm and catotelm has been used to differentiate between aerobic and anaerobic environments and their respective decomposition rates. However, the transition between middle and deep peat layers may be crucial for C cycling, marking the shift from relatively active upper layers to the more stable dynamics found beyond 100 cm below the surface. This zone experiences increased fluctuations in the water table, where oscillating conditions could enhance C loss.

The stability observed in bulk peat chemistry over five years suggests that, while surface and intermediate layers show signs of C loss, the bulk characteristics of all layers and deep peat C stocks remain largely unchanged. This resilience in deep C and peat chemical properties underscores the complexity of peatland C dynamics and indicates that deep peat may possess an inherent capacity to withstand environmental changes.

3.6. Conclusions

Our investigation into peatland C dynamics at the SPRUCE site over five years of warming and elevated CO_2 provides valuable insights applicable to global peatlands. While we observed no significant changes in bulk peat chemistry, the increase in C stocks within deep peat layers underscores the complexity of peatland C sequestration and emissions. This study highlights the critical balance between C sequestration and decomposition, illustrating the resilience of deep peat C.

Enhanced plant productivity and the vertical transport of organic matter to deeper layers, coupled with sustained waterlogged conditions, contribute to ongoing C accumulation in deep

peat. In conjunction with previous findings from this site, which indicate C loss due to treatment, our results suggest that this loss primarily occurs in surface layers, where warming accelerates decomposition and C emissions, while deeper peat layers continue to sequester C effectively.

The stability in bulk peat chemistry, despite significant changes in surface C fluxes and emissions, suggests that fundamental peat properties may be resilient to short-term (five-year) environmental changes. This implies that significant alterations in peat chemistry and C dynamics might require longer durations or more intense environmental stressors to become evident. These findings emphasize the importance of considering both short-term and long-term processes when assessing peatland C dynamics.

The resilience of deep peat to immediate warming and elevated CO_2 highlights the necessity for long-term studies to fully understand the interactions between C sequestration and emissions across various peatland types and climates. Given the critical role of peatlands in the global C cycle, understanding these complex dynamics is essential for predicting their responses to climate change and developing effective conservation and management strategies.

3.7. Figures

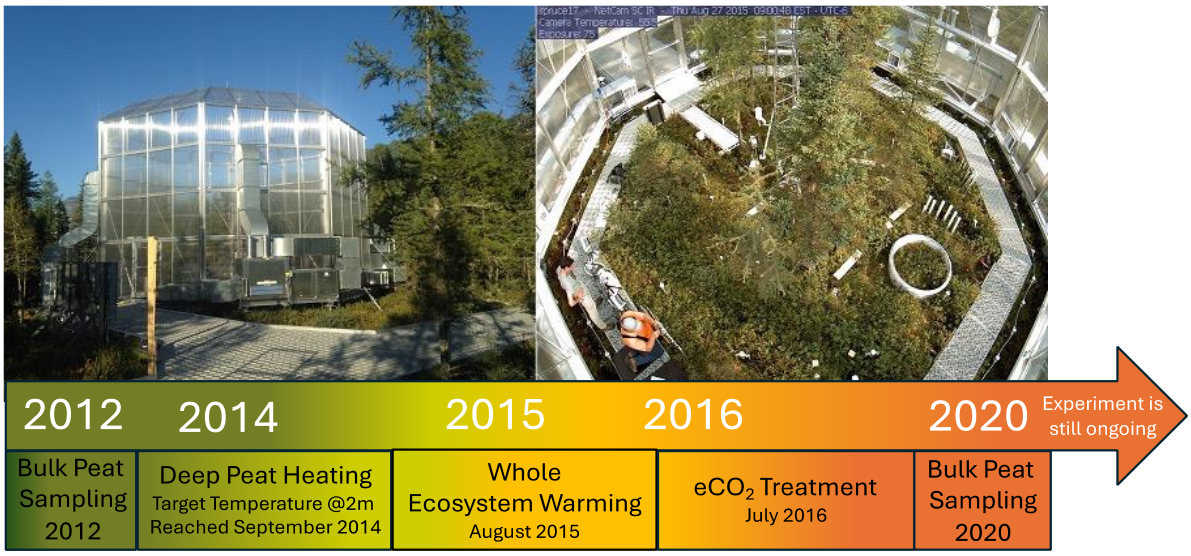

Figure 3.1 Experimental set up and timeline. A) Experimental chambers and supporting equipment of the SPRUCE site located in Minnesota. Along three boardwalks, chambers have been equipped with above and below ground heaters to achieve target temperatures. All warming treatments were held at either ambient CO_2 or elevated CO_2, the latter in the range of 800-900 ppm. B) Timeline of 2012 and 2020 sampling of bulk peat, as well as initiation of deep peat heating (DPH), whole ecosystem warming (WEW), and elevated CO_2 treatment. The initial sampling occurred following instalment of the experimental chambers, and the 2020 sampling occurred following 5 years of whole ecosystem warming.

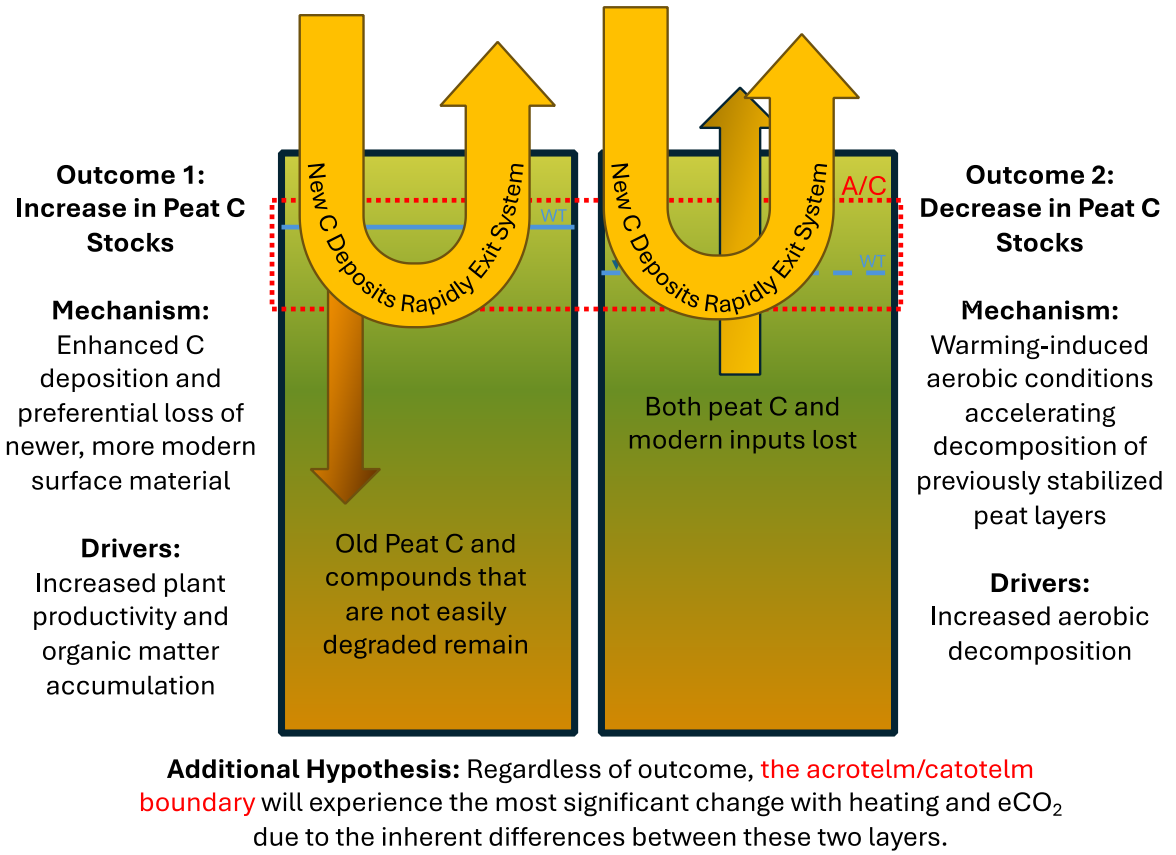

Figure 3.2 Conceptual diagram outlining the two potential outcomes of warming and elevated CO_2. Outcome 1: Increased C stock between 2012 and 2020 due to increased plant productivity and organic matter deposition that outpaces decomposition and contributed to peat C accumulation. Outcome 2: Decrease in C stock between 2012 and 2020 due to change in soil environment from anaerobic to predominantly aerobic, increasing the amount of C lost via microbial decomposition. The additional hypothesis is focused on the sensitivity of the acrotel/catotelm boundary which is denoted by a red box in both outcome 1 and 2. The peat profile is described by large rectangles with surface peat in light green at the top, middle peat in dark green, and deep peat in brown at the bottom. New C is represented in yellow and is depicted entering and exiting the peat profile as an arrow at the surface. Transport from the surface peat to the middle peat is denoted by a darker yellow arrow moving C from shallow to deeper peat layers, and deep peat C exiting the system is shown in a dark arrow moving from the deep layers to the surface. Size of arrow is a hypothetical estimation of relative amount of C within each of these fluxes.

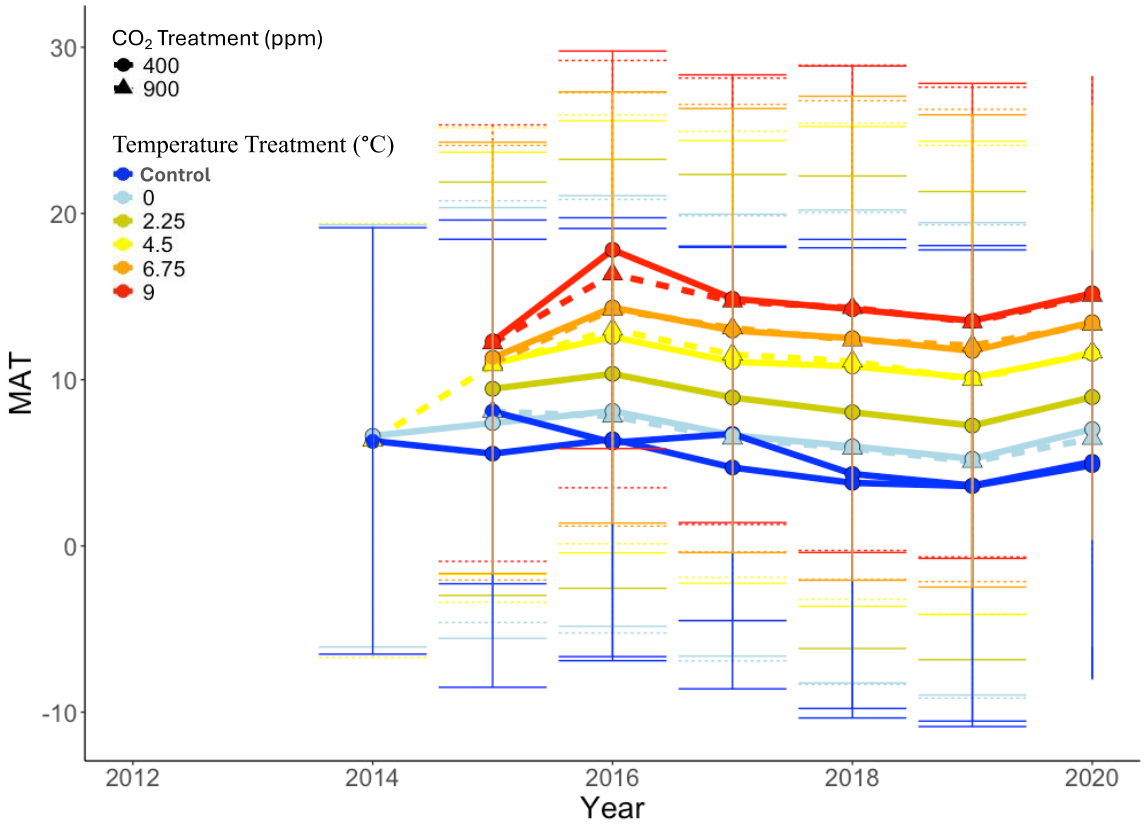

Figure 3.3 Mean annual temperatures within the experimental plots over time. Solid lines and circles denote plots with ambient CO_2 (400ppm) and triangles and dashed lines denote elevated CO_2 (900 ppm). Colors represent temperatures with blues being ambient and control (+0 °C), green +2.25°C, yellow +4.5 °C, orange +6.75°C, and red +9°C.

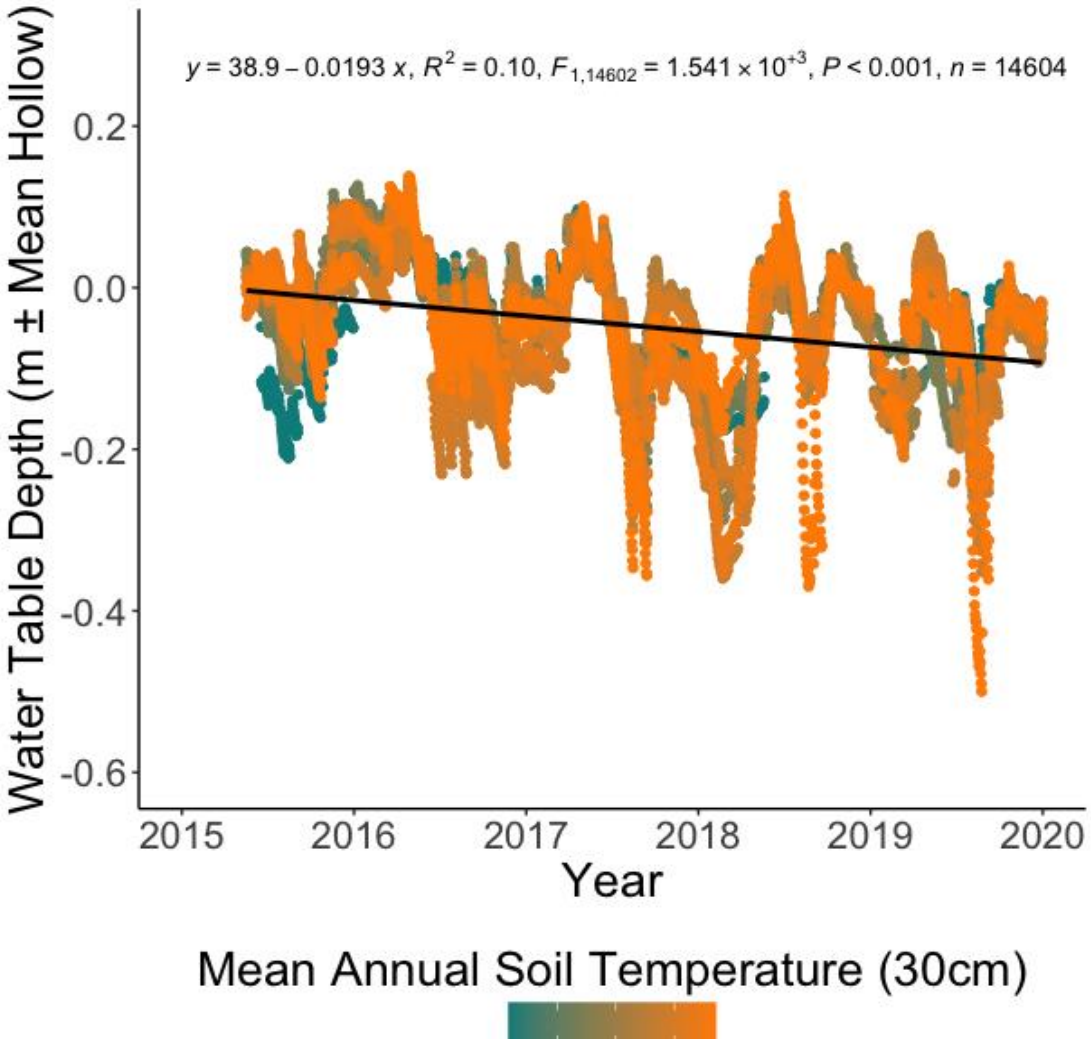

Figure 3.4 Water table depth over time. During the deep peat heating period water table depth was measured in 30 min measurement frequency and shows some trends associated with increased mean annual soil temperature, with blue coloring representing the cooler temperatures and orange representing the warmer temperatures. The overall drop in water table height over time was significant (R^2=0.1, F=1.541, df=14602, p<0.001)

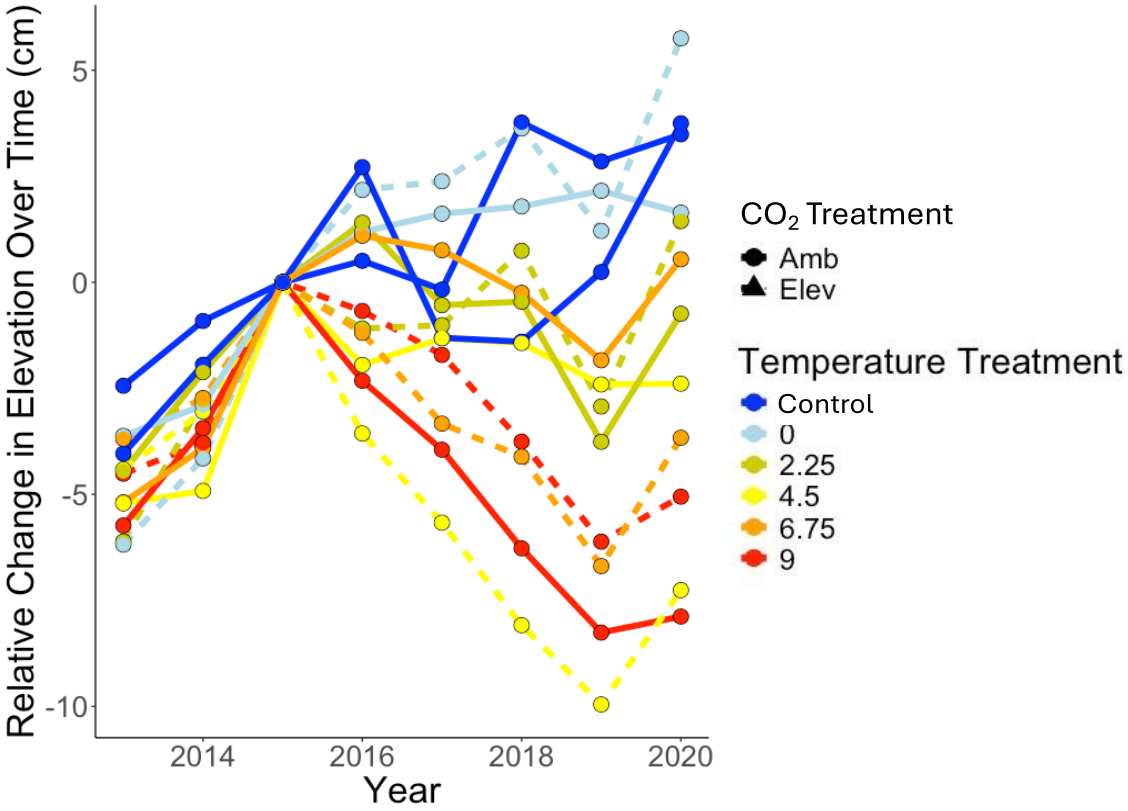

Figure 3.5 Relative difference in peat elevation compared to measurements taken in 2015 across the temperature treatments. Temperature is denoted by color with dark blue being open chamber control and light blue +0 °C, green +2.25°C, yellow +4.5 °C, orange +6.75°C, and red +9°C above ambient temperature. Elevated CO_2 treatments are shown by triangles and dashed lines, and ambient CO_2 plots are shown with circles and solid lines. Error bars represent standard deviations for averages from two SPRUCE Elevation Transect (SET) measurements of 9 peat heights taken from each plot every year (18 peat heights per plot per year).

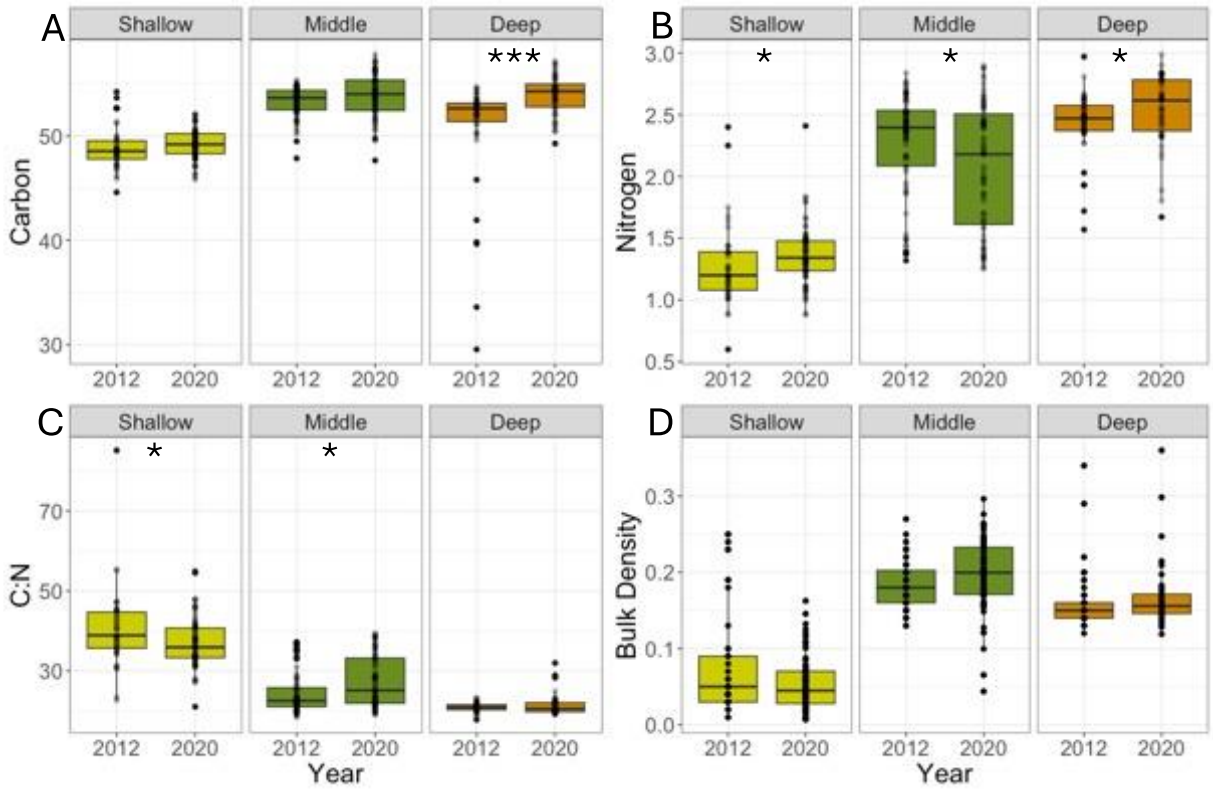

Figure 3.6 Comparison of peat soil characteristics between 2012 and 2020 for A) carbon B) nitrogen, C) C:N ratio, and D) bulk density for each depth increment, shallow (0-40cm), middle (40-100cm), and deep (100-200cm). These depths were pooled from all plots. Peat was sampled at the beginning of the SPRUCE experiment (2012) and after 5 years of whole ecosystem warming and elevated CO_2 (2020). Statistical results for this figure can be found in supplemental material Table S1. Significand codes: 0 '***' 0.001 '**' 0.01 '*' 0.1 ''.

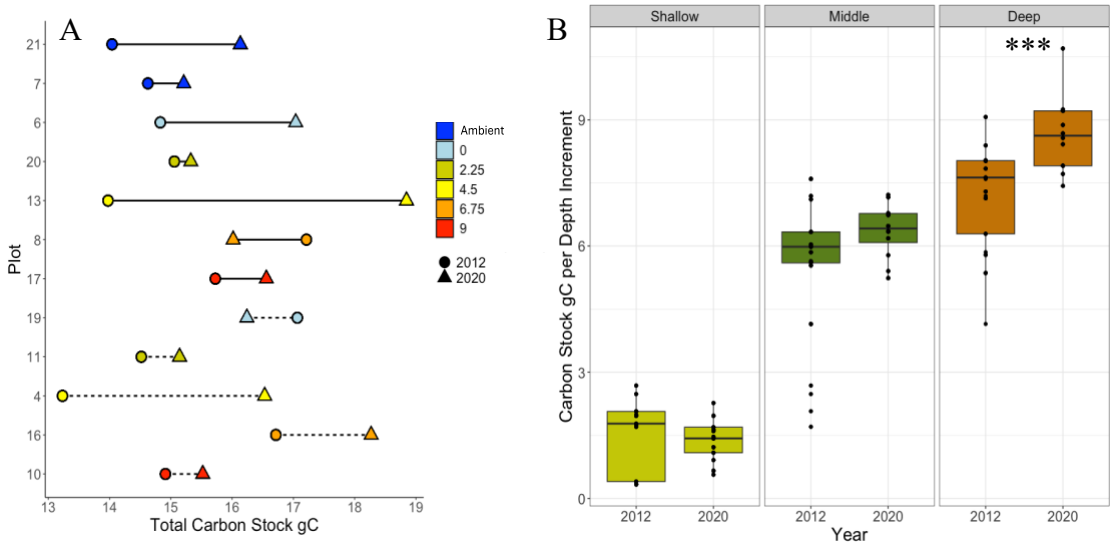

Figure 3.7 A) Change in total plot C stock between 2012 (circle) and 2020 (triangle). Colors represent temperatures with open control chambers in dark blue, light blue +0 °C, green +2.25°C, yellow +4.5 °C, orange +6.75°C, and red +9°C, and CO_2 treatment described by line type, with dashed lines indicating elevated plots and solid lines indicating ambient plots. B) Comparison of carbon stock for each depth increment, shallow (0-40cm), middle (40-100cm), and deep (100-200cm). These depths were pooled from all plots. Peat was sampled at the beginning of the SPRUCE experiment (2012) and after 5 years of whole ecosystem warming and elevated CO_2 (2020). Statistical results for this figure can be found in Table 1. Significand codes: 0 '***' 0.001 '**' 0.01 '*' 0.1 ' '.

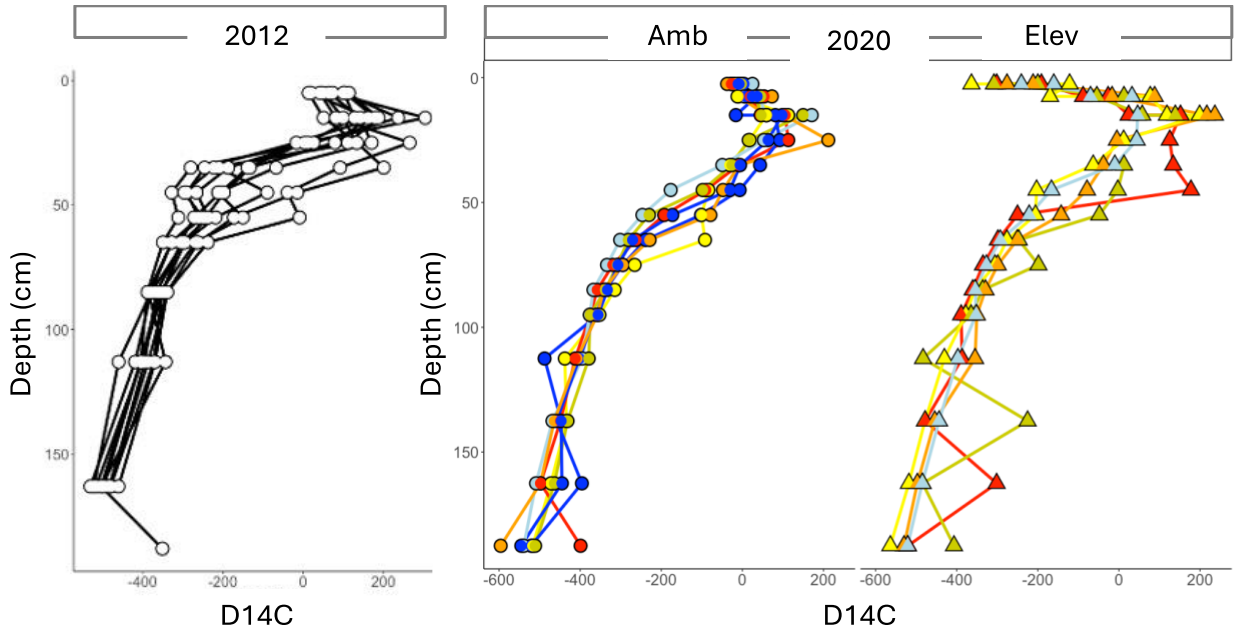

Figure 3.8 Bulk peat D ^{14}C composition of peat for A) all plots in 2012, B) ambient and elevated CO_2 plots in 2020. In A, the 2012 depth profiles are shown for all plots as white circles with solid black lines. The 2020 profiles are coloured by temperature treatment with open control chambers in dark blue, light blue +0 °C, green +2.25°C, yellow +4.5 °C, orange +6.75°C, and red +9°C. In b, CO_2 treatment described by point shape, with triangles indicating elevated plots and circles indicating ambient plots.

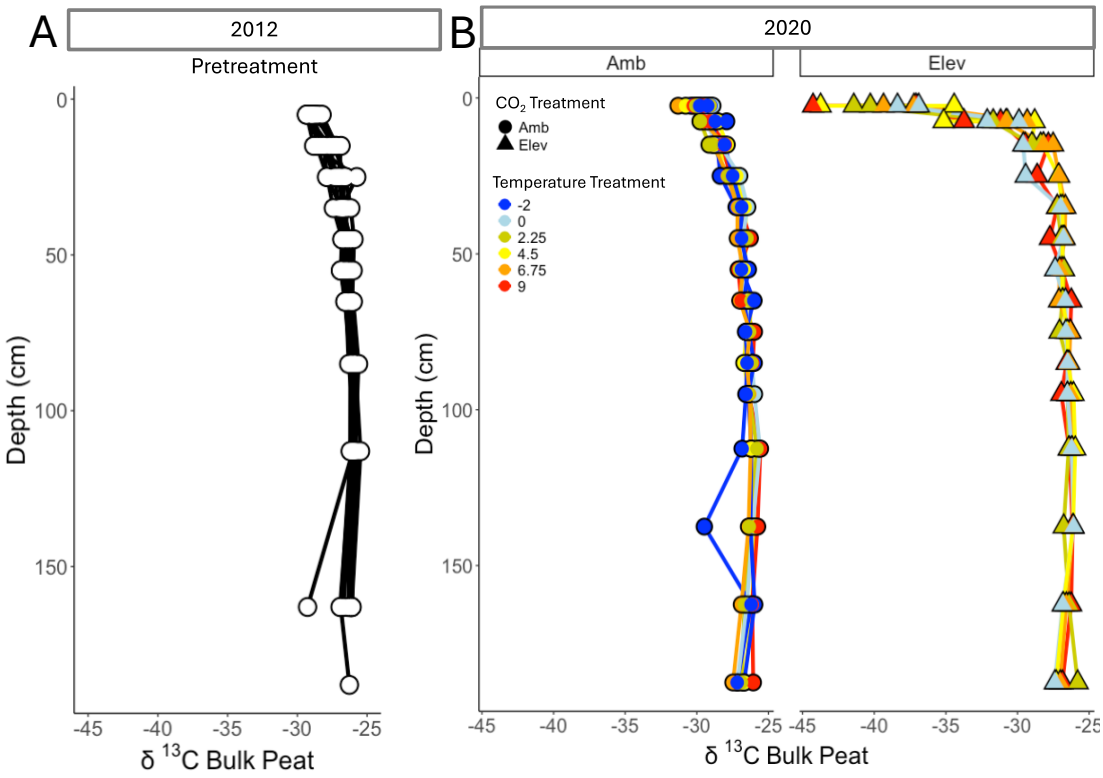

Figure 3.9 Bulk peat δ ^{13}C composition of peat for A) all plots in 2012, B) ambient and elevated CO_2 plots in 2020. In A, the 2012 depth profiles are shown for all plots as white circles with solid black lines. The 2020 profiles are coloured by temperature treatment with open control chambers in dark blue, light blue +0 °C, green +2.25°C, yellow +4.5 °C, orange +6.75°C, and red +9°C. In b, CO_2 treatment described by point shape, with triangles indicating elevated plots and circles indicating ambient plots.

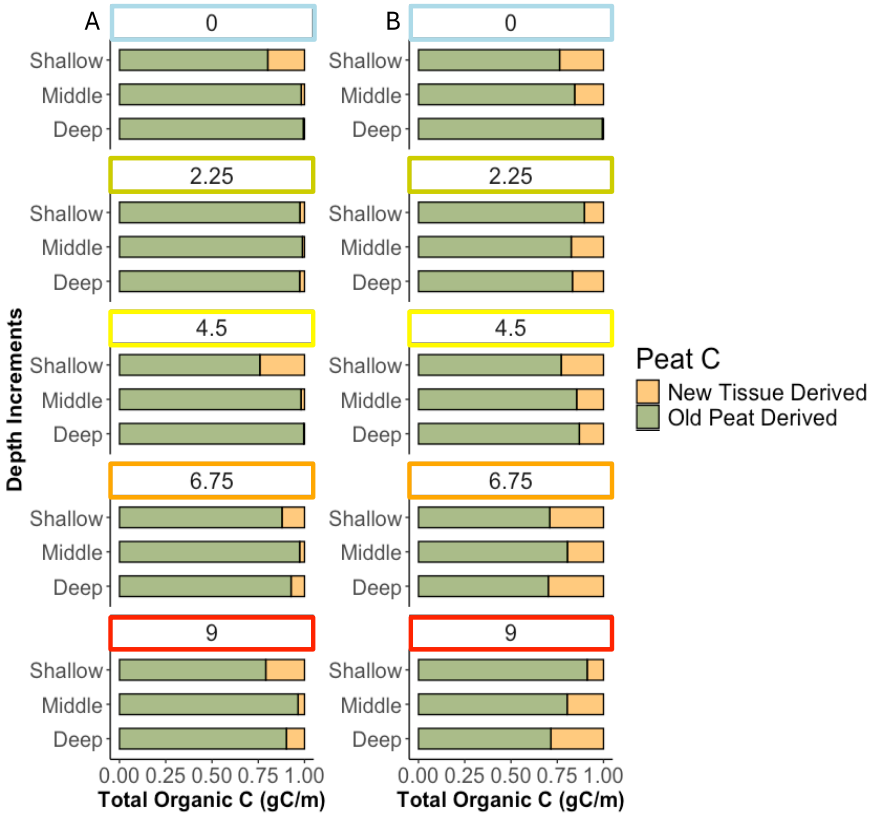

Figure 3.10 Peat carbon make up described by the end member mixing model using A) ^{13}C and B) ^{14}C. New tissue derived carbon content and older peat derived carbon content for the eCO_2 plots across the temperature treatment gradient. Colours represent temperatures with blues being ambient (dark blue) and control (light blue) +0 °C, green +2.25°C, yellow +4.5 °C, orange +6.75°C, and red +9°C. The proportion of older peat carbon is represented by green bars and the new tissue is represented by yellow bars.

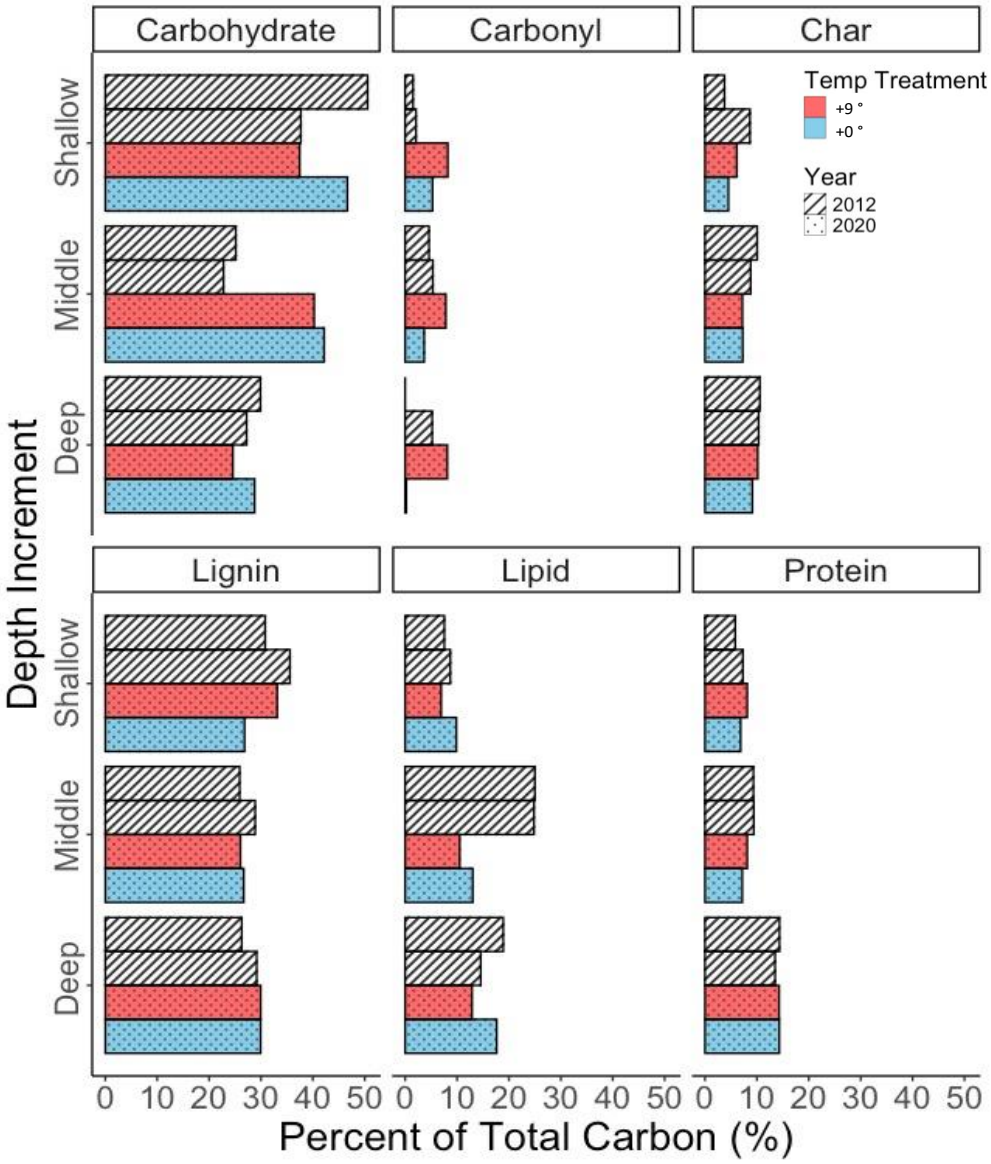

Figure 3.11 Proportion of total organic C attributed to each molecular component temperature and depth increments. Mixing model results showing change in the five molecular components described by the model. The bars represent average proportion of total organic C attributed to each molecular component. Colors indicate the temperature treatment with white representing 2012 ambient temperatures, red indicating +9°C above ambient and blue indicating +0° above ambient. Patterns of the bars denote year of sampling with diagonal lines denote 2012 and dots denote 2020.

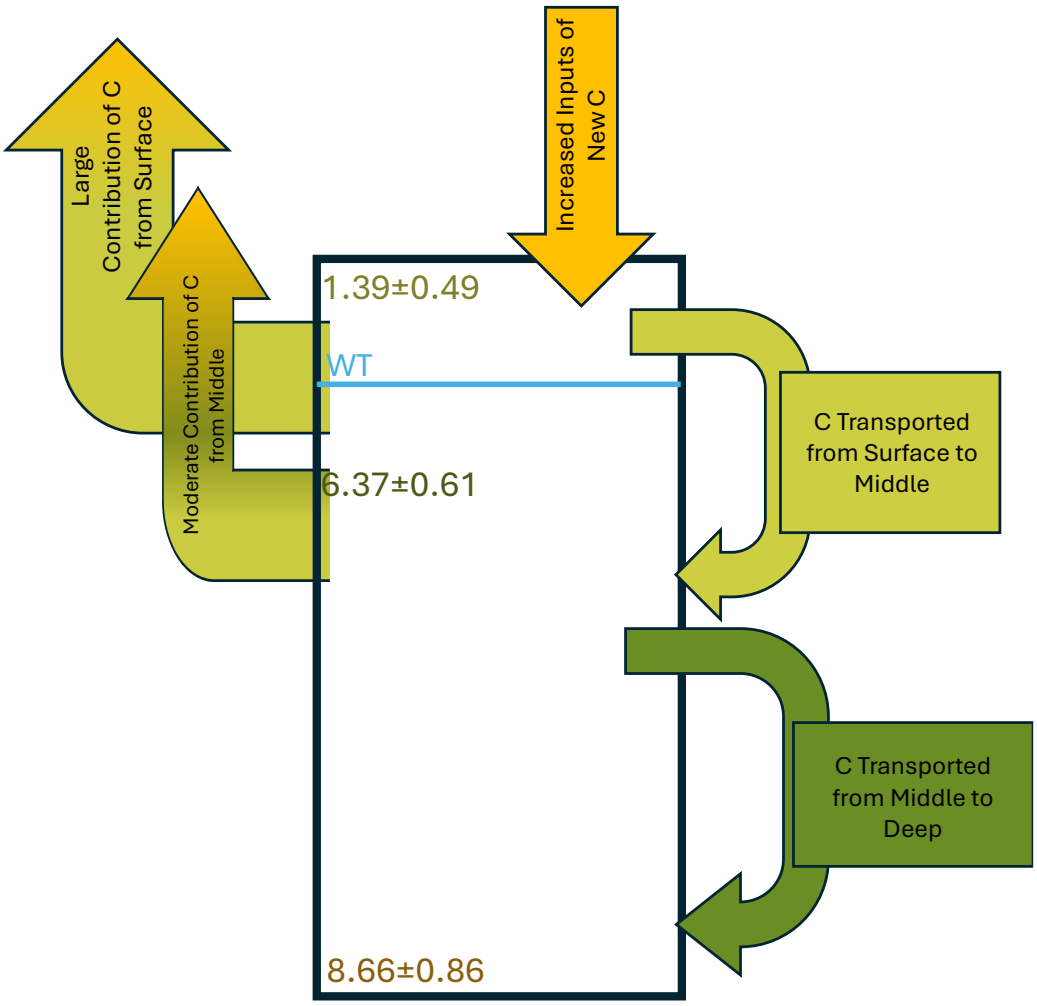

Figure 3.12 Conceptual model of potential C movement leading to an increase in deep peat C stocks at the SPRUCE peatland following 5 years of warming and elevated CO2 treatment. The peat profile is described by the large rectangle with surface peat in light green at the top, middle peat in dark green, and deep peat in brown at the bottom. Stocks measured for 2020 bulk peat are listed within each peat depth increment. New C is represented in yellow and is depicted entering the peat profile as an arrow at the surface. Transport from the surface peat to the middle peat is denoted by a light green arrow moving C from shallow to middle peat layers, and transport from middle to deep peat layers is shown by a dark green arrow. Export of C from the surface is shown by an arrow leaving the shallow peat gradient coloured with yellow and light green to represent the combination of C sources for these emissions and loss. Export of C from the middle peat is shown by an arrow leaving the mid profile layer and is gradient coloured with yellow, light green, and dark green to represent the combination of sources for this C loss. Size of arrow is a hypothetical estimation of relative amount of C within each of these fluxes.

3.8. Tables

Table 3-1 Results from Kruskal-Wallace test for carbon stock, carbon content, nitrogen content, C:N ratio, and bulk density. Comparisons are between years for each depth increment: Shallow (0-40cm), Middle (40-100cm), and Deep (100-200cm). Significand codes: 0 '***' 0.001 '**' 0.01 '*' 0.1 ''.

Variable	Year	Depth	n	Mean (sd)	Median	X2	p-value
Carbon Stock gC per Depth Increment	2012	Shallow	12	1.63 (0.82)	1.87	2.083	0.1489
	2020	Shallow	12	1.38 (0.51)	1.45		
	2012	Middle	17	5.17 (1.86)	5.64	3.797	0.0513
	2020	Middle	12	6.37 (0.63)	6.42		
	2012	Deep	16	6.94 (1.33)	7.24	11.172	0.0008***
	2020	Deep	12	8.66 (0.89)	8.62		
Carbon	2012	Shallow	45	48.9 (2.07)	48.50	4.074	0.0435
	2020	Shallow	83	49.3 (1.46)	49.20		
	2012	Middle	72	53.3 (1.46)	53.60	3.098	0.0784
	2020	Middle	72	53.8 (2.22)	54.00		
	2012	Deep	47	50.8 (5.29)	52.60	20.278	6.70E-06***
	2020	Deep	48	53.9 (1.85)	54.30		
Nitrogen	2012	Shallow	44	1.28 (0.331)	1.20	6.421	0.0113*
	2020	Shallow	83	1.36 (0.239)	1.30		
	2012	Middle	70	2.27 (0.419)	2.41	4.598	0.032*
	2020	Middle	72	2.08 (0.508)	2.18		
	2012	Deep	46	2.44 (0.243)	2.48	4.916	0.0266*
	2020	Deep	48	2.54 (0.288)	2.62		
C:N Ratio	2012	Shallow	45	40.5 (9.95)	38.90	5.244	0.022*
	2020	Shallow	83	37 (6.11)	35.90		
	2012	Middle	70	24.5 (5.20)	22.60	6.835	0.0089*
	2020	Middle	72	27.4 (6.46)	25.10		
	2012	Deep	45	20.9 (1.11)	21.00	0.064	0.7996
	2020	Deep	48	21.4 (21.4)	20.60		
Bulk Density	2012	Shallow	44	0.078(0.072)	0.05	1.287	0.2564
	2020	Shallow	87	0.053 (0.036)	0.04		
	2012	Middle	62	0.184 (0.033)	0.18	6.43	0.0112*
	2020	Middle	72	0.198 (0.046)	0.20		
	2012	Deep	35	0.166 (0.044)	0.15	0.359	0.5485
	2020	Deep	48	0.167 (0.042)	0.16		

3.9. Appendix

Appendix Table 3.1 Mixing model outputs for all depths sampled from the two plots used to compared peat chemistry between T0 and T5 of warming to +9C. Molecular component proportion of total C measured via ^{13}CNMR described by the mixing model (Wt%) developed by Baldock et al., 2004. The functional groups were determined from ^{13}C NMR spectra by integrating the area under the curve located at the assigned chemical shift region (ppm) for each group.

Plot_Year	Temp Treatment	Depth Increment	Depth (cm)	Molecular Component (Mixing Model Results)	Weight Percent (% of Total Peat Carbon)	Functional Group (13C NMR Results)	Measured Integral Area
17_2012	+9C	S	15	Carbohydrate	37.7	Alkyl	15.09
17_2012	+9C	S	15	Carbonyl	2.1	Aromatic	20.12
17_2012	+9C	S	15	Char	8.7	Phenolic	9.05
17_2012	+9C	S	15	Lignin	35.6	O-Alkyl	31.61
17_2012	+9C	S	15	Lipid	8.7	Di-O-Alkyl	9.83
17_2012	+9C	S	15	Protein	7.3	N-Alkyl/Methoxyl	7.54
17_2012	+9C	S	15			Amide/Carboxyl	6.11
17_2012	+9C	M	35	Carbohydrate	22.8	Alkyl	28.93
17_2012	+9C	M	35	Carbonyl	5.3	Aromatic	17.87
17_2012	+9C	M	35	Char	8.8	Phenolic	7.97
17_2012	+9C	M	35	Lignin	28.9	O-Alkyl	21.38
17_2012	+9C	M	35	Lipid	24.8	Di-O-Alkyl	6.66
17_2012	+9C	M	35	Protein	9.4	N-Alkyl/Methoxyl	6.94
17_2012	+9C	M	35			Amide/Carboxyl	8.86
17_2012	+9C	D	100	Carbohydrate	27.2	Alkyl	22.09
17_2012	+9C	D	100	Carbonyl	5.2	Aromatic	19.86
17_2012	+9C	D	100	Char	10.3	Phenolic	9.08
17_2012	+9C	D	100	Lignin	29.2	O-Alkyl	24.33
17_2012	+9C	D	100	Lipid	14.6	Di-O-Alkyl	7.34
17_2012	+9C	D	100	Protein	13.5	N-Alkyl/Methoxyl	7.73

17_2012	+9C	D	100			Amide/Carboxyl	9.84
17_2020	+9C	S	15	Carbohydrate	37.5	Alkyl	13.73
17_2020	+9C	S	15	Carbonyl	8.2	Aromatic	17.45
17_2020	+9C	S	15	Char	6.1	Phenolic	8.66
17_2020	+9C	S	15	Lignin	33.1	O-Alkyl	31.91
17_2020	+9C	S	15	Lipid	6.9	Di-O-Alkyl	9.2
17_2020	+9C	S	15	Protein	8.1	N-Alkyl/Methoxyl	6.64
17_2020	+9C	S	15			Amide/Carboxyl	9.02
17_2020	+9C	M	35	Carbohydrate	40.3	Alkyl	17.09
17_2020	+9C	M	35	Carbonyl	7.8	Aromatic	16.78
17_2020	+9C	M	35	Char	7.2	Phenolic	8.25
17_2020	+9C	M	35	Lignin	26.0	O-Alkyl	34.1
17_2020	+9C	M	35	Lipid	10.5	Di-O-Alkyl	9.25
17_2020	+9C	M	35	Protein	8.1	N-Alkyl/Methoxyl	6.38
17_2020	+9C	M	35			Amide/Carboxyl	9.53
17_2020	+9C	D	100	Carbohydrate	24.6	Alkyl	21.2
17_2020	+9C	D	100	Carbonyl	8.1	Aromatic	20.19
17_2020	+9C	D	100	Char	10.2	Phenolic	9.54
17_2020	+9C	D	100	Lignin	29.9	O-Alkyl	22.83
17_2020	+9C	D	100	Lipid	12.9	Di-O-Alkyl	6.89
17_2020	+9C	D	100	Protein	14.3	N-Alkyl/Methoxyl	7.87
17_2020	+9C	D	100			Amide/Carboxyl	11.51
6_2012	+0C	S	15	Carbohydrate	50.5	Alkyl	13.69
6_2012	+0C	S	15	Carbonyl	1.5	Aromatic	15.28
6_2012	+0C	S	15	Char	3.8	Phenolic	7.32
6_2012	+0C	S	15	Lignin	30.8	O-Alkyl	41.51
6_2012	+0C	S	15	Lipid	7.6	Di-O-Alkyl	10.87
6_2012	+0C	S	15	Protein	5.8	N-Alkyl/Methoxyl	7.66

6_2012	+0C	S	15			Amide/Carboxyl	5.37
6_2012	+0C	M	35	Carbohydrate	25.2	Alkyl	29.13
6_2012	+0C	M	35	Carbonyl	4.6	Aromatic	18.38
6_2012	+0C	M	35	Char	10.0	Phenolic	7.8
6_2012	+0C	M	35	Lignin	25.9	O-Alkyl	23.03
6_2012	+0C	M	35	Lipid	25.0	Di-O-Alkyl	7
6_2012	+0C	M	35	Protein	9.3	N-Alkyl/Methoxyl	7.18
6_2012	+0C	M	35			Amide/Carboxyl	8.83
6_2012	+0C	D	100	Carbohydrate	29.9	Alkyl	25.75
6_2012	+0C	D	100	Carbonyl	0.0	Aromatic	19.44
6_2012	+0C	D	100	Char	10.6	Phenolic	7.77
6_2012	+0C	D	100	Lignin	26.3	O-Alkyl	25.88
6_2012	+0C	D	100	Lipid	18.9	Di-O-Alkyl	7.6
6_2012	+0C	D	100	Protein	14.3	N-Alkyl/Methoxyl	9.1
6_2012	+0C	D	100			Amide/Carboxyl	7.13
6_2020	+0C	S	15	Carbohydrate	46.6	Alkyl	15.9
6_2020	+0C	S	15	Carbonyl	5.3	Aromatic	14.63
6_2020	+0C	S	15	Char	4.5	Phenolic	6.97
6_2020	+0C	S	15	Lignin	26.8	O-Alkyl	38.64
6_2020	+0C	S	15	Lipid	9.9	Di-O-Alkyl	9.88
6_2020	+0C	S	15	Protein	6.9	N-Alkyl/Methoxyl	6.85
6_2020	+0C	S	15			Amide/Carboxyl	7.54
6_2020	+0C	M	35	Carbohydrate	42.2	Alkyl	18.56
6_2020	+0C	M	35	Carbonyl	3.7	Aromatic	16.75
6_2020	+0C	M	35	Char	7.3	Phenolic	7.02
6_2020	+0C	M	35	Lignin	26.7	O-Alkyl	34.88
6_2020	+0C	M	35	Lipid	13.0	Di-O-Alkyl	8.98
6_2020	+0C	M	35	Protein	7.2	N-Alkyl/Methoxyl	7.3

6_2020	+0C	M	35			Amide/Carboxyl	7.03
6_2020	+0C	D	100	Carbohydrate	28.8	Alkyl	24.42
6_2020	+0C	D	100	Carbonyl	0.2	Aromatic	18.79
6_2020	+0C	D	100	Char	9.1	Phenolic	7.8
6_2020	+0C	D	100	Lignin	29.9	O-Alkyl	24.88
6_2020	+0C	D	100	Lipid	17.6	Di-O-Alkyl	7.4
6_2020	+0C	D	100	Protein	14.3	N-Alkyl/Methoxyl	8.65
6_2020	+0C	D	100			Amide/Carboxyl	7.56

Appendix Table 3.2 Carbon Stock: Type III Analysis of Variance Table with Satterthwaite's method

Variable	Sum of Squares	Df	F Value	p-value
Mean Annual Temperature (MAT)	0.84697	2	0.2618	0.7856
CO2 Treatment	0.24037	1	0.1486	0.7256
Depth Increment	0.40451	2	0.125	0.8847
MAT:CO2 Treatment	0.23548	2	0.0728	0.9314
MAT:Depth Increment	2.15105	4	0.3324	0.8471
CO2 Treatment : Depth Increment	0.64417	2	0.1991	0.8247
MAT:CO2 Treatment :Depth Increment	1.07168	4	0.1656	0.9482

Appendix Table 3.3 D14C: Anova Table (Type II)

Variable	Sum of Squares	Df	F Value	p-value	
Mean Annual Temperature (MAT)	19267	1	1.67	0.198	
CO2 Treatment	40380	1	3.50	0.063	.
Depth	5560321	1	481.62	<2e-16	***
MAT:CO2 Treatment	2021	1	0.18	0.676	
MAT:Depth	3	1	0.00	0.987	
CO2 Treatment : Depth	36582	1	3.17	0.077	.
MAT:CO2 Treatment :Depth	1201	1	0.10	0.748	

Signif. codes: 0 ‘***’ 0.001 ‘**’ 0.01 ‘*’ 0.05 ‘.’ 0.1 ‘ ’ 1

Appendix Table 3.4 d13C: Anova Table (Type II)

Variable	Sum of Squares	Df	F Value	p-value	
Mean Annual Temperature (MAT)	0.02	1	0.00	0.956	
CO2 Treatment	77.08	1	12.82	4.61E-04	***
Depth	394.93	1	65.67	1.58E-13	***
MAT:CO2 Treatment	0.01	1	0.00	0.969	
MAT:Depth	0.88	1	0.15	0.703	
CO2 Treatment : Depth	66.26	1	11.02	0.001	**
MAT:CO2 Treatment :Depth	0.03	1	0.01	0.944	

Signif. codes: 0 ‘***’ 0.001 ‘**’ 0.01 ‘*’ 0.05 ‘.’ 0.1 ‘ ’ 1

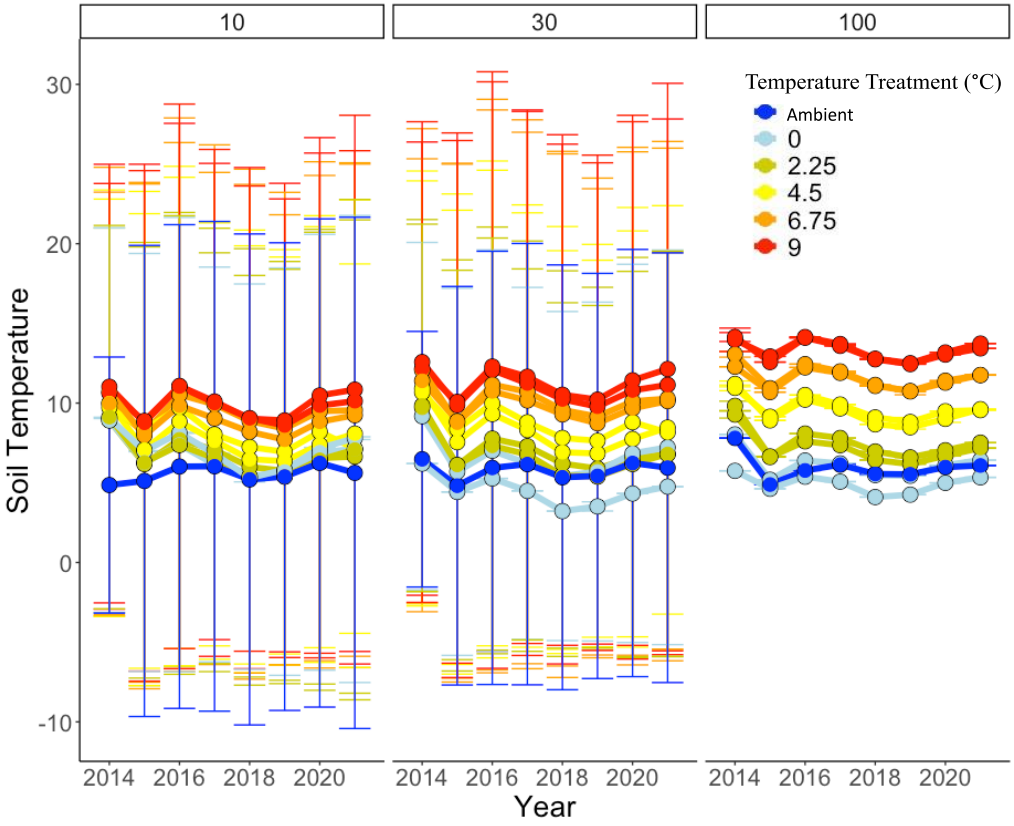

Appendix Figure 3-1 Below ground temperatures across relevant study period. These are averaged below ground temperatures from 2014 (start of deep peat heating) until 2021. Points and bars represent the averages and standard errors of three individual probes located in the plot, except for Plot 6 (+0C) where only two probes were included in the measurement. Depths shown here are 10cm, 30cm, and 100cm below the peat surface. Temperatures are represented by dark blue being ambient and light blue control (+0 °C), green +2.25°C, yellow +4.5 °C, orange +6.75°C, and red +9°C.

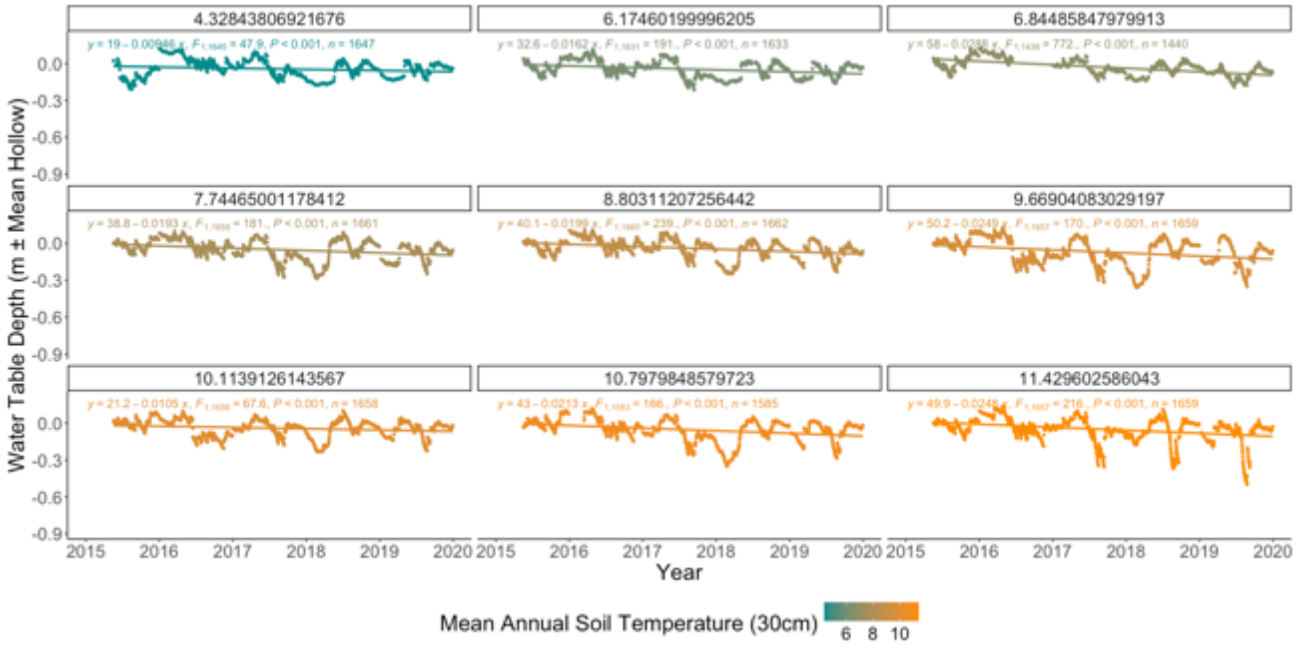

Appendix Figure 3-2 Water table depth over time. These plots have been faceted based on mean annual soil temperature measured at 30cm, with blue coloring representing the cooler temperatures measured and orange representing the warmer temperatures measured. Average mean annual temperatures at 1m above the peat are noted at the top of each plot. These values were taken at 30-minute time intervals over the deep peat heating period (2015-2020). A regression line through each of the plotted relationships shows that all slopes are negative, indicating a decrease in water table depth relative to hollow height, and that all relationships are significant (p-value<0.001 for all temperatures).

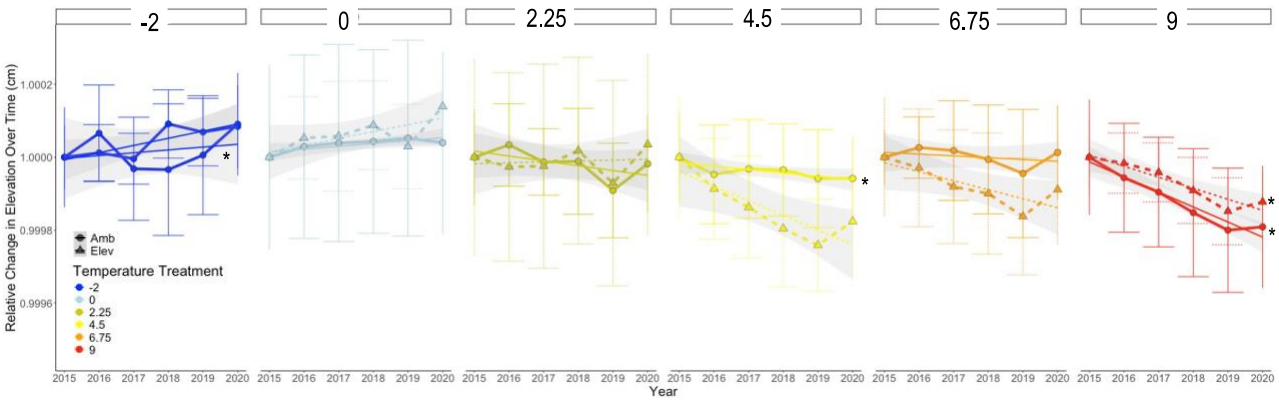

Appendix Figure 3-3 Relative change in peat elevation over time across various temperature treatments from 2015 to 2020, separated by temperature increase levels (°C) and color-coded by treatment. Dark blue represents control, light blue represents +0 °C, green represents +2.25 °C, yellow represents +4.5 °C, orange represents +6.75 °C, and red represents +9 °C. Each panel shows a different temperature treatment, with CO_2 treatments (ambient and elevated) distinguished by marker shapes (circles for ambient, triangles for elevated) and line types (solid for ambient, dashed for elevated). Error bars indicate standard deviations, while shaded regions show confidence intervals; significant differences ($p < 0.05$) between treatments are marked by asterisks, illustrating the effects of warming and CO_2 elevation on peat elevation stability.

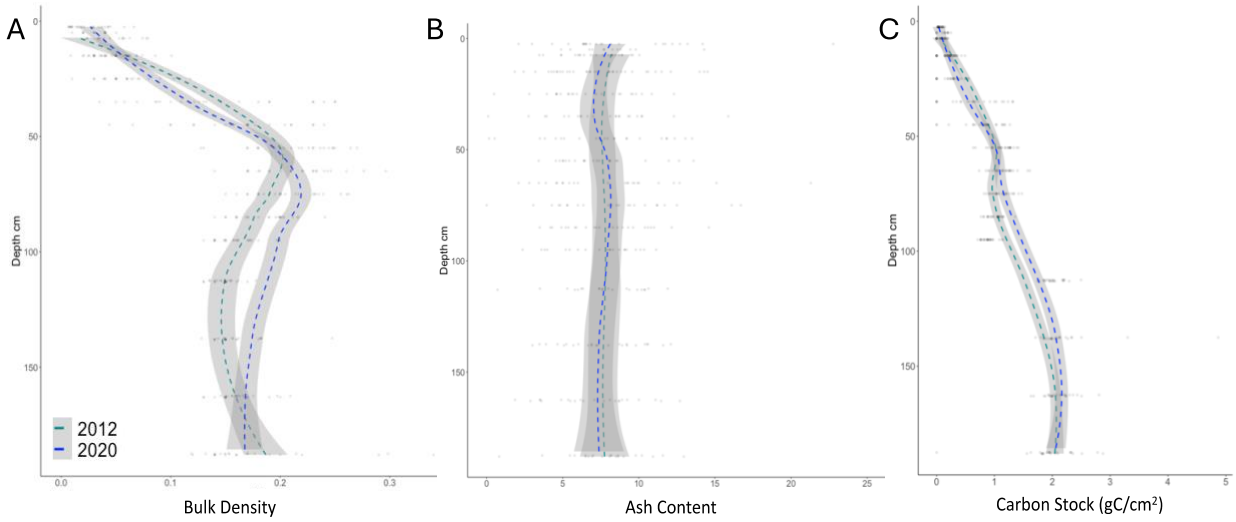

Appendix Figure 3-4 Depth profiles for A) bulk density, B) ash content, and C) Carbon stock for 2012 (light blue) and 2020 (dark blue).

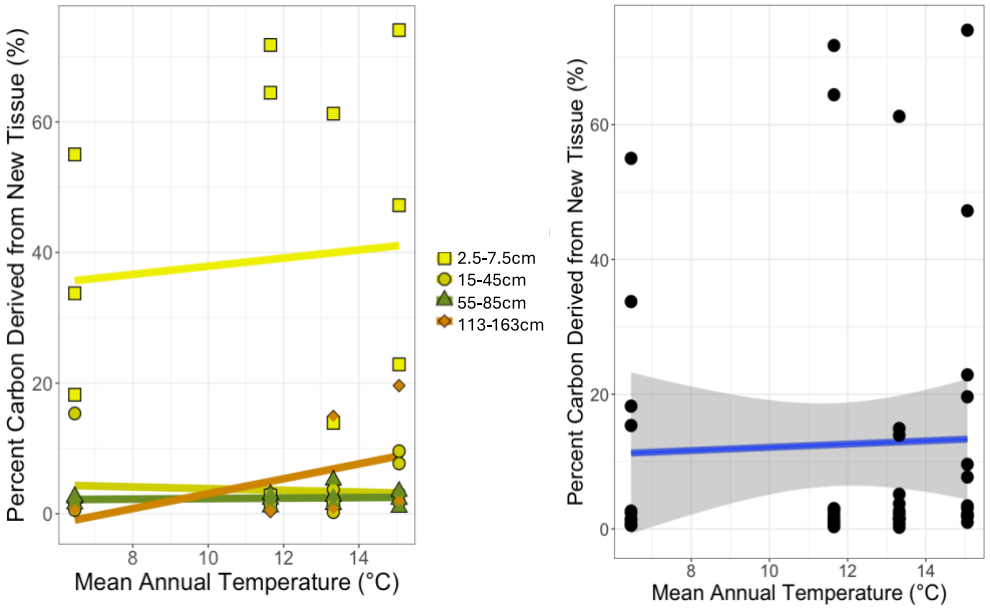

Appendix Figure 3-5 The contribution of new plant tissue derived carbon to bulk peat carbon at 2.5-163cm depth after 5 years of warming and elevated atmospheric CO2. A) The proportion of new carbon is plotted against average mean annual temperature from 2015-2021. Symbols and color represent different depth increments. Lines indicate regression trends between proportion of new carbon and temperature, however no significant trend was identified: 2.5-7.5cm, r2<0.01, p=0.808, F=0.0620, df=10; 15-45cm, r2<0.01, p=0.726, F=0.129, df=13; 55-85cm, r2<0.01, p=0.730, F=0.126, df=10; 113-163cm, r2=0.13, p=0.199, F=2.08, df=6). B) The proportion of new carbon is plotted against average mean annual temperature from 2015-2021 with no depth distinction. No significant trend was found between new carbon incorporation and temperature (r2<0.01, F=0.0614, p=0.805, df=45).

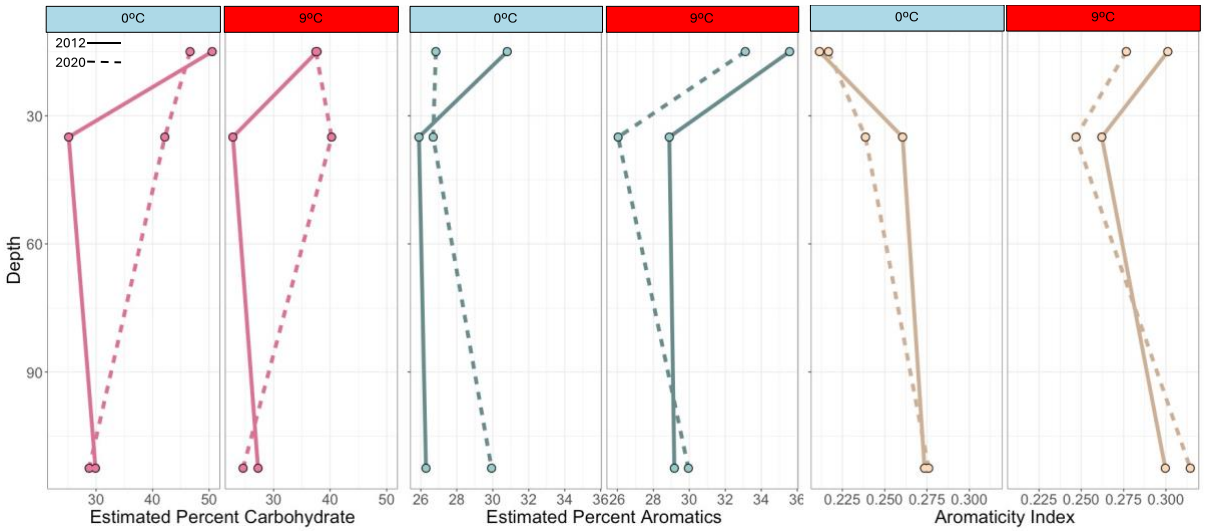

Appendix Figure 3-6 Proportion of total organic C attributed to each displayed molecular component and aromaticity index across temperature treatment. Colors indicate the temperature treatment with red indicating +9 ° above ambient and blue indicating +0° above ambient.

4. Peat Accumulation Patterns in Tropical Peatlands: Unveiling the Roles of Climate, Geography, and Productivity

4.1. Abstract

Tropical peatlands play a critical role in global carbon cycling, acting as long-term carbon sinks influenced by climate, geography, and productivity. This study investigates the long-term apparent rates of peat accumulation (LARPA) across four tropical regions: Southeast Asia, Africa, Central and South America, and Hawaii, using a comprehensive dataset from the International Soil Radiocarbon Database (ISRAD). Through radiocarbon dating, productivity metrics, and environmental data, the research identifies region-specific and shared drivers of peat accumulation. Key findings reveal that climatic factors, such as precipitation stability and proximity to the coast, strongly influence accumulation rates, while geographic factors like elevation and radiocarbon age also play significant roles. Southeast Asia and Africa exhibit the highest accumulation rates, driven by consistent rainfall and high productivity, whereas Hawaiian peatlands show slower rates, constrained by insular climate conditions. The study underscores the importance of understanding diverse environmental controls on tropical peatland dynamics to inform conservation and climate resilience strategies.

4.2. Introduction

Tropical peatlands are crucial for global carbon (C) cycling, acting as long-term C sinks that store significant amounts of organic C, thereby contributing to both ecosystem stability and climate regulation. These peatlands, concentrated in regions like Southeast Asia, Africa, Central and South America, and Hawaii, differ from their temperate counterparts in terms of their climate conditions and unique drivers of peat accumulation (Gumbricht et al., 2017; S. E. Page et al., 2011). Unlike temperate regions, where cooler climates and continuous waterlogging are major

drivers of peat formation, tropical peatlands are exposed to high temperatures, intense rainfall variability, and diverse vegetation types, all of which impact both the rate and stability of peat accumulation (Chimner, 2004; Dommain et al., 2011).

Peat formation in the tropics is especially influenced by bioclimatic factors like precipitation and temperature, as well as geographic elements such as elevation and proximity to the coast. For instance, year-round precipitation in Southeast Asia promotes rapid peat accumulation by maintaining waterlogged conditions that reduce decomposition rates (Dommain et al., 2011). Similarly, Amazonian and African peatlands, which experience more pronounced seasonal rainfall fluctuations, show slower peat accumulation, likely due to water table variation that can limit the buildup of organic matter (Draper et al., 2014). These previous findings underscore the role of stable hydrology in supporting tropical peat formation and suggest that regions with greater seasonal climate variability may accumulate peat at lower rates, potentially impacting their long-term C storage capacity.

In addition to climate, the role of vegetation productivity and C age are increasingly recognized as key factors in peatland dynamics. Tropical peatlands with high gross primary productivity (GPP) and net primary productivity (NPP) can contribute large volumes of organic material, fostering faster peat accumulation (Hergoualc'h & Verchot, 2011; S. E. Page et al., 2011). Radiocarbon age measurements ($\Delta^{14}C$), which provide insights into C turnover within peat profiles, are also valuable for understanding accumulation rates over time. Studies such as those by Chimner, (2004) and outlined by Mitsch and Gosselink, (2015) indicate that regions with younger C pools or more recent C inputs may support faster accumulation rates, while older C reserves typically correspond with slower, more stabilized peat layers. This distinction is

critical for understanding the resilience of these ecosystems and their capacity for long-term C sequestration.

Despite the recognized importance of these factors, few studies have compared the relative influence of environmental and geographic variables on peat accumulation across diverse tropical regions. As tropical peatlands face increased deforestation and land conversion, particularly in Southeast Asia and the Amazon basin, understanding the drivers of accumulation is essential for conservation and climate change mitigation efforts (Girkin et al., 2022; Miettinen et al., 2016; Omar et al., 2022; S. Page et al., 2022).

This study addresses this gap by examining long-term apparent rates of peat accumulation (LARPA) in tropical peatlands across four regions: Southeast Asia, Africa, Central and South America, and Hawaii. By leveraging a comprehensive dataset from the International Soil Radiocarbon Database (ISRAD), which includes radiocarbon measurements, precipitation, productivity, and geographic data, this research aims to identify both shared and region-specific drivers of peat accumulation in tropical ecosystems.

This study seeks to clarify the relative importance of climate, geographic, and productivity-related factors in shaping tropical peat accumulation by addressing the following hypothesis: **1) Climate-related factors, specifically precipitation and temperature, and proximity to the coast are hypothesized to be the primary drivers of tropical peat accumulation.** Based on prior research, we anticipate that regions with higher, stable precipitation and moderate temperatures will exhibit higher accumulation rates due to reduced decomposition and consistent organic input (Dommain et al., 2011; Gumbricht et al., 2017). **2) Geographic and productivity-related factors, such as radiocarbon age, elevation, and productivity (GPP and NPP), will have region-specific influences on peat accumulation.** Higher productivity and younger C

stores are expected to correlate with faster accumulation rates due to greater organic input and dynamic C turnover (Hergoualc'h & Verchot, 2011; S. E. Page et al., 2011).

4.3. Methods

4.3.1. Data Collection

The data for this study were compiled from the International Soil Radiocarbon Database (ISRAD) which houses radiocarbon measurements alongside associated environmental data. In addition, other published datasets and grey literature was included when possible. The easy access and ISRAD's stringent quality assurance protocols ensured a substantial amount of radiocarbon data and consistency across submitted datasets, and similar standards were applied to grey literature sources. This effort resulted in a robust dataset comprising 816 radiocarbon measurements from 142 peat profiles across 78 sites spanning 17 countries.

Environmental variables included in the analysis were derived from multiple sources. Productivity data, such as gross primary productivity (GPP) and net primary productivity (NPP), were obtained from MODIS products. Climate variables, including mean annual temperature (MAT) and mean annual precipitation (MAP), were sourced from WorldClim data layers within the ISRAD repository. Additional geographic features, such as elevation and proximity to the coast, were extracted using QGIS and corroborated with site-specific metadata. The resulting dataset represents diverse peatland conditions across Southeast Asia, Africa, Central and South America, and Hawaii.

4.3.2. Radiocarbon Calibration and Age-Depth Modeling

Age-depth models were generated for each peat core using the Bayesian BACON package in R (v.4.2.2). This method accounts for variable deposition rates and spatial-temporal

autocorrelation in sediment deposition, providing robust uncertainty estimates for each core. Long-term apparent rates of peat accumulation (LARPA) were calculated by analyzing the slope of the age-depth profiles, with steeper slopes representing faster accumulation rates.

4.3.3. Statistics

Statistical analyses were conducted in R v.4.2.2 (The R Foundation for Statistical Computing, 2022). Relationships between LARPA and all variables included in this analysis were assessed using Pearson correlation analysis. A full list of variables and their descriptions and matrix results, including r^2 values and significance, can be found in the appendix (Fig. A1-A4).

To investigate the drivers of peat accumulation, cores were categorized into high, medium, and low accumulation rates based on quantile classification, ensuring an even distribution of samples within each category. We applied Principal Component Analysis (PCA) using the *prcomp* function in R at the pantropical (all regions included) and regional scale. PCA was conducted on the standardized environmental variables to ensure that all variables contributed equally to the analysis, regardless of their original units. The principal components (PCs) were retained based on their eigenvalues, proportion of variance explained, and interpretability.

A linear regression model was used to evaluate the relationship between LARPA and the retained principal components. This approach allows for the exploration of how major environmental gradients influence peat accumulation while minimizing multicollinearity among predictors. The model's performance was assessed using R-squared, adjusted R-squared, and significance levels of individual predictors. Although linear regression assumes normality and homoscedasticity, it was employed here as an exploratory tool, with results interpreted cautiously to identify key trends (Gelman & Hill, 2021; Lumley et al., 2002). The regression model was fitted using the lm function in R, with LARPA as the dependent variable and the principal

components as independent variables. This approach allows exploration of how major environmental conditions (represented by the PCs) influenced the response variable while minimizing multicollinearity among predictors. Model performance was evaluated using R-squared, adjusted R-squared, and the significance of individual predictors based on t-tests.

4.4. Results

4.4.1. Tropical Peatland Extent

The final dataset for this analysis contained a total of 138 cores collected from 77 unique sites, which are categorized into four distinct regions: Hawaii, Central/South America, Africa, and Southeast Asia (Fig 1A). Each of these regions presents a unique climate profile, characterized by variations in average annual temperature and precipitation levels (Fig 1B). These climatic factors are critical in determining the initiation and development of peatlands, as they influence the hydrology, vegetation, and overall ecosystem dynamics of these areas. While the climate today differs considerably from that at the time of peatland formation, historical climate conditions have a lasting impact on peatland persistence. Elevation emerges as a significant factor influencing both temperature and precipitation across this dataset, strongly affecting where these peatland sites are situated within the climate space, represented by Mean Annual Precipitation versus Mean Annual Temperature (Fig 1B).

4.4.2. Patterns in Long-Term Apparent Rates of Peat Accumulation (LARPA)

Estimated peatland accumulation rates for each core were derived by calibrating the age of each peat layer and analyzing the slope of the resulting age-depth profile (Fig 2A&B). Cores with age-depth profiles exhibiting steeper slopes indicate faster accumulation rates, highlighting

more dynamic peatland sites, whereas shallower slopes correspond to slower accumulation processes.

This analysis revealed significant variability in accumulation rates, both across different tropical regions and within individual peatland sites. Southeast Asia and Africa host peatlands with the highest long-term apparent rates of peat accumulation (LARPA), measuring 0.987 cm/yr. and 0.864 cm/yr., respectively. In contrast, all of Hawaii's peatlands display slower LARPA rates; however, these rates fall within the range of the slower accumulating peatlands found in other regions. For instance, the slowest accumulating peatlands in both Hawaii and Southeast Asia accumulate peat at the same rate of 0.002 cm/yr. In the peatlands included in this analysis, the majority exhibit accumulation rates below 0.25 cm/yr. regardless of region (Fig 3).

Within each region, there is variability in peat accumulation rates both among different peat sites and occasionally within the same site. To better explore this variability, accumulation rates were categorized into bins for each region, allowing for a clearer distinction between "high," "medium," and "low" peat accumulation rates. This classification helps identify the underlying controls influencing peat accumulation across diverse tropical environments.

Density plots demonstrate that a significant proportion of peatlands across all regions exhibit "low" accumulation rates (Fig 4). This trend persists despite the variations in accumulation rates within each region; notably, the highest density of data points consistently aligns with the lower end of the accumulation rate spectrum. This suggests that, while there may be some peatlands with higher rates, the majority tend to accumulate peat at slower rates.

4.4.3. Environmental Drivers of Peat Accumulation: Regional and Pantropical Analysis of LARPA

Environmental factors included in this analysis play a key role in differentiating both regional (Fig 5A) and rate-based groupings (Fig 5B) of the peat sites, with PC1 (59.14% variance explained) and PC2 (20.2% variance explained) capturing the primary gradients of variation. Distinct clustering of peat development sites based on regional origin, with Hawaii (HI, yellow) forming a tighter cluster, suggesting relatively uniform environmental characteristics, while Africa (AFR, magenta), Southeast Asia (SEA, cyan), and Central/South America (CSA, turquoise) display greater spread, reflecting higher variability. Key environmental variables, such as gross primary productivity (GPP), Subsoil pH, elevation, mean annual temperature (MAT_C), and precipitation of the driest quarter, influence these patterns. For instance, GPP and elevation strongly drive variation along PC1, while MAT_C and Precipitation contribute more to PC2. There is also evidence that environmental conditions also drive differences in rates of peat accumulation. Sites with high-rates of LARPA align with GPP and Subsoil pH, suggesting positive associations with these variables, while low-rate sites are more associated with elevation and precipitation, reflecting distinct environmental drivers. Medium-rate sites fall between the high and low categories, indicating a transitional influence of these variables.

The five principal components used in this analysis provide insights into the major environmental gradients driving variation across the sites. Together, these components reveal distinct environmental gradients: temperature-elevation (PC1), bioproductivity-soil pH (PC2), soil pH-productivity trade-offs (PC3), precipitation-temperature interactions (PC4), and elevation-temperature variability (PC5) (Appendix Table 2). These axes collectively describe the complex interplay of climate, soil, and productivity in shaping environmental variability across

the sites. PC1 represents climactic conditions and includes the effect of the temperature-elevation gradient on location of peat development and LARPA, with mean annual temperature and elevation being the dominant variables. This suggests that sites at higher elevations, associated with cooler temperatures, reflect a climatic or geographic gradient. PC2 captures the bioproductivity-soil pH characteristics, dominated by GPP and subsoil pH, suggesting a link between productivity and peat soil conditions (Fig 5, Appendix Table 2). PC3 describes a soil pH versus productivity gradient, with an inverse relationship between subsoil pH and GPP, suggesting that soil pH can limit or support vegetation growth depending on the conditions. PC4 highlights a precipitation-temperature interaction, with precipitation during the driest quarter and mean annual temperature as dominant variables, capturing regions where seasonal moisture availability coincides with cooler temperatures. Finally, PC5 reflects elevation-related temperature variability, dominated by elevation and mean annual temperature, pointing to localized microclimatic conditions linked to elevation.

The linear model examines the relationship between LARPA, and the five principal components (PC1 to PC5) derived from the dataset (Table 1). The model explains approximately 10.76% of the variance in LARPA (Multiple R-squared = 0.11), and the adjusted R-squared (0.08) reflects modest explanatory power. The overall model is statistically significant (F-statistic = 3.304, $p = 0.008$), indicating that the predictors collectively contribute to explaining variation in the LARPA values. Among the principal components, PC1 (temperature-elevation gradient) has a significant negative effect (Estimate = -0.02, $p = 0.02$), suggesting that increases in PC1 are associated with a slight decrease in LARPA. Similarly, PC3 (soil pH-productivity) shows a significant negative relationship (Estimate = -0.05, $p = 0.003$), highlighting a potential stronger influence of these factors on LARPA. In contrast, PC2 (bioproductivity-soil pH), PC4

(precipitation-temperature interaction), and PC5 (elevation-temperature variability) do not significantly contribute to the model ($p > 0.1$), indicating weaker or no effects on the response variable (LARPA). The residuals, ranging from -0.23 to 0.75 with a median near zero, support the assumption of reasonable model fit (Table 1). Overall, the results suggest that while PC1 and PC3 significantly influence LARPA, the model's modest explanatory power indicates that additional factors not captured by these principal components may play an important role.

4.4.3.1. Africa

In African peatlands, precipitation and soil factors were the strongest correlates of LARPA. Precipitation during the wettest quarter (Bioclim16) was positively associated with accumulation rates, suggesting that hydrological stability during peak rainfall seasons supports peat formation (Appendix Figure A2). Conversely, high elevation negatively correlated with accumulation, likely due to cooler temperatures and limited productivity.

The PCA results show the two principal components, PC1 and PC2 together explained 79.16% of the variance, with PC1 (59.14%) dominated by temperature and elevation gradients (Fig 6A). High-accumulation sites were strongly aligned with PC2, reflecting associations with seasonal precipitation and root oxygen availability. Low-accumulation sites clustered with higher elevation and cooler temperatures. PC2 captured bioproductivity and soil characteristics, driven by GPP and subsoil pH. High-accumulation sites were associated with higher productivity and neutral to slightly acidic soil conditions, while low-accumulation sites corresponded with harsher soil conditions and limited hydrology. The ellipses around each group represent 95% confidence intervals, with smaller ellipses for high-accumulation sites, suggesting lower variability within this group. This pattern indicates that sites with high accumulation rates are influenced by distinct environmental gradients compared to low and medium rates.

Overall, the results demonstrate that peatland accumulation rates are shaped by a combination of elevation, productivity, and bioclimatic variables (Fig 6B). PC1 represents a gradient influenced by elevation, NPP, and GPP, with higher accumulation rates possibly associated with greater productivity and lower elevations. PC2 captures variability driven by factors such as root oxygen availability (Root_O2), precipitation during the driest quarter, and annual temperature range.

The regression model for African peatlands explained only 14.95% of the variance in LARPA (Adjusted $R^2 = 0.0048$) and was not statistically significant ($F = 1.033$, $p = 0.4253$). Only PC6 approached significance ($p = 0.0692$), highlighting possible unexplored gradients influencing LARPA. These results suggest that other, unmeasured factors may play a dominant role in African peat accumulation dynamics (Appendix Table A4).

4.4.3.2. Central South America

In Central and South America, correlations between LARPA and productivity variables (GPP, NPP) were prominent (Appendix Figure A3). Coastal proximity exhibited moderate positive correlations, reflecting the role of marine influence and hydrological inputs. Conversely, high elevation negatively correlated with accumulation, similar to Africa (Appendix Figure A2).

The PCA analysis shows clustering of Central South American peatland sites, with PC1 and PC2 explaining 58.83% and 28.91% of the total variance, respectively (Fig 7A). High-accumulation sites clustered along PC1, emphasizing the importance of productivity. Low-accumulation sites aligned with PC2 variables, reflecting elevation constraints and oxygen-limited conditions. The clustering of medium-accumulation sites suggests transitional environmental conditions, where moderate productivity and hydrological stability balance limitations such as soil oxygen deficits. The 95% confidence ellipses for each group illustrate

variability, with the high-rate sites showing less dispersion compared to low and medium sites. This suggests that sites with high accumulation rates are more homogenous in their environmental characteristics, while low-accumulation sites are associated with greater variability, potentially reflecting more diverse limiting factors.

PC1 reflects a gradient driven by variables such as NPP, GPP, and mean annual temperature, with positive loadings indicating higher productivity and warmer conditions (Fig 7B). PC2 captures a gradient influenced by latitude and elevation, with elevation showing a strong negative loading. Root oxygen availability and temperature variability (annual temperature range and mean diurnal range) also align with PC2, highlighting their importance in separating sites based on accumulation rates. High-accumulation sites are associated with high productivity (GPP, NPP) and favorable climatic conditions, whereas low-accumulation sites align more with restricting factors like high elevation and reduced oxygen availability.

The regression model explained 45.38% of the variance in LARPA (Adjusted $R^2 = 29.77\%$), with PC1 ($p = 0.00948$) and PC2 ($p = 0.00910$) as significant positive predictors (Appendix Table A6). PC5 showed a significant negative association ($p = 0.04317$), indicating that elevation-related constraints reduce accumulation rates.

4.4.3.3. Southeast Asia

In Southeast Asia, significant correlations were observed between peat accumulation rates and variables associated with productivity (GPP, NPP) and hydrological stability (precipitation metrics) (Appendix Figure A1). Gross primary productivity exhibited a strong positive correlation with LARPA, suggesting that organic matter input plays a critical role in supporting rapid peat formation. Subsoil pH showed moderate correlations, indicating potential soil chemical constraints on productivity.

The PCA results identified five components, with PC1 explaining 48.4% of the variance and PC2 accounting for 22.95% (Fig 8). The distribution of peatland sites categorized by accumulation rates (high, medium, and low) along the first two principal components (Fig 8A). High-accumulation sites clustered closely along PC1, reflecting favorable conditions for organic matter preservation and peat accumulation. PC2 highlighted the influence of coastal proximity and precipitation during the warmest quarter, suggesting that both geographic and hydrological factors contribute to site variability. High-accumulation sites aligned with variables driving PC1, emphasizing the role of stable productivity and hydrology in this region. Medium-accumulation sites exhibited intermediate traits, influenced by both PC1 and PC2. Low-accumulation sites diverged from these variables, reflecting possible hydrological instability or productivity constraints.

PC1 represents a gradient driven by aboveground biomass, GPP, and precipitation seasonality, with positive loadings suggesting that high biomass and productivity are positively associated with high accumulation rates (Fig 8B, Appendix Table A7). PC2 reflects variability driven by coastal proximity (Coastal_km) and precipitation during the warmest quarter, highlighting their influence in differentiating sites. High-accumulation sites align with favorable conditions such as higher biomass and productivity, while low-accumulation sites are associated with limiting conditions such as reduced precipitation. These results underscore the role of productivity, hydrological factors, and coastal influence in shaping peatland accumulation rates in Southeast Asia.

The regression model explained 51.22% of the variance in LARPA (Adjusted $R^2 = 44.26\%$) and was statistically significant ($F = 7.351$, $p < 0.001$). PC1 ($p < 0.001$) and PC5 ($p = 0.0015$) were significant predictors of LARPA (Appendix Table A8). The positive influence of PC1

corroborates the importance of productivity and hydrological stability, while PC5 highlights the role of elevation and temperature variability as localized drivers.

4.4.3.4. Hawaii

Hawaiian peatlands showed limited significant correlations, likely due to the small sample size (n = 6) (Appendix Figure A4). However, precipitation metrics (MAP, Bioclim13) positively correlated with LARPA, suggesting hydrology as a key driver. Productivity variables showed weaker correlations, reflecting the volcanic and nutrient-limited nature of Hawaiian soils.

The PCA examines the environmental controls on peat accumulation rates in Hawaii, represented by high (green), medium (yellow), and low (red) accumulation rate sites (Fig 9A & B). PC1 (72.67%) was dominated by GPP, NPP, and precipitation, while PC2 (26.67%) captured MAP variability and coastal proximity. High-accumulation sites aligned with high productivity and favorable precipitation patterns. Low-accumulation sites clustered along PC2, reflecting hydrological constraints. The overlap of medium-accumulation sites suggests that intermediate hydrological conditions are transitional between extremes of productivity and nutrient availability. The regression model had limited explanatory power due to the small sample size and was excluded from the analysis.

4.5. Discussion

This study underscores the pivotal role of hydrology, productivity, and geographic factors in shaping peat accumulation rates across tropical regions. The results support the initial hypothesis that climate-related factors, particularly precipitation and temperature, are primary drivers of peat accumulation, with stable hydrology and moderate temperatures promoting higher accumulation rates. In Southeast Asia, where conditions align with this hypothesis, the highest rates were observed, driven by consistent rainfall and high productivity. Similarly, the hypothesis

is validated in African and South American peatlands, where precipitation patterns and soil characteristics influence accumulation dynamics, albeit at slower rates. Hawaiian peatlands, while consistent with expectations of localized constraints such as nutrient limitations and hydrological variability, demonstrate the unique challenges faced by isolated ecosystems. The second hypothesis—that geographic and productivity factors such as elevation, GPP, and NPP have region-specific influences—is also supported. Across regions, elevation emerged as a critical constraint in sites with low accumulation rates, while productivity variables aligned strongly with high-accumulation sites. The variability observed across regions reflects how these factors interact with local environmental conditions, further emphasizing the need for region specific study and tailored conservation approaches.

Southeast Asia exhibits the highest long-term apparent rates of peat accumulation, with values reaching up to 0.987 cm/yr. These rates are strongly correlated with high gross primary productivity and net primary productivity, reflecting the critical role of organic input in supporting rapid peat formation. Consistent, year-round precipitation (mean annual precipitation >2000 mm) further contributes to waterlogged conditions, which suppress aerobic decomposition and enhance C sequestration. These findings align with Dommain et al. (2011) and Page et al. (2011), who demonstrated that the extensive peat domes in Southeast Asia are underpinned by hydrological stability and high productivity.

PCA results reinforce the importance of productivity and hydrology in shaping accumulation rates. High-accumulation sites align with PC1, driven by GPP, NPP, and precipitation seasonality. Coastal proximity (PC2) further differentiates sites, with coastal peatlands benefiting from marine influences that stabilize hydrology. Medium- and low-accumulation sites exhibit greater variability along PC2 and PC3, suggesting that inland and marginal peatlands may face

seasonal water table fluctuations, reducing organic matter preservation. These results are consistent with Gumbricht et al. (2017), who highlighted the role of hydrological connectivity in maintaining peatland function.

Despite their remarkable accumulation rates, Southeast Asian peatlands face significant anthropogenic threats. Land conversion for agriculture, particularly oil palm and acacia plantations, has led to large-scale drainage, which drastically reduces water table levels and triggers peat subsidence and fires (Hooijer et al., 2012; Miettinen et al., 2016). Linear regression results emphasize the sensitivity of LARPA to PC1 and PC5, suggesting that disruptions to hydrological and productivity gradients could disproportionately impact high-accumulation sites. Protecting these peatlands requires immediate action to maintain waterlogged conditions, prevent further drainage, and restore degraded areas.

African peatlands demonstrate moderate accumulation rates, with LARPA reaching up to 0.864 cm/yr in some regions. These rates are closely linked to seasonal wetland dynamics, where consistent wet-season precipitation sustains organic matter accumulation. High-accumulation sites are strongly associated with precipitation during the wettest quarter (Bioclim16), highlighting the importance of hydrological stability. However, precipitation seasonality introduces variability, with low-accumulation sites more likely to experience water table fluctuations. These findings align with Dargie et al. (2017), who identified vast Cuvette peatlands in the Congo Basin supported by seasonal flooding.

PCA results indicate that PC1, driven by temperature and elevation, explains much of the variance in accumulation rates. High-elevation sites, associated with cooler temperatures, show limited productivity and reduced accumulation rates. PC2 captures gradients of bioproductivity and soil pH, revealing that high-accumulation sites align with moderate pH values conducive to

vegetation growth, while low-accumulation sites correlate with harsher soil conditions. This variability underscores the role of both climatic and edaphic factors in influencing African peatlands.

Linear regression results suggest that while climatic and soil factors are important, additional unmeasured variables may contribute to the observed patterns. PC6, which approached significance ($p = 0.0692$), highlights potential unexplored gradients such as vegetation composition or anthropogenic impacts. The moderate accumulation rates observed in African peatlands suggest resilience to short-term disturbances, but long-term risks from land-use changes and climate variability, including altered rainfall patterns and deforestation, could destabilize these ecosystems.

In Central and South America, LARPA ranges from low to moderate, with most sites below 0.5 cm/yr. High-accumulation sites are concentrated in coastal and lowland areas, where consistent hydrology supports organic matter preservation. Precipitation during the wettest quarter and coastal proximity emerge as significant predictors of accumulation rates, reflecting the role of stable hydrological inputs. These findings align with past studies that report lowland Amazonian peatlands store significant C but rely on hydrological connectivity for peat formation (Wang et al., 2018).

PCA results show that PC1, dominated by productivity variables, explains most of the variance in accumulation rates. High-accumulation sites align with moderate GPP and NPP values, while low-accumulation sites are constrained by PC3 variables such as soil oxygen deficits and high elevation. Inland peatlands near the Andes experience greater variability due to steep gradients and seasonal water availability, limiting their potential for long-term C storage.

These findings are consistent with Draper et al. (2014), who identified hydrological and topographical constraints in Amazonian peatlands.

The regression model highlights the importance of PC1 and PC2 in predicting accumulation rates, while PC5 indicates that elevation-related constraints negatively impact accumulation. These results emphasize that while lowland peatlands benefit from stable hydrology, upland and marginal systems are more vulnerable to environmental variability. Conservation strategies should prioritize lowland peatlands and address hydrological disruptions caused by deforestation, agriculture, and infrastructure development.

Hawaiian peatlands exhibit the slowest accumulation rates, with most LARPA values below 0.25 cm/yr. These systems are strongly influenced by localized hydrology and volcanic topography. High-accumulation sites are rare and align with moderate precipitation (Bioclim13) and productivity metrics such as GPP, reflecting the importance of organic matter input even in nutrient-limited volcanic soils. There is evidence from Hawaii focused studies that describe how Hawaiian wetlands rely heavily on localized hydrological stability to support peat formation, consistent with the findings here (Chimner, 2004).

PCA results reveal that PC1, dominated by GPP and NPP, explains 72.67% of the variance, while PC2 captures precipitation variability and coastal proximity. High-accumulation sites align with PC1 variables, highlighting the role of productivity. Low-accumulation sites are influenced by PC2, reflecting hydrological constraints and seasonal precipitation variability. These results suggest that Hawaiian peatlands operate under unique conditions distinct from other tropical systems. However, the sensitivity of Hawaiian peatlands to hydrological variability underscores the need for careful management of water resources. Protecting these systems requires a nuanced

understanding of their localized constraints and the impacts of climate change on precipitation patterns.

4.5.1. Pantropical Implications

Tropical peatlands play a critical role in the global C cycle, serving as both significant C sinks and, under disturbed conditions, as potent sources of greenhouse gas emissions. Across the tropics, this study underscores hydrological stability and high productivity as the dominant drivers of peat accumulation, consistent with findings from other studies (Dargie et al., 2017; Dommain et al., 2011; S. E. Page et al., 2011). However, variability in accumulation rates across regions highlights the unique interplay of climatic, geographic, and anthropogenic factors in shaping the dynamics of these ecosystems.

Regions like Southeast Asia represent ideal conditions for rapid peat accumulation, driven by stable waterlogged conditions, year-round precipitation, and high organic input. However, these peatlands are also among the most vulnerable. Deforestation and land conversion for agriculture and plantations, particularly for oil palm, have already degraded millions of hectares of peatlands, turning them into net C emitters (Hooijer et al., 2012; Miettinen et al., 2016). In Indonesia and Malaysia alone, drained peatlands contribute approximately 500 million tons of CO_2 annually (Hergoualc'h & Verchot, 2011). These emissions exacerbate global warming, creating a feedback loop that further threatens peatland stability. Protecting these peatlands requires urgent conservation actions, such as rewetting degraded areas and implementing sustainable land-use practices.

African and South American peatlands, while accumulating C at slower rates, demonstrate resilience to seasonal variability. African peatlands, particularly those in the Congo Basin, store immense quantities of C—approximately 30 billion tons—making them the largest tropical

peatland complex globally (Dargie et al., 2017). However, seasonal flooding patterns that support these systems are highly sensitive to climate variability. Shifts in precipitation patterns, as predicted under many climate change scenarios, could destabilize these ecosystems, leading to reduced C sequestration or even C release. In the Amazon, Draper et al. (2014) found that lowland peatlands remain C sinks primarily due to stable hydrological conditions, but upland and Andean-adjacent peatlands are far more vulnerable to climatic variability and deforestation. These findings highlight the importance of hydrological connectivity and suggest that regions with slower accumulation rates may be at equal or greater risk from long-term climate changes compared to high-accumulation peatlands.

Hawaiian peatlands, while unique in their volcanic and nutrient-limited contexts, offer critical insights into the influence of localized constraints on peat dynamics. Their slow accumulation rates highlight how volcanic topography, nutrient availability, and hydrology interact to limit C storage. Similar constraints are observed in tropical peatlands on small islands, such as those in the Caribbean and Pacific (Chimner, 2004). Despite their limited spatial extent, these systems provide a valuable window into how climate and geology jointly influence peatland development, particularly under extreme or nutrient-poor conditions.

From a pantropical perspective, these findings reinforce the importance of maintaining hydrological stability as a universal priority for tropical peatland conservation. Drainage, whether for agriculture, logging, or urban development, disrupts the waterlogged conditions essential for peat accumulation, leading to rapid C losses (Hooijer et al., 2012; Moore et al., 2013). In addition, climate change presents a looming threat, with rising temperatures and altered precipitation patterns likely to exacerbate peatland degradation. Studies suggest that even small

increases in temperature can significantly increase peat decomposition rates, transforming peatlands from C sinks to sources (Hopple et al., 2020; Wilson et al., 2016).

Despite these challenges, tropical peatlands also present opportunities for climate mitigation. Restoring degraded peatlands, particularly in Southeast Asia, has been shown to rapidly reduce emissions while enhancing biodiversity and hydrological functions (Joosten & FAO, 2012; S. E. Page & Baird, 2016). Conservation of intact peatlands in Africa and the Amazon is equally critical, given their role as long-term C reservoirs. Policy frameworks such as the REDD+ mechanism provide an avenue for integrating peatland conservation into global climate strategies, offering financial incentives for countries to protect and restore these ecosystems (Hergoualc'h & Verchot, 2011; Joosten & Clarke, 2002).

Integrating regional findings into a global framework highlights the interconnectedness of tropical peatland dynamics. While the drivers of peat accumulation may vary across regions, the overarching principles of hydrological stability and productivity are universal. Conservation strategies must be tailored to regional contexts, addressing specific threats while leveraging global mechanisms to promote sustainable management. By recognizing the critical role of tropical peatlands in C storage, biodiversity support, and climate regulation, we can develop comprehensive strategies to safeguard these vital ecosystems for future generations.

4.6. Figures

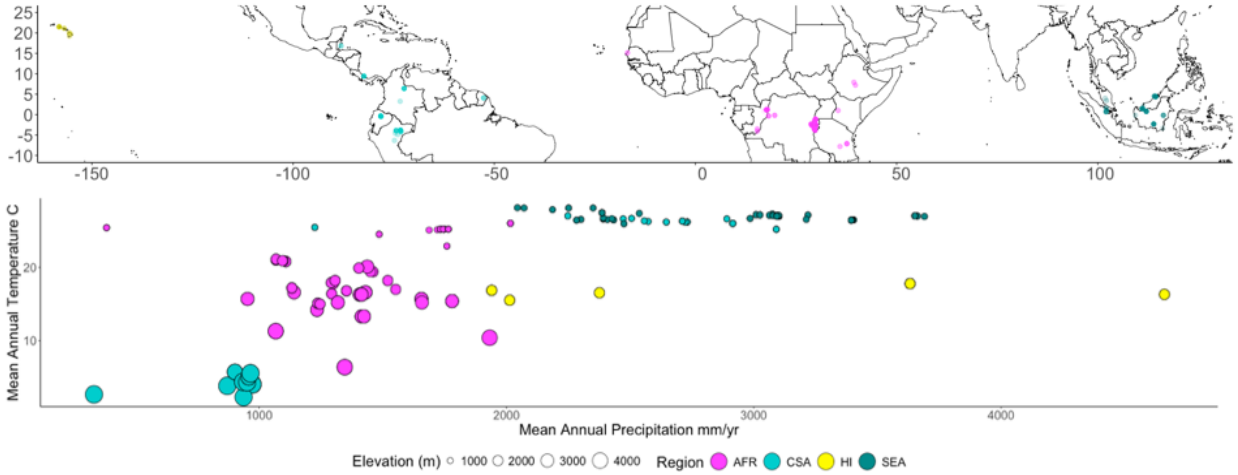

Figure 4.1 Map of tropical peat sites used in this analysis and where they plot in climate space. A) Peatland coordinates were collected from the ISRAD database, and colors denote peatland regions with yellow indicating Hawaii (HI), cyan indicating Central/South America (CSA), magenta representing Africa (AFR), and teal representing Southeast Asia (SEA). B) Climate space for each peatland site as described by the relationship between Mean Annual Precipitation and Mean Annual temperature. The size of the circles represents the elevation of the peatlands, with larger circles indicating those at higher elevations, and illustrates the relationship between climate space and elevation.

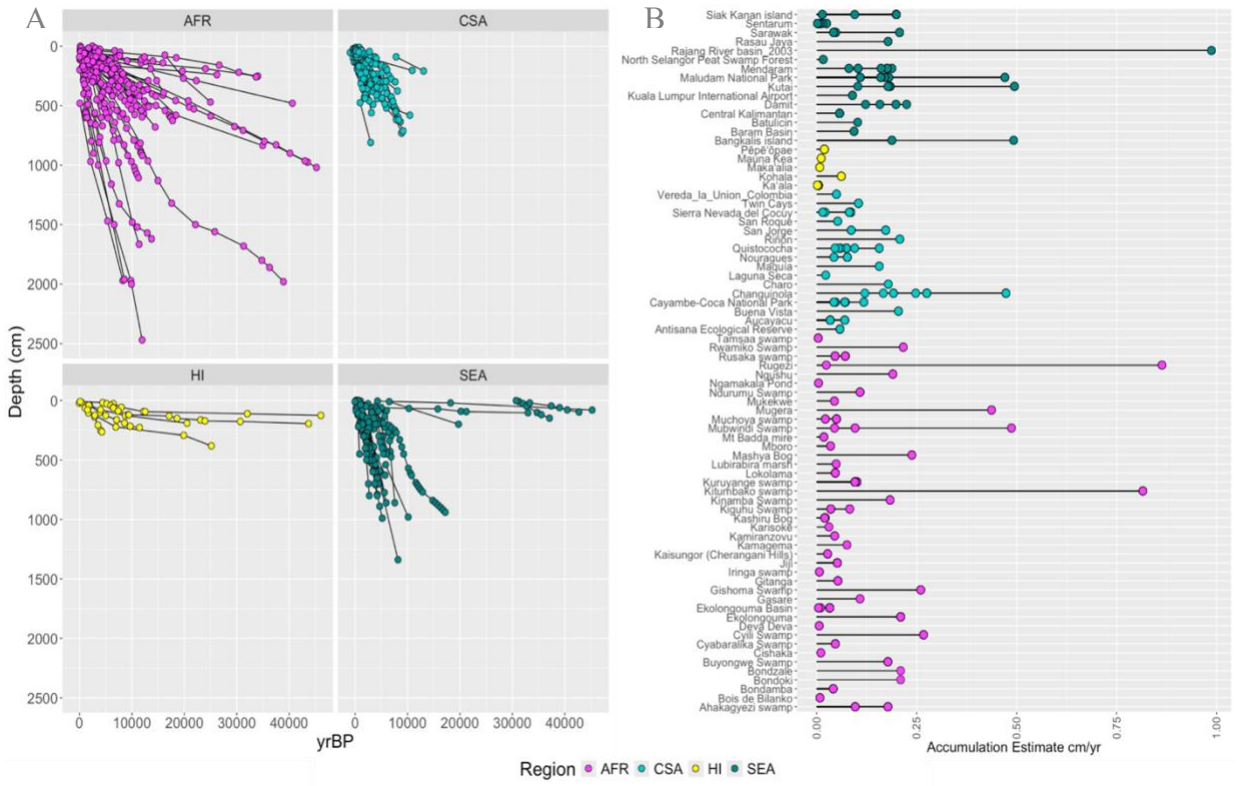

Figure 4.2 Rates of peatland accumulation and their distribution across the tropics. A) Age-depth profiles for each core faceted by region. Cores with steep slopes indicate peatland sites that accumulate faster than cores with more gradual slopes. B) Estimated peat accumulation rates for each site included in this analysis. Each circle represents a single core that was used to calculate a long-term apparent accumulation rate (LORCA). Some sites have multiple rate estimates due to the extraction of several cores from the same location.

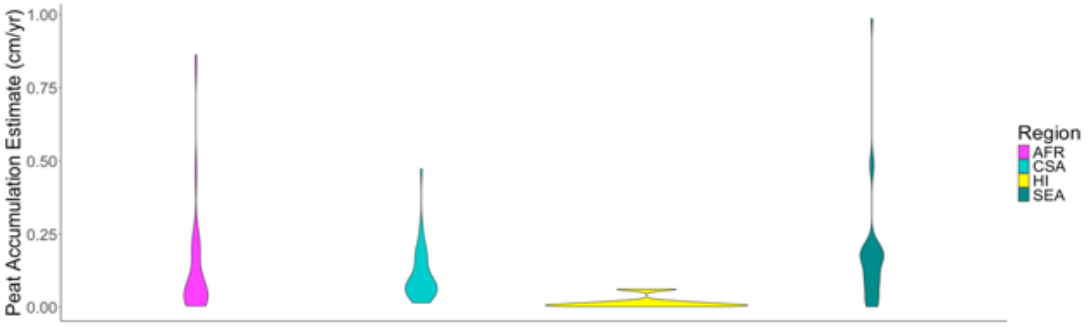

Figure 4.3 Violin plot comparing peatland accumulation rates across various tropical regions. This plot illustrates the distribution of long-term apparent rates of peat accumulation (LARCA) for each color-coded region: Africa (magenta), Central/South America (cyan), Hawaii (yellow), and Southeast Asia (teal). It highlights differences in median accumulation rates and variability among regions. The wider sections of the violins indicate areas of higher concentration of accumulation rates, while the central box represents the median and interquartile range. This visualization emphasizes the substantial variability in peatland dynamics across tropical ecosystems.

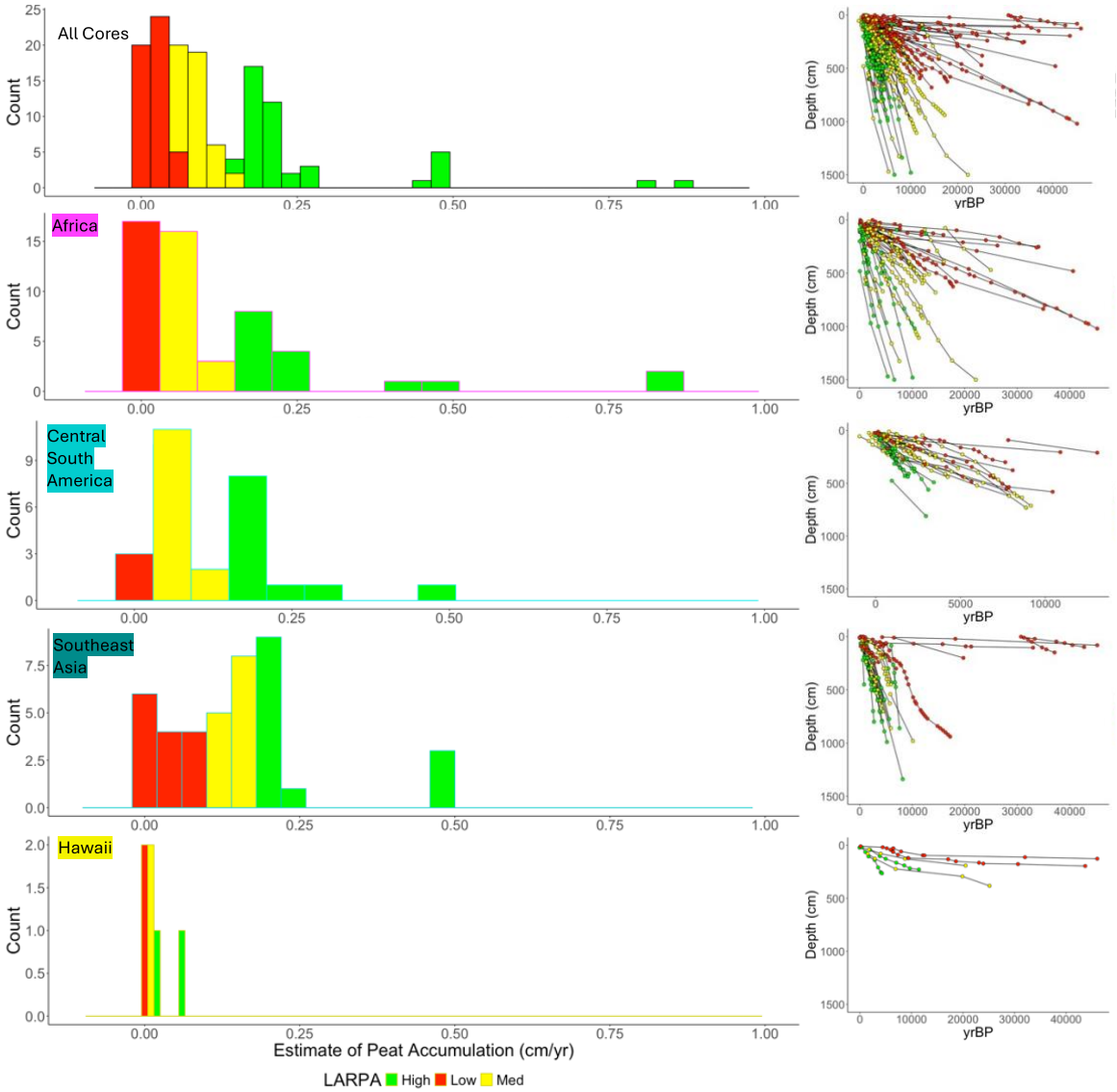

Figure 4.4 Histograms of peat accumulation estimates and age-depth plots for A) all cores, B) Africa, C) Central South America, D) Southeast Asia, and E) Hawaii. Each plot displays the distribution of long-term apparent rates of peat accumulation (LARCA) for the specified color-coded region: Africa (magenta), Central/South America (cyan), Hawaii (yellow), and Southeast Asia (teal). The histograms provide insight into the variation and central tendencies of accumulation rates, highlighting differences in peatland dynamics among these regions. Each region exhibits distinct frequencies of accumulation rates, and bins for accumulation rates have been defined separately for each region (see Appendix Table for specific bin ranges). Green indicates "high" accumulation rates, yellow represents "medium" accumulation rates, and red signifies "low" accumulation rates.

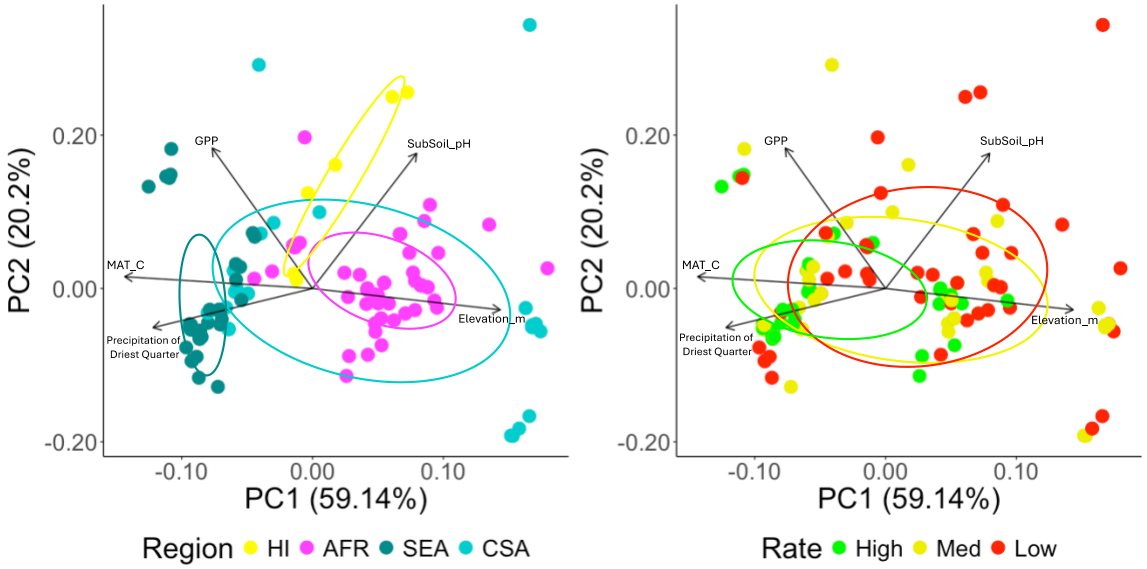

Figure 4.5 Principal Component Analysis (PCA) biplots depicting the variation in environmental variables across A) regions and B) peat accumulation rates for the complete dataset. The left panel shows samples grouped by region (HI = yellow, AFR = magenta, SEA = cyan, CSA = turquoise), while the right panel highlights groupings based on rate categories (High = green, Medium = yellow, Low = red). Arrows represent the environmental variables contributing to the variation along PC1 (59.14%) and PC2 (20.2%), including Gross Primary Productivity (GPP), Subsoil pH, Elevation, Mean Annual Temperature (MAT_C), and Precipitation of the Driest Quarter. Ellipses indicate 95% confidence intervals for group centroids.

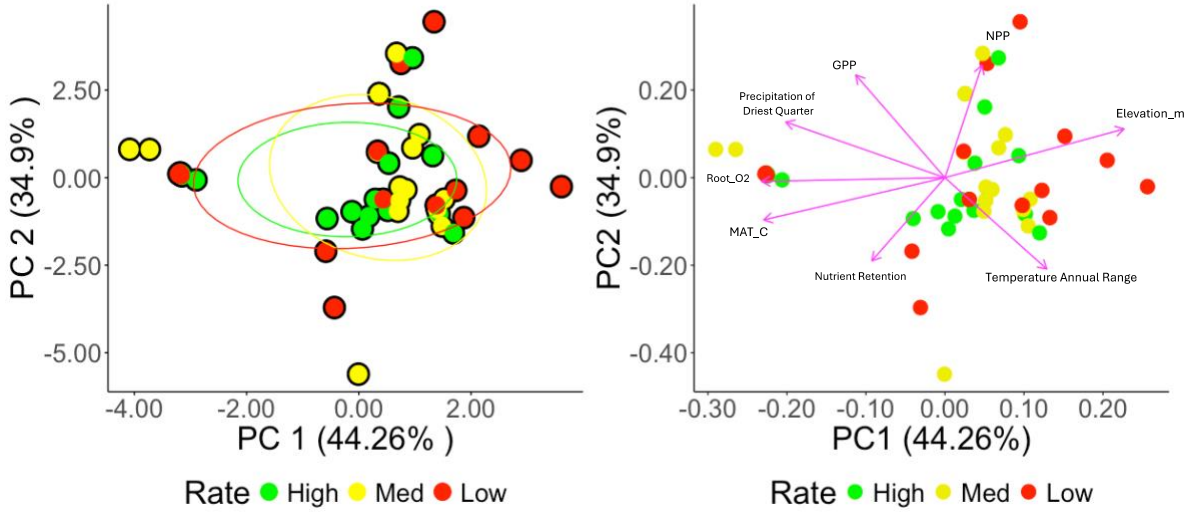

Figure 4.6 Principal Component Analysis (PCA) of African Peatland Accumulation Rates. A) PCA plot with peatland sites categorized by accumulation rates: high (green), medium (yellow), and low (red). The clustering and ellipses indicate the variation within each group along the two principal components, PC1 (44.26%) and PC2 (34.9%). B) Biplot of environmental and bioclimatic variables influencing the principal components, with vectors representing the direction and strength of each variable's influence. Key variables include root oxygen availability (Root_O2), Elevation_m, Bioclim factors, net primary productivity (NPP), and gross primary productivity (GPP).

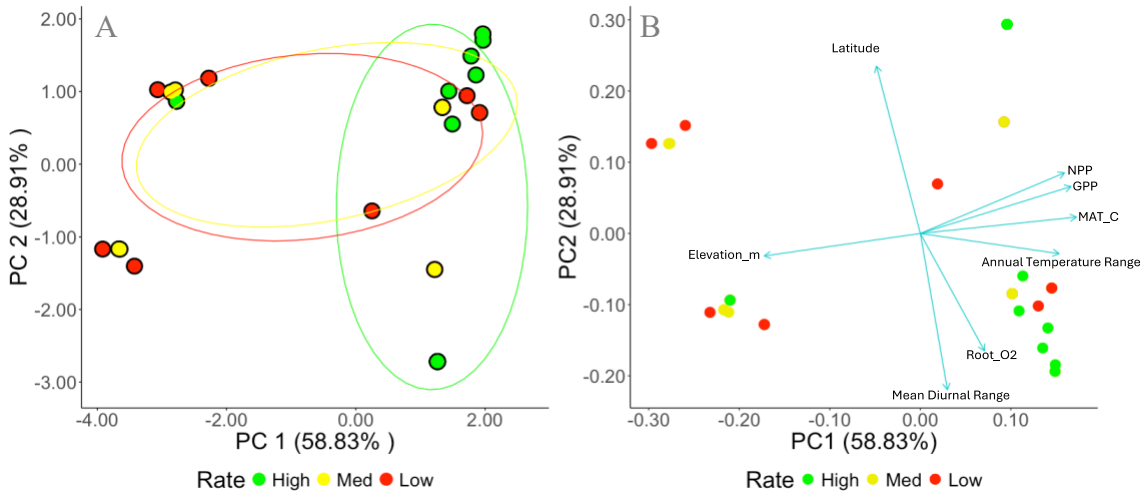

Figure 4.7 Principal Component Analysis (PCA) of Environmental Drivers of Peatland Accumulation Rates for Central South America. A) PCA plot showing peatland sites categorized by accumulation rates: high (green), medium (yellow), and low (red). The first two principal components (PC1 and PC2) explain 58.83% and 28.91% of the variance, respectively. Clustering patterns and 95% confidence ellipses indicate that high-accumulation sites form a distinct, tightly clustered group, while low-accumulation sites exhibit greater variability. Medium-accumulation sites overlap both groups, reflecting transitional environmental conditions. B) Biplot illustrating the environmental variables contributing to the principal components.

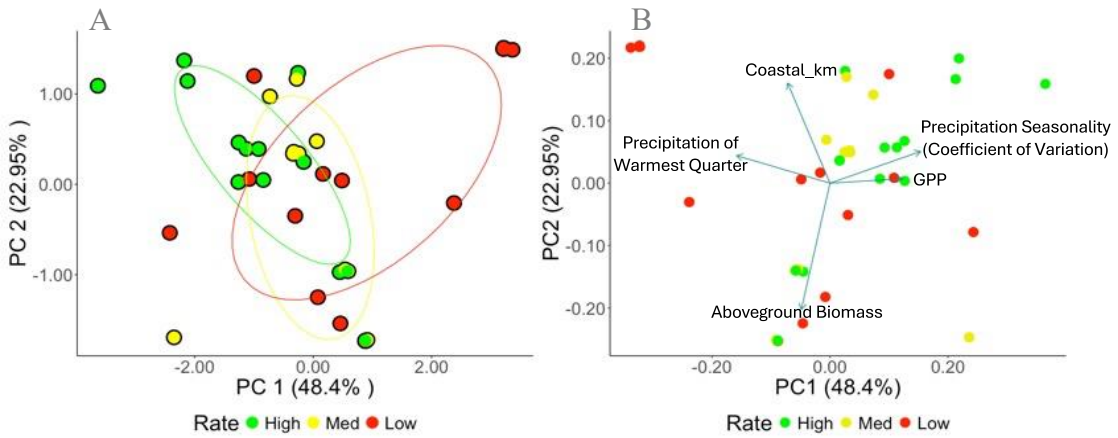

Figure 4.8 Principal Component Analysis (PCA) of Peatland Accumulation Rates for Southeast Asia. A) PCA plot with peatland sites categorized by accumulation rates: high (green), medium (yellow), and low (red). The clustering and ellipses indicate the variation within each group along the two principal components, PC1 (77.37%) and PC2 (10.42%). B) Biplot of environmental and bioclimatic variables influencing the principal components, with vectors representing the direction and strength of each variable's influence. Key variables include Elevation_m, radiocarbon value, Bioclim factors, and longitude.

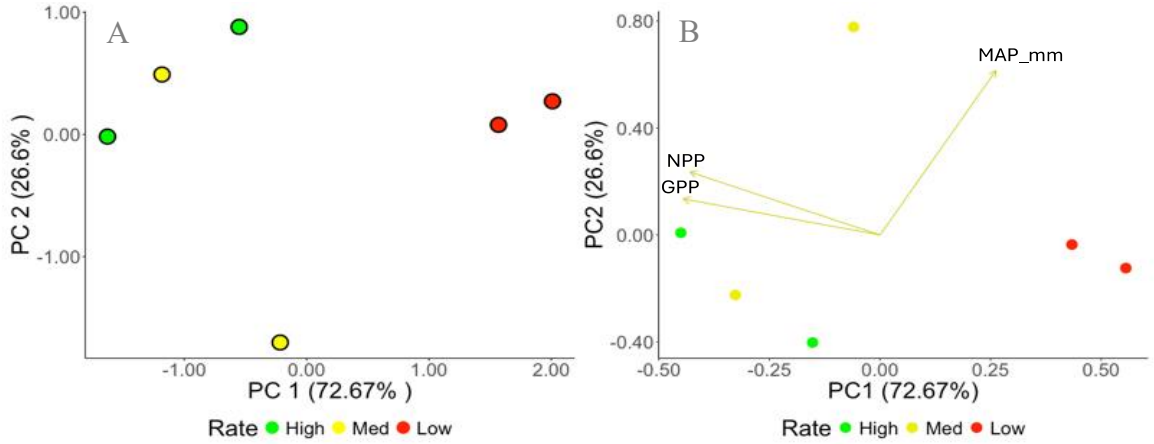

Figure 4.9 Principal Component Analysis (PCA) of Environmental Drivers of Peat Accumulation Rates in Hawaii. A) PCA plot showing peatland sites categorized by accumulation rates: high (green), medium (yellow), and low (red). The first two principal components, PC1 (72.67% variance explained) and PC2 (26.67% variance explained), account for 99.34% of the total variability. Clustering patterns indicate distinct separation between high- and low-accumulation rate sites, with medium-accumulation sites overlapping both groups, reflecting transitional environmental conditions. B) Biplot showing the environmental variables contributing to the principal components. Note: The Hawaii segment of this dataset is limited to just 6 cores. This small sample size may affect the robustness and generalizability of this analysis. Therefore, caution should be exercised when interpreting these correlations, as they may not fully represent the broader patterns observed in larger datasets or different regions.

4.7. Tables

Table 4-1 Regression output describing effect of PCA components on peat accumulation estimate across all regions and rates. Variation inflation factor (VIF) listed for all components included in the model.

Model Statistics	Value
Df	137
Residual Standard Error	0.15
R^2	0.11
R^2 adj	0.08
F Value	3.30
p-value	0.01

Component	VIF	Estimate	Std.Error	t Value	Pr(>|t|)	
(Intercept)		1.3E-01	1.2E-02	1.0E+01	<2e -16	***
PC1	1	-1.7E-02	7.2E-03	-2.4E+00	2.0E-02	*
PC2	1	-1.4E-03	1.2E-02	-1.2E-01	9.1E-01	
PC3	1	-4.9E-02	1.6E-02	-3.1E+00	2.5E-03	**
PC4	1	-2.1E-02	1.9E-02	-1.1E+00	2.7E-01	
PC5	1	5.2E-02	1.1E-01	4.8E-01	6.3E-01	

Signif. codes: 0 '***' 0.001 '**' 0.01 '*' 0.05 '.' 0.1 ' ' 1

Table 4-2 Metadata, units, and source for variables used in correlation matrixes for each region.

Variable	Description	Units	Source
$\Delta^{14}C$	Describes the radiocarbon concentrations of the peat layers reported as $\Delta^{14}C$	Δ14C	ISRAD
Vegetation_Cover	Total Plant Area Index based solely on GEDI lidar and validated with independent data.	m2 m^{-2}	NASA Global Ecosystem Dynamics Investigation (GEDI)
Topsoil_pH	pH, measured in a soil-water solution, is a measure for the acidity and alkalinity of the soil. This field gives the soil reaction of top- (0–30cm) soil.		Harmonized World Soil Database
TMIN_C	Min Temperature of Coldest Month	°C	ISRAD via WorldClim
TMAX_C	Max Temperature of Warmest Month	°C	ISRAD via WorldClim
Subsoil_pH	pH, measured in a soil-water solution, is a measure for the acidity and alkalinity of the soil. This field gives the soil reaction of sub- (30-100 cm) soil.		Harmonized World Soil Database
Site_long	Peatland site longitude	dec. degrees	ISRAD
Site_lat	Peatland site latitude	dec. degrees	ISRAD
Region	Peatland region as determined by geographic location	NA	Determined within this analysis using data from ISRAD
Nutrient_Retention	Nutrient retention capacity refers to the capacity of the soil to retain added nutrients against losses caused by leaching.		Harmonized World Soil Database
NPP	Net Primary Productivity	kg*C/m^2	MODIS
MAT_C	Mean Annual Temperature	°C	ISRAD via WorldClim
MAP_mm	Mean Annual Precipitation	mm	ISRAD via WorldClim

LARPA	LARCA, or long-term apparent rate of peat accumulation, is a measure of how quickly organic matter accumulates within a peatland	cm/year	Calculated for this study
Inundation	Inundation classification described by one of three states: upland area (0), minimum inundation area (1), maximum inundation area (2), long-term maximum inundation area (3)	NA	Global Inundation Extent from Multiple-Satellites (GIEMS)
GPP	Gross Primary Productivity	$kg*C/m^2$	MODIS
Elevation_m	Elevation of peatland site	m	Qgis
Coasta_km	Peatland distance/proximity to coast	km	Qgis
CalBP	Calibrated age; CalBP is an abbreviation for "calibrated years before the present" or "calendar years before the present" and is a notation which signifies that the raw radiocarbon date cited has been corrected using current methodologies.	CalBP (age)	Calculated for this study
Aboveground_Biomass	Predicted aboveground biomass density based solely on GEDI lidar and validated with independent data.	$Mg\ ha^{-1}$	NASA Global Ecosystem Dynamics Investigation (GEDI)
	Mean temperature of warmest quarter	°C	ISRAD via WorldClim
	Mean temperature of coldest quarter	°C	ISRAD via WorldClim
	Precipitation of Wettest Month	mm	ISRAD via WorldClim
	Precipitation of Driest Month	mm	ISRAD via WorldClim
	Precipitation Seasonality (Coefficient of Variation)		ISRAD via WorldClim
	Precipitation of Wettest Quarter	mm	ISRAD via WorldClim
	Precipitation of Driest Quarter	mm	ISRAD via WorldClim
	Precipitation of Warmest Quarter	mm	ISRAD via WorldClim
	Precipitation of Coldest Quarter	mm	ISRAD via WorldClim

	Mean Diurnal Range (Mean of monthly (max temp - min temp))	°C	ISRAD via WorldClim
	Isothermality (Bioclim2/Bioclim7) (×100)	°C	ISRAD via WorldClim
	Temperature Seasonality (standard deviation ×100)	°C	ISRAD via WorldClim
	Temperature Annual Range (BIO5-BIO6)	°C	ISRAD via WorldClim
	Mean Temperature of Wettest Quarter	°C	ISRAD via WorldClim
	Mean Temperature of Driest Quarter	°C	ISRAD via WorldClim

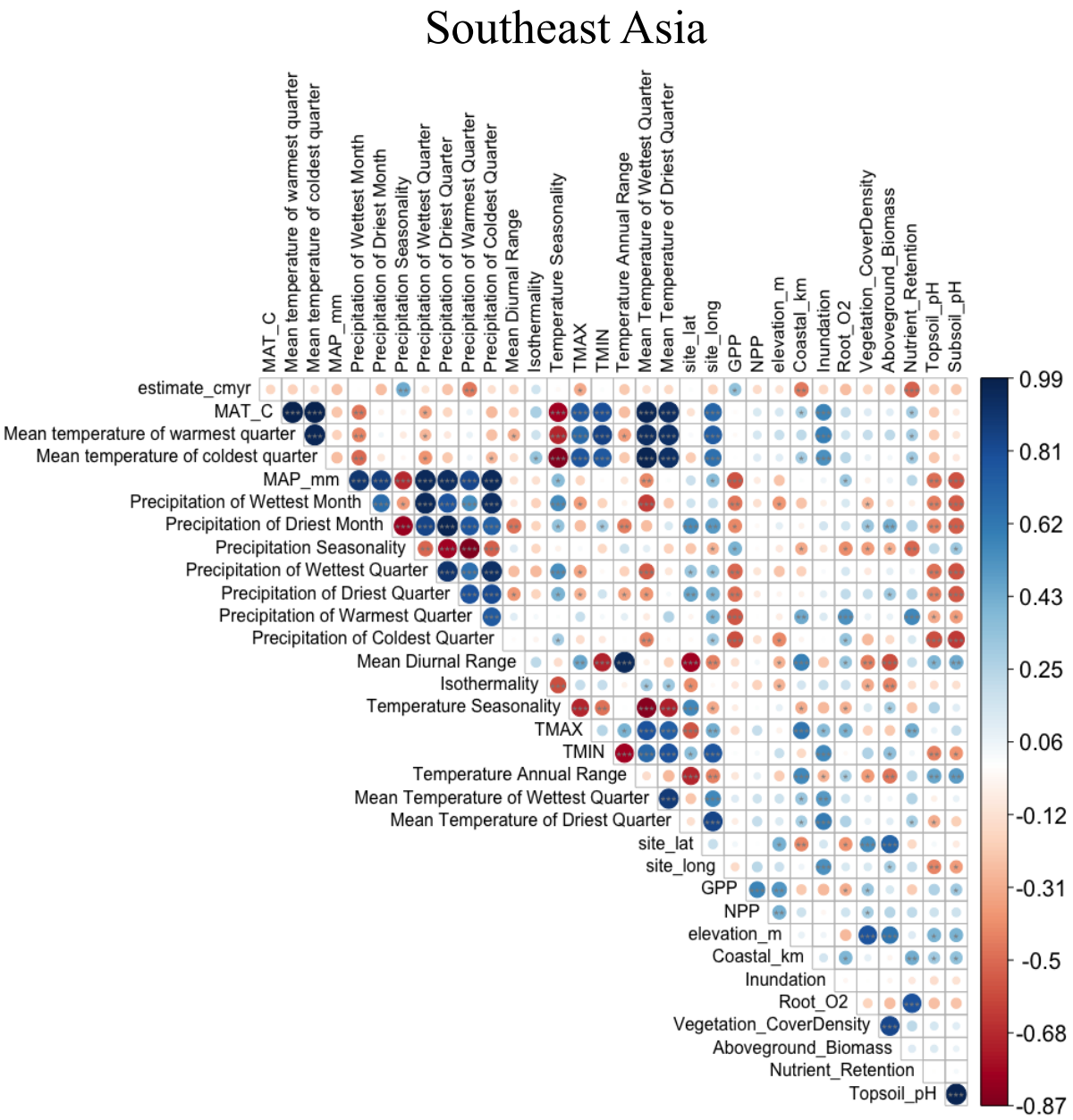

Appendix Figure 4-1 Correlation plot showing relationships between variables included in this study dataset for Southeast Asia. Variables that are positively correlated are indicated in blue, and variables that are negatively corelated are indicated in red. The significance of these correlations is indicated by the transparency of the circles, as well as by asterisks, where significance codes are as follows: 0 '***' 0.001 '**' 0.01 '*' 0.1 ' '

Africa

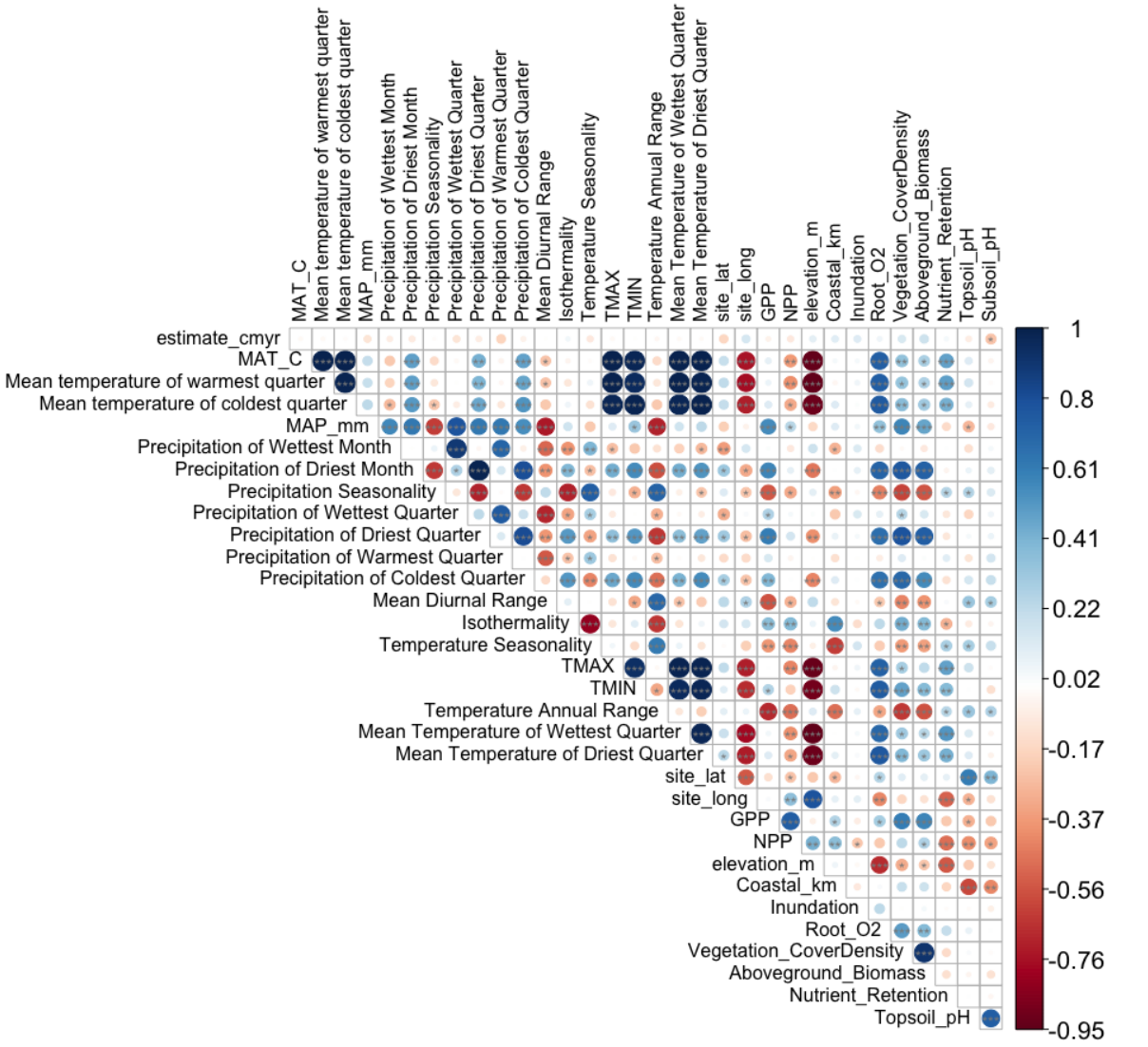

Appendix Figure 4-2 Correlation plot showing relationships between variables included in this study dataset for Africa. Variables that are positively correlated are indicated in blue, and variables that are negatively corelated are indicated in red. The significance of these correlations is indicated by the transparency of the circles, as well as by asterisks, where significance codes are as follows: 0 '***' 0.001 '**' 0.01 '*' 0.1 ' '

Central/South America

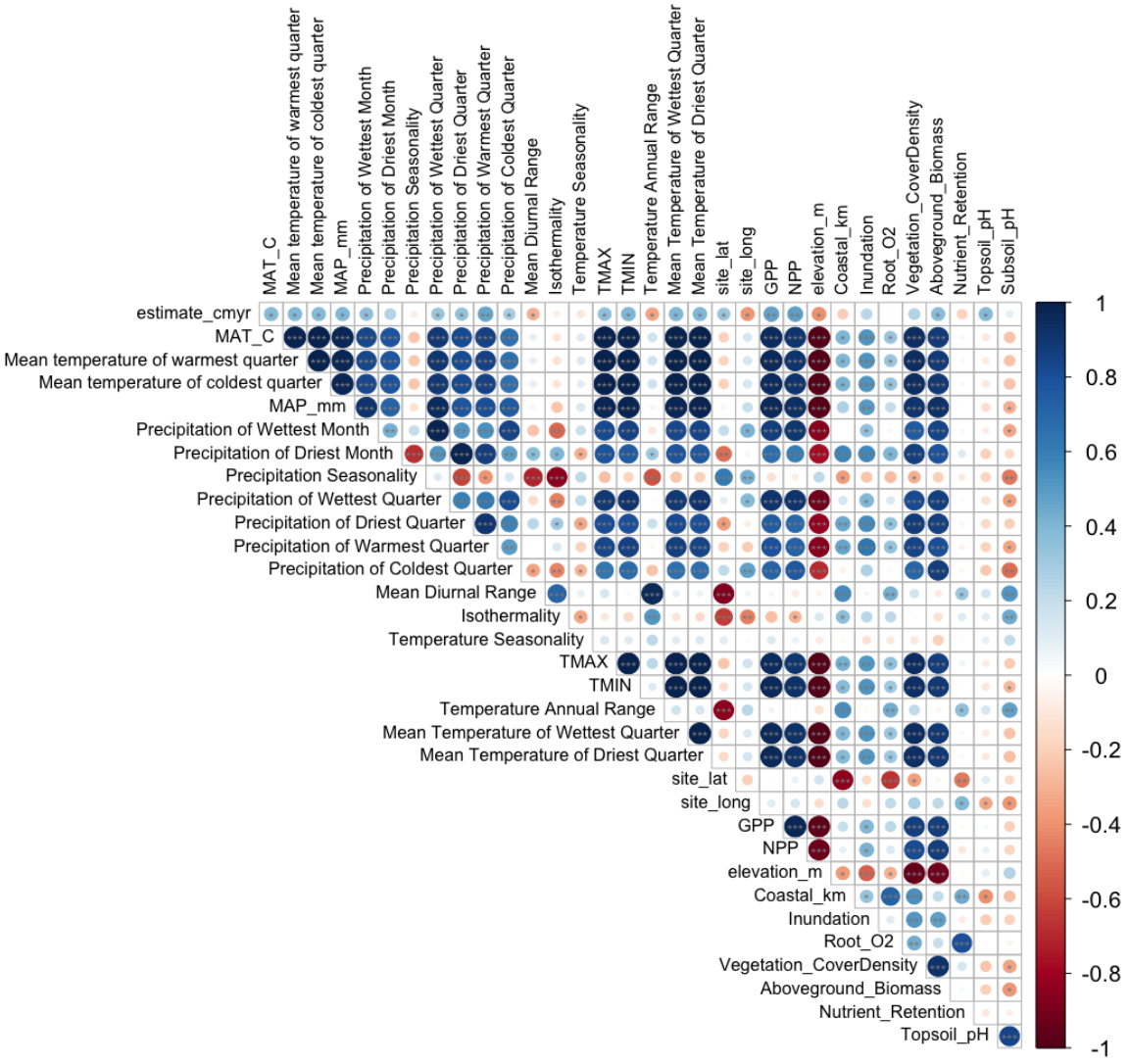

Appendix Figure 4-3 Correlation plot showing relationships between variables included in this study dataset for Central/South America. Variables that are positively correlated are indicated in blue, and variables that are negatively corelated are indicated in red. The significance of these correlations is indicated by the transparency of the circles, as well as by asterisks, where significance codes are as follows: 0 '***' 0.001 '**' 0.01 '*' 0.1 ' '

Hawaii

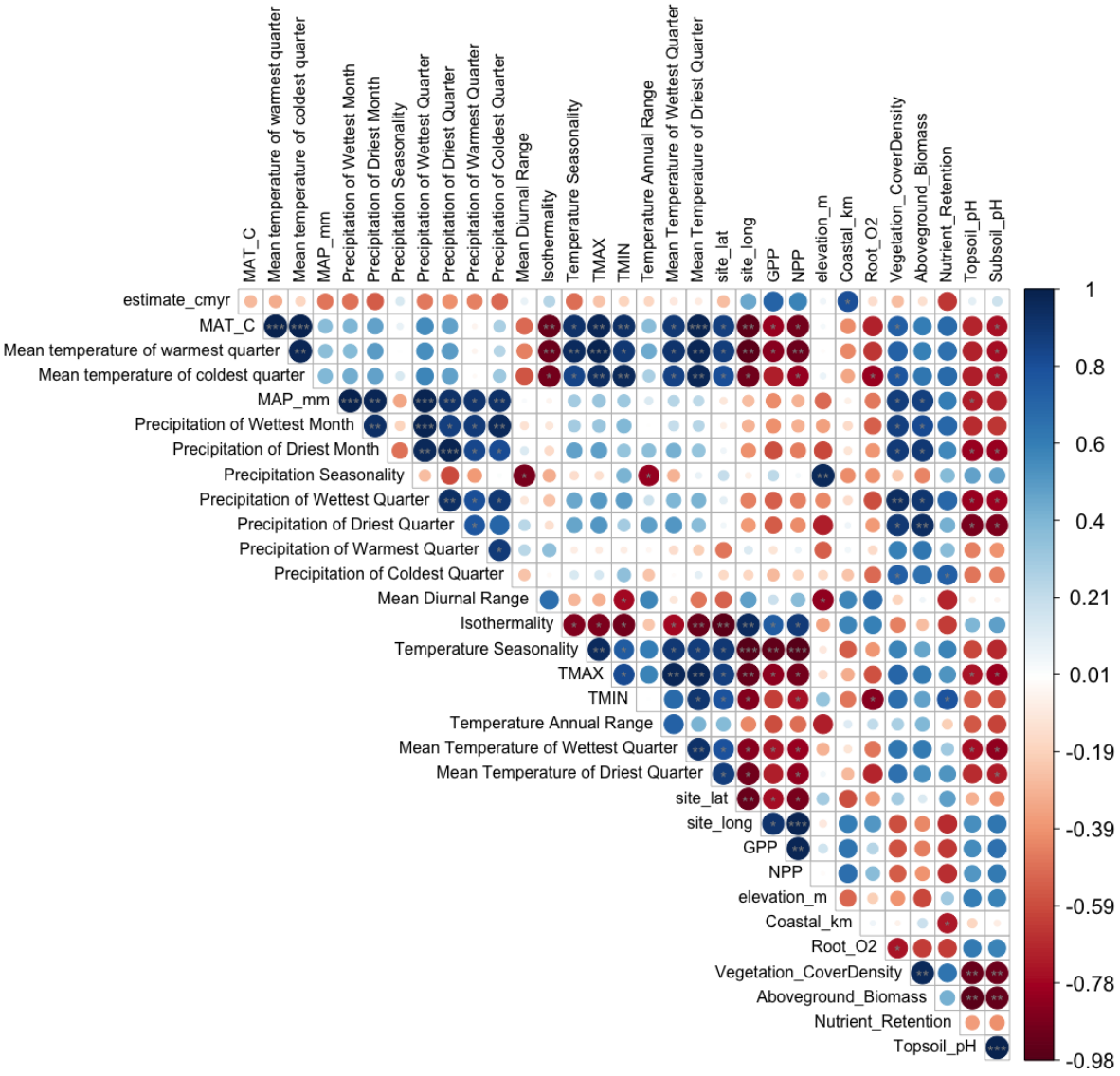

Appendix Figure 4-4 Correlation plot showing relationships between variables included in this study dataset for Hawaii. Variables that are positively correlated are indicated in blue, and variables that are negatively corelated are indicated in red. The significance of these correlations is indicated by the transparency of the circles, as well as by asterisks, where significance codes are as follows: 0 '***' 0.001 '**' 0.01 '*' 0.1 ' '

It is important to note that the Hawaii segment of this dataset is limited to just 6 cores. This small sample size may affect the robustness of the correlation results and their generalizability. Therefore, caution should be exercised when interpreting these correlations, as they may not fully represent the broader patterns observed in larger datasets or different regions.

Appendix Table 4.1 Principal Component Analysis (PCA) of possible drivers of peat accumulation and development across tropical regions. Peatland sites from different tropical regions: Africa, Central and South America, Hawaii, and Southeast Asia. Rates described as High (>0.16 cm/yr), Med (0.16 to 0.05 cm/yr) and low (<0.05 cm/yr). Table shows eigenvalues and loadings for the five principal components.

	PC1	**PC2**	**PC3**	**PC4**	**PC5**
Eigenvalues	**2.957**	**1.01**	**0.604**	**0.416**	**0.01**
Variable					
MAT_C	-0.55	0.06	0.20	-0.42	0.69
Elevation_m	0.55	-0.11	-0.29	0.30	0.71
Precipitation of Driest Quarter	-0.47	-0.2	0.24	0.83	0.08
GPP	-0.29	0.70	-0.62	0.18	0.0
Subsoil_pH	0.30	0.67	0.65	0.14	0.08

Appendix Table 4.2 Principal Component Analysis (PCA) of possible drivers of peat accumulation and development across African peatland sites included in this analysis. Table shows eigenvalues and loadings for the eight principal components.

	PC1	**PC2**	**PC3**	**PC4**	**PC5**	**PC6**	**PC7**	**PC8**
Eigenvalues	3.54	2.79	0.68	0.38	0.3	0.19	0.09	0.04
Variables								
MAT_C	-0.47	-0.20	0.04	-0.35	0.38	0.06	-0.19	0.66
elevation_m	0.46	0.23	-0.12	0.26	-0.28	-0.29	-0.16	0.68
Precipitation of Driest Quarter	-0.41	0.26	-0.30	0.29	-0.40	0.55	-0.35	0.03
GPP	-0.23	0.48	0.35	-0.22	-0.31	0.08	0.64	0.20
Nutrient_Retention	-0.19	-0.39	0.73	0.41	-0.28	-0.08	-0.17	0.04
Temperature Annual Range	0.26	-0.43	-0.04	-0.60	-0.57	0.22	-0.08	0.03
Root_O2	-0.48	-0.02	-0.29	-0.12	-0.34	-0.73	-0.07	-0.15
NPP	0.10	0.53	0.39	-0.37	0.05	-0.10	-0.61	-0.20

Appendix Table 4.3 Regression output describing effect of PCA components on peat accumulation estimate across African peatlands included in the analysis.

Model Statistics					
Df	47				
Residual Standard Error	0.17				
R2	0.15				
R2 adj	0.00				
F Value	1.03				
p-value	0.43				
Components	**Estimate**	**Std.Error**	**t Value**	**Pr(>|t|)**	
(Intercept)	0.12	0.02	5.22	<2e-16	***
PC1	0.01	0.01	0.51	0.61	
PC2	-0	0.01	-0.3	0.75	
PC3	-0	0.03	-0.2	0.85	
PC4	0.04	0.04	1.07	0.29	
PC5	-0	0.04	-0	0.98	
PC6	-0.1	0.05	-1.9	0.07	.
PC7	0.06	0.08	0.78	0.44	
PC8	0.2	0.12	1.63	0.11	

Signif. codes: 0 '***' 0.001 '**' 0.01 '*' 0.05 '.' 0.1 ' ' 1

Appendix Table 4.4 Principal Component Analysis (PCA) of possible drivers of peat accumulation and development across Central South America peatland sites included in this analysis. Table shows eigenvalues and loadings for the eight principal components.

	PC1	**PC2**	**PC3**	**PC4**	**PC5**	**PC6**	**PC7**	**PC8**
Eigenvalues	4.71	2.31	0.57	0.28	0.09	0.03	0.01	0.00
Variables								
MAT_C	0.45	0.06	0.00	-0.08	0.42	0.34	-0.09	-0.69
Mean Diurnal Range	0.08	-0.58	0.50	-0.37	-0.36	0.36	-0.05	0.01
Latitude	-0.13	0.62	-0.11	-0.08	-0.49	0.58	-0.11	-0.02
Elevation_m	-0.45	-0.08	0.00	0.04	-0.37	-0.29	0.25	-0.71
Temperature Annual Range	0.40	-0.07	0.20	0.82	-0.34	0.02	0.00	-0.03
GPP	0.44	0.17	-0.02	-0.25	-0.15	-0.08	0.82	0.09
Root_O2	0.19	-0.43	-0.83	-0.04	-0.26	0.11	-0.08	-0.01
NPP	0.42	0.22	0.07	-0.33	-0.33	-0.56	-0.48	-0.08

Appendix Table 4.5 Regression output describing effect of PCA components on peat accumulation estimate across Central South American peatlands included in the analysis.

Model Statistics	
Df	28
Residual Standard Error	0.08
R2	0.45
R2 adj	0.30
F Value	2.91
p-value	0.02

Components	**Estimate**	**Std.Error**	**t Value**	**Pr(>|t|)**	
(Intercept)	0.11	0.01	8.99	0.00	***
PC1	0.02	0.01	2.79	0.01	**
PC2	0.02	0.01	2.80	0.01	**
PC3	-0.02	0.02	-1.00	0.33	
PC4	0.02	0.02	0.64	0.53	
PC5	-0.09	0.04	-2.12	0.04	*
PC6	0.06	0.07	0.88	0.39	
PC7	-0.01	0.12	-0.07	0.94	
PC8	-0.52	0.52	-0.99	0.33	

Signif. codes: 0 '***' 0.001 '**' 0.01 '*' 0.05 '.' 0.1 ' ' 1

Appendix Table 4.6 Principal Component Analysis (PCA) of possible drivers of peat accumulation and development across Southeast Asia peatland sites included in this analysis. Table shows eigenvalues and loadings for the five principal components.

	PC1	**PC2**	**PC3**	**PC4**	**PC5**
Eigenvalues	2.42	1.15	0.87	0.42	0.14
Variables					
Precipitation Seasonality (Coefficient of Variation)	0.58	0.19	-0.08	0.48	0.63
Coastal_km	-0.27	0.60	0.63	0.39	-0.15
Precipitation of Warmest Quarter	-0.59	0.17	-0.05	-0.32	0.72
GPP	0.46	0.03	0.60	-0.64	0.13
Aboveground_Biomass	-0.18	-0.76	0.49	0.33	0.21

Appendix Table 4.7 Regression output describing effect of PCA components on peat accumulation estimate across Southeast Asia peatlands included in the analysis.

Model Statistics	
Df	35
Residual Standard Error	0.13
R2	0.51
R2 adj	0.44
F Value	7.35
p-value	8.45E-05

Components	**Estimate**	**Std.Error**	**t Value**	**Pr(>|t|)**	
(Intercept)	0.17	0.02	8.16	1.32E-09	***
PC1	0.06	0.01	4.77	3.25E-05	***
PC2	0.02	0.02	1.24	0.22	
PC3	-0.01	0.02	-0.31	0.76	
PC4	-0.02	0.03	-0.77	0.45	
PC5	0.19	0.06	3.44	1.52E-03	**

Signif. codes: 0 '***' 0.001 '**' 0.01 '*' 0.05 '.' 0.1 ' ' 1

Appendix Table 4.8 Principal Component Analysis (PCA) of possible drivers of peat accumulation and development across Hawaii peatland sites included in this analysis. Table shows eigenvalues and loadings for the three principal components.

	PC1	**PC2**	**PC3**
Eigenvalues	2.18	0.80	0.02
Variables			
MAP_mm	0.39	0.91	-0.10
NPP	-0.64	0.35	0.68
GPP	-0.66	0.20	-0.72

5. Concluding thoughts and a message for future peatland research

Peatlands are among the most crucial C reservoirs on Earth, serving as long-term C sinks that help regulate atmospheric greenhouse gases, particularly CO_2 and CH_4. However, peatlands are also highly vulnerable to the accelerating impacts of climate change and human disturbances, placing their stability as C sinks in jeopardy. This dissertation has highlighted the importance of peatland ecosystems within the global C cycle by investigating the complex C dynamics of tropical and boreal peatlands, along with insights from a global synthesis of radiocarbon profiles. Together, these findings underscore the need for intensified research and conservation efforts, as peatlands' dual role as both C reservoirs and potential sources of greenhouse gases makes them critical ecosystems for effective climate mitigation.

The results of this dissertation point to critical, understudied processes that govern peatland C storage. In tropical peatlands, where this research has shown that surface-derived dissolved organic carbon is an essential contributor to microbial respiration at depth, our understanding of C cycling is broadened, suggesting that surface C inputs have a deeper, more extensive influence on the ecosystem than previously thought. This dynamic raises concerns, as any changes to surface vegetation or hydrology could have cascading impacts on deep C stability, a particular risk in tropical peatlands, where climate shifts and land-use pressures are intense. In boreal peatlands, the experimental results demonstrate that surface and shallow peat layers are especially vulnerable to warming, potentially transforming these regions from C sinks into sources as temperatures rise. The relatively stable C found in deeper peat layers, while encouraging, cannot counterbalance the accelerated C losses from shallower layers. These findings highlight the importance of conserving boreal peatlands' surface and intermediate layers to prevent substantial greenhouse gas releases under warming scenarios.

Looking ahead, there is an urgent need to focus peatland research on region-specific processes that dictate C retention and vulnerability across tropical, temperate, and boreal peatlands. Comparative studies are essential to identify how varying climate conditions, hydrological shifts, and microbial pathways contribute to each peatland's capacity to store C and regulate methane emissions. This understanding is critical to accurately model peatland responses to future climate change, as changes in precipitation, temperature, and human land use will likely stress these ecosystems further. Expanding interdisciplinary research efforts that integrate field studies, remote sensing, isotopic analysis, and modeling will be instrumental in building a holistic understanding of peatland responses. Moreover, prioritizing research on methane dynamics in peatlands is critical, as these emissions have high short-term climate impacts, making them a focal point for immediate climate action.

This dissertation underscores the necessity of proactive peatland conservation and restoration measures worldwide, particularly as evidence mounts that climate-driven changes are pushing peatlands closer to becoming net C sources. Protecting these ecosystems is not only a matter of preserving biodiversity but also an essential strategy for reducing greenhouse gas emissions on a global scale. Governments, researchers, and conservationists must intensify efforts to protect intact peatlands, restore degraded ones, and consider peatland dynamics in climate policy. Peatlands are natural climate regulators, but their role is contingent on maintaining the delicate balance of conditions that have allowed them to sequester C for millennia. Without decisive action to protect these ecosystems, peatlands could become a powerful, destabilizing force in the global climate system rather than a mitigating one. The future of peatlands is therefore not just a matter of scientific interest but a pressing component of effective, urgent climate action.

6. References

Aliev, A. E. (2020). Solid state NMR spectroscopy. In P. Hodgkinson (Ed.), *Nuclear Magnetic Resonance* (1st ed., pp. 139–187). The Royal Society of Chemistry. https://doi.org/10.1039/9781788010665-00139

Anderson, J. A. R., & Muller, J. (1975). Palynological study of a holocene peat and a miocene coal deposit from NW Borneo. *Review of Palaeobotany and Palynology*, *19*(4), 291–351. https://doi.org/10.1016/0034-6667(75)90049-4

Aravena, R., Warner, B. G., Charman, D. J., Belyea, L. R., Mathur, S. P., & Dinel, H. (1993). Carbon Isotopic Composition of Deep Carbon Gases in an Ombrogenous Peatland, Northwestern Ontario, Canada. *Radiocarbon*, *35*(2), 271–276. https://doi.org/10.1017/S0033822200064948

Bader, C., Müller, M., Schulin, R., & Leifeld, J. (2018). Peat decomposability in managed organic soils in relation to land use, organic matter composition and temperature. *Biogeosciences*, *15*(3), 703–719. https://doi.org/10.5194/bg-15-703-2018

Baldock, J. A., Masiello, C. A., Gélinas, Y., & Hedges, J. I. (2004). Cycling and composition of organic matter in terrestrial and marine ecosystems. *Marine Chemistry*, *92*(1–4), 39–64. https://doi.org/10.1016/j.marchem.2004.06.016

Barreto, C., & Lindo, Z. (2020). Decomposition in Peatlands: Who Are the Players and What Affects Them? *Frontiers for Young Minds*, *8*, 107. https://doi.org/10.3389/frym.2020.00107

Beilman, D. W., Massa, C., Nichols, J. E., Elison Timm, O., Kallstrom, R., & Dunbar-Co, S. (2019). Dynamic Holocene Vegetation and North Pacific Hydroclimate Recorded in a Mountain Peatland, Moloka‘i, Hawai‘i. *Frontiers in Earth Science*, *7*, 188. https://doi.org/10.3389/feart.2019.00188

Blodau, C., Basiliko, N., & Moore, T. R. (2004). Carbon turnover in peatland mesocosms exposed to different water table levels. *Biogeochemistry*, *67*(3), 331–351. https://doi.org/10.1023/B:BIOG.0000015788.30164.e2

Broek, T. A. B., Ognibene, T. J., McFarlane, K. J., Moreland, K. C., Brown, T. A., & Bench, G. (2021). Conversion of the LLNL/CAMS 1 MV biomedical AMS system to a semi-automated natural abundance 14C spectrometer: System optimization and performance evaluation. *Nuclear Instruments and Methods in Physics Research Section B: Beam Interactions with Materials and Atoms*, *499*, 124–132. https://doi.org/10.1016/j.nimb.2021.01.022

Chanton, J. P., Bauer, J. E., Glaser, P. A., Siegel, D. I., Kelley, C. A., Tyler, S. C., Romanowicz, E. H., & Lazrus, A. (1995). Radiocarbon evidence for the substrates supporting methane formation within northern Minnesota peatlands. *Geochimica et Cosmochimica Acta*, *59*(17), 3663–3668. https://doi.org/10.1016/0016-7037(95)00240-Z

Chanton, J. P., Glaser, P. H., Chasar, L. S., Burdige, D. J., Hines, M. E., Siegel, D. I., Tremblay, L. B., & Cooper, W. T. (2008). Radiocarbon evidence for the importance of surface vegetation on fermentation and methanogenesis in contrasting types of boreal peatlands. *Global Biogeochemical Cycles*, *22*(4), 2008GB003274. https://doi.org/10.1029/2008GB003274

Charman, D. J., Aravena, R., Bryant, C. L., & Harkness, D. D. (1999). Carbon isotopes in peat, DOC, CO2, and CH4 in a Holocene peatland on Dartmoor, southwest England. *Geology*, *27*(6), 539. https://doi.org/10.1130/0091-7613(1999)027<0539:CIIPDC>2.3.CO;2

Chen, X., Xue, D., Wang, Y., Qiu, Q., Wu, L., Wang, M., Liu, J., & Chen, H. (2023). Variations in the archaeal community and associated methanogenesis in peat profiles of three typical

peatland types in China. *Environmental Microbiome*, *18*(1), 48. https://doi.org/10.1186/s40793-023-00503-y

Chimner, R. A. (2004). Soil respiration rates of tropical peatlands in Micronesia and Hawaii. *Wetlands*, *24*(1), 51–56. https://doi.org/10.1672/0277-5212(2004)024[0051:SRROTP]2.0.CO;2

Clymo, R. S., & Bryant, C. L. (2008). Diffusion and mass flow of dissolved carbon dioxide, methane, and dissolved organic carbon in a 7-m deep raised peat bog. *Geochimica et Cosmochimica Acta*, *72*(8), 2048–2066. https://doi.org/10.1016/j.gca.2008.01.032

Clymo, R. S., Turunen, J., & Tolonen, K. (1998). Carbon Accumulation in Peatland. *Oikos*, *81*(2), 368. https://doi.org/10.2307/3547057

Cobb, A. R., Hoyt, A. M., Gandois, L., Eri, J., Dommain, R., Abu Salim, K., Kai, F. M., Haji Su'ut, N. S., & Harvey, C. F. (2017). How temporal patterns in rainfall determine the geomorphology and carbon fluxes of tropical peatlands. *Proceedings of the National Academy of Sciences*, *114*(26). https://doi.org/10.1073/pnas.1701090114

Cohen, A. D., Raymond, R., Ramirez, A., Morales, Z., & Ponce, F. (1989). The Changuinola peat deposit of northwestern Panama: A tropical, back-barrier, peat(coal)-forming environment. *International Journal of Coal Geology*, *12*(1–4), 157–192. https://doi.org/10.1016/0166-5162(89)90050-5

Conrad, R. (2020). Importance of hydrogenotrophic, aceticlastic and methylotrophic methanogenesis for methane production in terrestrial, aquatic and other anoxic environments: A mini review. *Pedosphere*, *30*(1), 25–39. https://doi.org/10.1016/S1002-0160(18)60052-9

Corbett, J. E., Tfaily, M. M., Burdige, D. J., Cooper, W. T., Glaser, P. H., & Chanton, J. P. (2013). Partitioning pathways of CO2 production in peatlands with stable carbon isotopes. *Biogeochemistry*, *114*(1–3), 327–340. https://doi.org/10.1007/s10533-012-9813-1

Cusack, D. F., Markesteijn, L., Condit, R., Lewis, O. T., & Turner, B. L. (2018). Soil carbon stocks across tropical forests of Panama regulated by base cation effects on fine roots. *Biogeochemistry*, *137*(1–2), 253–266. https://doi.org/10.1007/s10533-017-0416-8

Dargie, G. C., Lewis, S. L., Lawson, I. T., Mitchard, E. T. A., Page, S. E., Bocko, Y. E., & Ifo, S. A. (2017). Age, extent and carbon storage of the central Congo Basin peatland complex. *Nature*, *542*(7639), 86–90. https://doi.org/10.1038/nature21048

Dhandapani, S., Evers, S., Boyd, D., Evans, C. D., Page, S., Parish, F., & Sjogersten, S. (2023). Assessment of differences in peat physico-chemical properties, surface subsidence and GHG emissions between the major land-uses of Selangor peatlands. *CATENA*, *230*, 107255. https://doi.org/10.1016/j.catena.2023.107255

Dhandapani, S., Girkin, N. T., & Evers, S. (2022). Spatial variability of surface peat properties and carbon emissions in a tropical peatland oil palm monoculture during a dry season. *Soil Use and Management*, *38*(1), 381–395. https://doi.org/10.1111/sum.12741

Dommain, R., Cobb, A. R., Joosten, H., Glaser, P. H., Chua, A. F. L., Gandois, L., Kai, F., Noren, A., Salim, K. A., Su'ut, N. S. H., & Harvey, C. F. (2015). Forest dynamics and tip-up pools drive pulses of high carbon accumulation rates in a tropical peat dome in Borneo (Southeast Asia). *Journal of Geophysical Research: Biogeosciences*, *120*(4), 617–640. https://doi.org/10.1002/2014JG002796

Dommain, R., Couwenberg, J., & Joosten, H. (2011). Development and carbon sequestration of tropical peat domes in south-east Asia: Links to post-glacial sea-level changes and

Holocene climate variability. *Quaternary Science Reviews*, *30*(7–8), 999–1010. https://doi.org/10.1016/j.quascirev.2011.01.018

Draper, F. C., Roucoux, K. H., Lawson, I. T., Mitchard, E. T. A., Honorio Coronado, E. N., Lähteenoja, O., Torres Montenegro, L., Valderrama Sandoval, E., Zaráte, R., & Baker, T. R. (2014). The distribution and amount of carbon in the largest peatland complex in Amazonia. *Environmental Research Letters*, *9*(12), 124017. https://doi.org/10.1088/1748-9326/9/12/124017

Elizabeth Corbett, J., Burdige, D. J., Tfaily, M. M., Dial, A. R., Cooper, W. T., Glaser, P. H., & Chanton, J. P. (2013). Surface production fuels deep heterotrophic respiration in northern peatlands. *Global Biogeochemical Cycles*, *27*(4), 1163–1174. https://doi.org/10.1002/2013GB004677

Farmer, J., Matthews, R., Smith, J. U., Smith, P., & Singh, B. K. (2011). Assessing existing peatland models for their applicability for modelling greenhouse gas emissions from tropical peat soils. *Current Opinion in Environmental Sustainability*, *3*(5), 339–349. https://doi.org/10.1016/j.cosust.2011.08.010

Fritts, R. (2022). Tropical Wetlands Emit More Methane Than Previously‐Thought. *Eos*, *103*. https://doi.org/10.1029/2022EO220443

Gandois, L., Teisserenc, R., Cobb, A. R., Chieng, H. I., Lim, L. B. L., Kamariah, A. S., Hoyt, A., & Harvey, C. F. (2014). Origin, composition, and transformation of dissolved organic matter in tropical peatlands. *Geochimica et Cosmochimica Acta*, *137*, 35–47. https://doi.org/10.1016/j.gca.2014.03.012

Gelman, A., & Hill, J. (2021). *Data analysis using regression and multilevel/hierarchical models* (23rd printing). Cambridge Univ. Press.

Gill, A. L., Giasson, M., Yu, R., & Finzi, A. C. (2017). Deep peat warming increases surface methane and carbon dioxide emissions in a black spruce-dominated ombrotrophic bog. *Global Change Biology*, *23*(12), 5398–5411. https://doi.org/10.1111/gcb.13806

Girkin, N. T., Cooper, H. V., Ledger, M. J., O'Reilly, P., Thornton, S. A., Åkesson, C. M., Cole, L. E. S., Hapsari, K. A., Hawthorne, D., & Roucoux, K. H. (2022). Tropical peatlands in the Anthropocene: The present and the future. *Anthropocene*, *40*, 100354. https://doi.org/10.1016/j.ancene.2022.100354

Girkin, N. T., Dhandapani, S., Evers, S., Ostle, N., Turner, B. L., & Sjögersten, S. (2020). Interactions between labile carbon, temperature and land use regulate carbon dioxide and methane production in tropical peat. *Biogeochemistry*, *147*(1), 87–97. https://doi.org/10.1007/s10533-019-00632-y

Girkin, N. T., Turner, B. L., Ostle, N., Craigon, J., & Sjögersten, S. (2018). Root exudate analogues accelerate CO2 and CH4 production in tropical peat. *Soil Biology and Biochemistry*, *117*, 48–55. https://doi.org/10.1016/j.soilbio.2017.11.008

Girkin, N. T., Turner, B. L., Ostle, N., & Sjögersten, S. (2018). Composition and concentration of root exudate analogues regulate greenhouse gas fluxes from tropical peat. *Soil Biology and Biochemistry*, *127*, 280–285. https://doi.org/10.1016/j.soilbio.2018.09.033

Girkin, N. T., Vane, C. H., Cooper, H. V., Moss-Hayes, V., Craigon, J., Turner, B. L., Ostle, N., & Sjögersten, S. (2019). Spatial variability of organic matter properties determines methane fluxes in a tropical forested peatland. *Biogeochemistry*, *142*(2), 231–245. https://doi.org/10.1007/s10533-018-0531-1

Goldstein, A., Turner, W. R., Spawn, S. A., Anderson-Teixeira, K. J., Cook-Patton, S., Fargione, J., Gibbs, H. K., Griscom, B., Hewson, J. H., Howard, J. F., Ledezma, J. C., Page, S.,

Koh, L. P., Rockström, J., Sanderman, J., & Hole, D. G. (2020). Protecting irrecoverable carbon in Earth's ecosystems. *Nature Climate Change*, *10*(4), 287–295. https://doi.org/10.1038/s41558-020-0738-8

Gruca-Rokosz, R., & Koszelnik, P. (2018). Production pathways for CH4 and CO2 in sediments of two freshwater ecosystems in south-eastern Poland. *PLOS ONE*, *13*(6), e0199755. https://doi.org/10.1371/journal.pone.0199755

Gumbricht, T., Roman-Cuesta, R. M., Verchot, L., Herold, M., Wittmann, F., Householder, E., Herold, N., & Murdiyarso, D. (2017). An expert system model for mapping tropical wetlands and peatlands reveals South America as the largest contributor. *Global Change Biology*, *23*(9), 3581–3599. https://doi.org/10.1111/gcb.13689

Hanson, P. J., Griffiths, N. A., Iversen, C. M., Norby, R. J., Sebestyen, S. D., Phillips, J. R., Chanton, J. P., Kolka, R. K., Malhotra, A., Oleheiser, K. C., Warren, J. M., Shi, X., Yang, X., Mao, J., & Ricciuto, D. M. (2020). Rapid Net Carbon Loss From a Whole-Ecosystem Warmed Peatland. *AGU Advances*, *1*(3). https://doi.org/10.1029/2020AV000163

Hanson, P. J., Riggs, J. S., Nettles, W. R., Phillips, J. R., Krassovski, M. B., Hook, L. A., Gu, L., Richardson, A. D., Aubrecht, D. M., Ricciuto, D. M., Warren, J. M., & Barbier, C. (2017). Attaining whole-ecosystem warming using air and deep-soil heating methods with an elevated CO₂ atmosphere. *Biogeosciences*, *14*(4), 861–883. https://doi.org/10.5194/bg-14-861-2017

Hanson, P., Phillips, J., Brice, D., Hook, L., & Guilliams, M. (2018). *SPRUCE Bog Surface Elevation Assessments with SET Instrument Beginning in 2013* [Dataset]. Oak Ridge National Laboratory (ORNL), Oak Ridge, TN (United States). https://doi.org/10.25581/SPRUCE.055/1455014

Hanson, P., Riggs, J., Nettles, W., Krassovski, M., & Hook, L. (2016). *SPRUCE Whole Ecosystems Warming (WEW) Environmental Data Beginning August 2015* [Dataset]. ORNL (Oak Ridge National Laboratory (ORNL), Oak Ridge, TN (United States)). https://doi.org/10.3334/CDIAC/SPRUCE.032

Harenda, K. M., Lamentowicz, M., Samson, M., & Chojnicki, B. H. (2018). The Role of Peatlands and Their Carbon Storage Function in the Context of Climate Change. In T. Zielinski, I. Sagan, & W. Surosz (Eds.), *Interdisciplinary Approaches for Sustainable Development Goals* (pp. 169–187). Springer International Publishing. https://doi.org/10.1007/978-3-319-71788-3_12

Hergoualc'h, K., & Verchot, L. V. (2011). Stocks and fluxes of carbon associated with land use change in Southeast Asian tropical peatlands: A review: PEATLAND CARBON DYNAMICS AND LAND USE CHANGE IN SOUTHEAST ASIA. *Global Biogeochemical Cycles*, *25*(2), n/a-n/a. https://doi.org/10.1029/2009GB003718

Hirano, T., Jauhiainen, J., Inoue, T., & Takahashi, H. (2009). Controls on the Carbon Balance of Tropical Peatlands. *Ecosystems*, *12*(6), 873–887. https://doi.org/10.1007/s10021-008-9209-1

Hodgkins, S. B., Richardson, C. J., Dommain, R., Wang, H., Glaser, P. H., Verbeke, B., Winkler, B. R., Cobb, A. R., Rich, V. I., Missilmani, M., Flanagan, N., Ho, M., Hoyt, A. M., Harvey, C. F., Vining, S. R., Hough, M. A., Moore, T. R., Richard, P. J. H., De La Cruz, F. B., … Chanton, J. P. (2018). Tropical peatland carbon storage linked to global latitudinal trends in peat recalcitrance. *Nature Communications*, *9*(1), 3640. https://doi.org/10.1038/s41467-018-06050-2

Holden, J., & Burt, T. P. (2003). Hydrological studies on blanket peat: The significance of the acrotelm-catotelm model. *Journal of Ecology*, *91*(1), 86–102. https://doi.org/10.1046/j.1365-2745.2003.00748.x

Holmes, M. E., Chanton, J. P., Tfaily, M. M., & Ogram, A. (2015). CO_2 and CH_4 isotope compositions and production pathways in a tropical peatland. *Global Biogeochemical Cycles*, *29*(1), 1–18. https://doi.org/10.1002/2014GB004951

Hooijer, A., Page, S., Jauhiainen, J., Lee, W. A., Lu, X. X., Idris, A., & Anshari, G. (2012). Subsidence and carbon loss in drained tropical peatlands. *Biogeosciences*, *9*(3), 1053–1071. https://doi.org/10.5194/bg-9-1053-2012

Hopple, A. M., Wilson, R. M., Kolton, M., Zalman, C. A., Chanton, J. P., Kostka, J., Hanson, P. J., Keller, J. K., & Bridgham, S. D. (2020). Massive peatland carbon banks vulnerable to rising temperatures. *Nature Communications*, *11*(1), 2373. https://doi.org/10.1038/s41467-020-16311-8

Hornibrook, E. R. C., Longstaffe, F. J., & Fyfe, W. S. (2000). Evolution of stable carbon isotope compositions for methane and carbon dioxide in freshwater wetlands and other anaerobic environments. *Geochimica et Cosmochimica Acta*, *64*(6), 1013–1027. https://doi.org/10.1016/S0016-7037(99)00321-X

Hoyos-Santillan, J. (2014). *2014 Hoyos Controls of Carbon Turnover in Tropical Peatlands*. https://doi.org/10.13140/2.1.3387.2329

Hoyos-Santillan, J., Lomax, B. H., Large, D., Turner, B. L., Boom, A., Lopez, O. R., & Sjögersten, S. (2015). Getting to the root of the problem: Litter decomposition and peat formation in lowland Neotropical peatlands. *Biogeochemistry*, *126*(1–2), 115–129. https://doi.org/10.1007/s10533-015-0147-7

Hoyos-Santillan, J., Lomax, B. H., Large, D., Turner, B. L., Boom, A., Lopez, O. R., & Sjögersten, S. (2016). Quality not quantity: Organic matter composition controls of CO2 and CH4 fluxes in neotropical peat profiles. *Soil Biology and Biochemistry*, *103*, 86–96. https://doi.org/10.1016/j.soilbio.2016.08.017

Hoyos-Santillan, J., Lomax, B. H., Large, D., Turner, B. L., Lopez, O. R., Boom, A., Sepulveda-Jauregui, A., & Sjögersten, S. (2019). Evaluation of vegetation communities, water table, and peat composition as drivers of greenhouse gas emissions in lowland tropical peatlands. *Science of The Total Environment*, *688*, 1193–1204. https://doi.org/10.1016/j.scitotenv.2019.06.366

Hoyt, A. (2014). *Methane production and transport in a tropical peatland*. *Vol. 2014*. https://agu.confex.com/agu/fm14/meetingapp.cgi/Paper/30346

Hoyt, A., Cadillo-Quiroz, H., Xu, X., Torn, M., Bazán Pacaya, A., Jacobs, M., Shapiama Peña, R., Ramirez Navarro, D., Urquiza-Muñoz, D., & Trumbore, S. (2020). *Isotopic Insights into Methane Production and Emission in Diverse Amazonian Peatlands* [Other]. oral. https://doi.org/10.5194/egusphere-egu2020-12960

Hoyt, A. M., Gandois, L., Eri, J., Kai, F. M., Harvey, C. F., & Cobb, A. R. (2019). CO_2 emissions from an undrained tropical peatland: Interacting influences of temperature, shading and water table depth. *Global Change Biology*, *25*(9), 2885–2899. https://doi.org/10.1111/gcb.14702

Ingram, H. A. P. (1987). Ecohydrology of Scottish peatlands. *Transactions of the Royal Society of Edinburgh: Earth Sciences*, *78*(4), 287–296. https://doi.org/10.1017/S0263593300011226

Intergovernmental Panel On Climate Change (Ipcc). (2023). *Climate Change 2021 – The Physical Science Basis: Working Group I Contribution to the Sixth Assessment Report of the Intergovernmental Panel on Climate Change* (1st ed.). Cambridge University Press. https://doi.org/10.1017/9781009157896

Iversen, C. M. (2014). Using root form to improve our understanding of root function. *New Phytologist*, *203*(3), 707–709. https://doi.org/10.1111/nph.12902

Jastrow, J. D., Amonette, J. E., & Bailey, V. L. (2007). Mechanisms controlling soil carbon turnover and their potential application for enhancing carbon sequestration. *Climatic Change*, *80*(1–2), 5–23. https://doi.org/10.1007/s10584-006-9178-3

Jauhiainen, J., Takahashi, H., Heikkinen, J. E. P., Martikainen, P. J., & Vasander, H. (2005). Carbon fluxes from a tropical peat swamp forest floor. *Global Change Biology*, *11*(10), 1788–1797. https://doi.org/10.1111/j.1365-2486.2005.001031.x

Joosten, H., & Clarke, D. (with International Peat Society, & International Mire Conservation Group). (2002). *Wise use of mires and peatlands: Background and principles including a framework for decision-making*. International Peat Society ; International Mire Conservation Group.

Joosten, H. & FAO (Eds.). (2012). *Peatlands—Guidance for climate change mitigation through conservation, rehabilitation and sustainable use* (2. ed). FAO [u.a.].

Kettridge, N., Turetsky, M. R., Sherwood, J. H., Thompson, D. K., Miller, C. A., Benscoter, B. W., Flannigan, M. D., Wotton, B. M., & Waddington, J. M. (2015). Moderate drop in water table increases peatland vulnerability to post-fire regime shift. *Scientific Reports*, *5*(1), 8063. https://doi.org/10.1038/srep08063

Kolka, R. (Ed.). (2011). *Peatland biogeochemistry and watershed hydrology at the Marcell Experimental Forest*. CRC Press.

Kotsyurbenko, O. R., Chin, K.-J., Glagolev, M. V., Stubner, S., Simankova, M. V., Nozhevnikova, A. N., & Conrad, R. (2004). Acetoclastic and hydrogenotrophic methane production and methanogenic populations in an acidic West-Siberian peat bog. *Environmental Microbiology*, *6*(11), 1159–1173. https://doi.org/10.1111/j.1462-2920.2004.00634.x

Lähteenoja, O., Reátegui, Y. R., Räsänen, M., Torres, D. D. C., Oinonen, M., & Page, S. (2012). The large A mazonian peatland carbon sink in the subsiding P astaza- M arañón foreland basin, P eru. *Global Change Biology*, *18*(1), 164–178. https://doi.org/10.1111/j.1365-2486.2011.02504.x

Lampela, M., Jauhiainen, J., & Vasander, H. (2014). Surface peat structure and chemistry in a tropical peat swamp forest. *Plant and Soil*, *382*(1–2), 329–347. https://doi.org/10.1007/s11104-014-2187-5

Li, D., Ni, H., Jiao, S., Lu, Y., Zhou, J., Sun, B., & Liang, Y. (2021). Coexistence patterns of soil methanogens are closely tied to methane generation and community assembly in rice paddies. *Microbiome*, *9*(1), 20. https://doi.org/10.1186/s40168-020-00978-8

Li, Q., Leroy, F., Zocatelli, R., Gogo, S., Jacotot, A., Guimbaud, C., & Laggoun-Défarge, F. (2021). Abiotic and biotic drivers of microbial respiration in peat and its sensitivity to temperature change. *Soil Biology and Biochemistry*, *153*, 108077. https://doi.org/10.1016/j.soilbio.2020.108077

Liebner, S., Ganzert, L., Kiss, A., Yang, S., Wagner, D., & Svenning, M. M. (2015). Shifts in methanogenic community composition and methane fluxes along the degradation of

discontinuous permafrost. *Frontiers in Microbiology*, *6*. https://doi.org/10.3389/fmicb.2015.00356

Loisel, J., Gallego-Sala, A. V., Amesbury, M. J., Magnan, G., Anshari, G., Beilman, D. W., Benavides, J. C., Blewett, J., Camill, P., Charman, D. J., Chawchai, S., Hedgpeth, A., Kleinen, T., Korhola, A., Large, D., Mansilla, C. A., Müller, J., Van Bellen, S., West, J. B., … Wu, J. (2021). Expert assessment of future vulnerability of the global peatland carbon sink. *Nature Climate Change*, *11*(1), 70–77. https://doi.org/10.1038/s41558-020-00944-0

Lumley, T., Diehr, P., Emerson, S., & Chen, L. (2002). The Importance of the Normality Assumption in Large Public Health Data Sets. *Annual Review of Public Health*, *23*(1), 151–169. https://doi.org/10.1146/annurev.publhealth.23.100901.140546

McFarlane, K. J., Hanson, P. J., Iversen, C. M., Phillips, J. R., & Brice, D. J. (2018). Local Spatial Heterogeneity of Holocene Carbon Accumulation throughout the Peat Profile of an Ombrotrophic Northern Minnesota Bog. *Radiocarbon*, *60*(3), 941–962. https://doi.org/10.1017/RDC.2018.37

McNicol, G., Knox, S. H., Guilderson, T. P., Baldocchi, D. D., & Silver, W. L. (2020). Where old meets new: An ecosystem study of methanogenesis in a reflooded agricultural peatland. *Global Change Biology*, *26*(2), 772–785. https://doi.org/10.1111/gcb.14916

McPartland, M. Y., Montgomery, R. A., Hanson, P. J., Phillips, J. R., Kolka, R., & Palik, B. (2020). Vascular plant species response to warming and elevated carbon dioxide in a boreal peatland. *Environmental Research Letters*, *15*(12), 124066. https://doi.org/10.1088/1748-9326/abc4fb

Miettinen, J., Shi, C., & Liew, S. C. (2016). Land cover distribution in the peatlands of Peninsular Malaysia, Sumatra and Borneo in 2015 with changes since 1990. *Global Ecology and Conservation*, *6*, 67–78. https://doi.org/10.1016/j.gecco.2016.02.004

Mitsch, W. J., & Gosselink, J. G. (2015). *Wetlands* (Fifth edition). John Wiley and Sons, Inc.

Mobilian, C., & Craft, C. B. (2022). Wetland Soils: Physical and Chemical Properties and Biogeochemical Processes. In *Encyclopedia of Inland Waters* (pp. 157–168). Elsevier. https://doi.org/10.1016/B978-0-12-819166-8.00049-9

Moore, S., Evans, C. D., Page, S. E., Garnett, M. H., Jones, T. G., Freeman, C., Hooijer, A., Wiltshire, A. J., Limin, S. H., & Gauci, V. (2013). Deep instability of deforested tropical peatlands revealed by fluvial organic carbon fluxes. *Nature*, *493*(7434), 660–663. https://doi.org/10.1038/nature11818

Noon, M. L., Goldstein, A., Ledezma, J. C., Roehrdanz, P. R., Cook-Patton, S. C., Spawn-Lee, S. A., Wright, T. M., Gonzalez-Roglich, M., Hole, D. G., Rockström, J., & Turner, W. R. (2021). Mapping the irrecoverable carbon in Earth's ecosystems. *Nature Sustainability*, *5*(1), 37–46. https://doi.org/10.1038/s41893-021-00803-6

Norris, M. W., Turnbull, J. C., Howarth, J. D., & Vandergoes, M. J. (2020). Pretreatment of Terrestrial Macrofossils. *Radiocarbon*, *62*(2), 349–360. https://doi.org/10.1017/RDC.2020.8

Nottingham, A. T., Bååth, E., Reischke, S., Salinas, N., & Meir, P. (2019). Adaptation of soil microbial growth to temperature: Using a tropical elevation gradient to predict future changes. *Global Change Biology*, *25*(3), 827–838. https://doi.org/10.1111/gcb.14502

Ofiti, N. O. E., Schmidt, M. W. I., Abiven, S., Hanson, P. J., Iversen, C. M., Wilson, R. M., Kostka, J. E., Wiesenberg, G. L. B., & Malhotra, A. (2023). Climate warming and

elevated CO2 alter peatland soil carbon sources and stability. *Nature Communications*, *14*(1), 7533. https://doi.org/10.1038/s41467-023-43410-z

Ofiti, N. O. E., Solly, E. F., Hanson, P. J., Malhotra, A., Wiesenberg, G. L. B., & Schmidt, M. W. I. (2022). Warming and elevated CO $_2$ promote rapid incorporation and degradation of plant-derived organic matter in an ombrotrophic peatland. *Global Change Biology*, *28*(3), 883–898. https://doi.org/10.1111/gcb.15955

Omar, M. S., Ifandi, E., Sukri, R. S., Kalaitzidis, S., Christanis, K., Lai, D. T. C., Bashir, S., & Tsikouras, B. (2022). Peatlands in Southeast Asia: A comprehensive geological review. *Earth-Science Reviews*, *232*, 104149. https://doi.org/10.1016/j.earscirev.2022.104149

Osaki, M., Kato, T., Kohyama, T., Takahashi, H., Haraguchi, A., Yabe, K., Tsuji, N., Shiodera, S., Rahajoe, J. S., Atikah, T. D., Oide, A., Matsui, K., Wetadewi, R. I., & Silsigia, S. (2021). Basic Information About Tropical Peatland Ecosystems. In M. Osaki, N. Tsuji, N. Foead, & J. Rieley (Eds.), *Tropical Peatland Eco-management* (pp. 3–62). Springer Singapore. https://doi.org/10.1007/978-981-33-4654-3_1

Page, S. E., & Baird, A. J. (2016). Peatlands and Global Change: Response and Resilience. *Annual Review of Environment and Resources*, *41*(1), 35–57. https://doi.org/10.1146/annurev-environ-110615-085520

Page, S. E., Rieley, J. O., & Banks, C. J. (2011). Global and regional importance of the tropical peatland carbon pool. *Global Change Biology*, *17*(2), 798–818. https://doi.org/10.1111/j.1365-2486.2010.02279.x

Page, S., Mishra, S., Agus, F., Anshari, G., Dargie, G., Evers, S., Jauhiainen, J., Jaya, A., Jovani-Sancho, A. J., Laurén, A., Sjögersten, S., Suspense, I. A., Wijedasa, L. S., & Evans, C. D. (2022). Anthropogenic impacts on lowland tropical peatland biogeochemistry. *Nature*

Reviews Earth & Environment, *3*(7), 426–443. https://doi.org/10.1038/s43017-022-00289-6

Phillips, J., Hanson, P., & McFarlane, K. (2022). *SPRUCE Peat Physical and Chemical Characteristics from Experimental Plot Cores, Post-Treatment 2020* [Dataset]. Oak Ridge National Laboratory (ORNL), Oak Ridge, TN (United States). https://doi.org/10.25581/SPRUCE.102/1878603

Phillips, S., & Bustin, R. M. (1996). Sedimentology of the Changuinola peat deposit: Organic and clastic sedimentary response to punctuated coastal subsidence. *Geological Society of America Bulletin*, *108*(7), 794–814. https://doi.org/10.1130/0016-7606(1996)108<0794:SOTCPD>2.3.CO;2

Phillips, S., Rouse, G. E., & Bustin, R. M. (1997). Vegetation zones and diagnostic pollen profiles of a coastal peat swamp, Bocas del Toro, Panamá. *Palaeogeography, Palaeoclimatology, Palaeoecology*, *128*(1–4), 301–338. https://doi.org/10.1016/S0031-0182(97)81129-7

Ribeiro, K., Pacheco, F. S., Ferreira, J. W., De Sousa-Neto, E. R., Hastie, A., Krieger Filho, G. C., Alvalá, P. C., Forti, M. C., & Ometto, J. P. (2021). Tropical peatlands and their contribution to the global carbon cycle and climate change. *Global Change Biology*, *27*(3), 489–505. https://doi.org/10.1111/gcb.15408

Schlesinger, W. H., & Bernhardt, E. S. (2020). Wetland Ecosystems. In *Biogeochemistry* (pp. 249–291). Elsevier. https://doi.org/10.1016/B978-0-12-814608-8.00007-4

Sjögersten, S., Aplin, P., Gauci, V., Peacock, M., Siegenthaler, A., & Turner, B. L. (2018). Temperature response of ex-situ greenhouse gas emissions from tropical peatlands:

Interactions between forest type and peat moisture conditions. *Geoderma*, *324*, 47–55. https://doi.org/10.1016/j.geoderma.2018.02.029

Sjögersten, S., Cheesman, A. W., Lopez, O., & Turner, B. L. (2011). Biogeochemical processes along a nutrient gradient in a tropical ombrotrophic peatland. *Biogeochemistry*, *104*(1–3), 147–163. https://doi.org/10.1007/s10533-010-9493-7

Stuiver, M., & Polach, H. A. (1977). Discussion Reporting of ^{14}C Data. *Radiocarbon*, *19*(3), 355–363. https://doi.org/10.1017/S0033822200003672

Sugimoto, A., & Wada, E. (1993). Carbon isotopic composition of bacterial methane in a soil incubation experiment: Contributions of acetate and. *Geochimica et Cosmochimica Acta*, *57*(16), 4015–4027. https://doi.org/10.1016/0016-7037(93)90350-6

Sun, C. L., Brauer, S. L., Cadillo-Quiroz, H., Zinder, S. H., & Yavitt, J. B. (2012). Seasonal Changes in Methanogenesis and Methanogenic Community in Three Peatlands, New York State. *Frontiers in Microbiology*, *3*. https://doi.org/10.3389/fmicb.2012.00081

Szajdak, L. W., Meysner, T., Inisheva, L. I., Lapshina, E., Szczepański, M., & Gaca, W. (2019). Dynamics of organic matter and mineral components in Sphagnum- and Carex-dominated organic soils. *Mires and Peat*, *24*, 1–15. https://doi.org/10.19189/MaP.2019.BG.StA.1754

Thompson, M., Gamage, D., Hirotsu, N., Martin, A., & Seneweera, S. (2017). Effects of Elevated Carbon Dioxide on Photosynthesis and Carbon Partitioning: A Perspective on Root Sugar Sensing and Hormonal Crosstalk. *Frontiers in Physiology*, *8*, 578. https://doi.org/10.3389/fphys.2017.00578

Thormann, M. N. (2006). Diversity and function of fungi in peatlands: A carbon cycling perspective. *Canadian Journal of Soil Science*, *86*(Special Issue), 281–293. https://doi.org/10.4141/S05-082

Troxler, T. G. (2007). Patterns of phosphorus, nitrogen and δ ^{15} N along a peat development gradient in a coastal mire, Panama. *Journal of Tropical Ecology*, *23*(6), 683–691. https://doi.org/10.1017/S0266467407004464

Troxler, T. G., Ikenaga, M., Scinto, L., Boyer, J. N., Condit, R., Perez, R., Gann, G. D., & Childers, D. L. (2012). Patterns of Soil Bacteria and Canopy Community Structure Related to Tropical Peatland Development. *Wetlands*, *32*(4), 769–782. https://doi.org/10.1007/s13157-012-0310-z

United Nations Environment Programme, Global Environment Facility, Asia Pacific Network for Global Change Research, Global Environment Centre (Malaysia), & Wetlands International (Eds.). (2008). *Assessment on peatlands, biodiversity, and climate change*. Global Environment Centre & Wetlands International, Wageningen.

Upton, A., Vane, C. H., Girkin, N., Turner, B. L., & Sjögersten, S. (2018). Does litter input determine carbon storage and peat organic chemistry in tropical peatlands? *Geoderma*, *326*, 76–87. https://doi.org/10.1016/j.geoderma.2018.03.030

Waldron, S., Vihermaa, L., Evers, S., Garnett, M. H., Newton, J., & Henderson, A. C. G. (2019). C mobilisation in disturbed tropical peat swamps: Old DOC can fuel the fluvial efflux of old carbon dioxide, but site recovery can occur. *Scientific Reports*, *9*(1), 11429. https://doi.org/10.1038/s41598-019-46534-9

Wang, S., Zhuang, Q., Lähteenoja, O., Draper, F. C., & Cadillo-Quiroz, H. (2018). Potential shift from a carbon sink to a source in Amazonian peatlands under a changing climate.

Proceedings of the National Academy of Sciences, *115*(49), 12407–12412. https://doi.org/10.1073/pnas.1801317115

Wiesenberg, G. L. B., Dorodnikov, M., & Kuzyakov, Y. (2010). Source determination of lipids in bulk soil and soil density fractions after four years of wheat cropping. *Geoderma*, *156*(3–4), 267–277. https://doi.org/10.1016/j.geoderma.2010.02.026

Wilson, R. M., Griffiths, N. A., Visser, A., McFarlane, K. J., Sebestyen, S. D., Oleheiser, K. C., Bosman, S., Hopple, A. M., Tfaily, M. M., Kolka, R. K., Hanson, P. J., Kostka, J. E., Bridgham, S. D., Keller, J. K., & Chanton, J. P. (2021). Radiocarbon Analyses Quantify Peat Carbon Losses With Increasing Temperature in a Whole Ecosystem Warming Experiment. *Journal of Geophysical Research: Biogeosciences*, *126*(11), e2021JG006511. https://doi.org/10.1029/2021JG006511

Wilson, R. M., Hopple, A. M., Tfaily, M. M., Sebestyen, S. D., Schadt, C. W., Pfeifer-Meister, L., Medvedeff, C., McFarlane, K. J., Kostka, J. E., Kolton, M., Kolka, R. K., Kluber, L. A., Keller, J. K., Guilderson, T. P., Griffiths, N. A., Chanton, J. P., Bridgham, S. D., & Hanson, P. J. (2016). Stability of peatland carbon to rising temperatures. *Nature Communications*, *7*(1), 13723. https://doi.org/10.1038/ncomms13723

Wilson, R. M., Tfaily, M. M., Kolton, M., Johnston, E. R., Petro, C., Zalman, C. A., Hanson, P. J., Heyman, H. M., Kyle, J. E., Hoyt, D. W., Eder, E. K., Purvine, S. O., Kolka, R. K., Sebestyen, S. D., Griffiths, N. A., Schadt, C. W., Keller, J. K., Bridgham, S. D., Chanton, J. P., & Kostka, J. E. (2021). Soil metabolome response to whole-ecosystem warming at the Spruce and Peatland Responses under Changing Environments experiment. *Proceedings of the National Academy of Sciences*, *118*(25), e2004192118. https://doi.org/10.1073/pnas.2004192118

Wright, E. L., Black, C. R., Cheesman, A. W., Drage, T., Large, D., Turner, B. L., & Sjögersten, S. (2011). Contribution of subsurface peat to CO2 and CH4 fluxes in a neotropical peatland: CARBON FLUXES IN A NEOTROPICAL PEATLAND. *Global Change Biology*, *17*(9), 2867–2881. https://doi.org/10.1111/j.1365-2486.2011.02448.x

Wright, E. L., Black, C. R., Turner, B. L., & Sjögersten, S. (2013). Environmental controls of temporal and spatial variability in CO_2 and CH_4 fluxes in a neotropical peatland. *Global Change Biology*, *19*(12), 3775–3789. https://doi.org/10.1111/gcb.12330

Yu, Z., Loisel, J., Brosseau, D. P., Beilman, D. W., & Hunt, S. J. (2010). Global peatland dynamics since the Last Glacial Maximum. *Geophysical Research Letters*, *37*(13), 2010GL043584. https://doi.org/10.1029/2010GL043584

Zhang, Y., Ma, A., Zhuang, G., & Zhuang, X. (2019). The acetotrophic pathway dominates methane production in Zoige alpine wetland coexisting with hydrogenotrophic pathway. *Scientific Reports*, *9*(1), 9141. https://doi.org/10.1038/s41598-019-45590-5

Zhong, Y., Jiang, M., & Middleton, B. A. (2020). Effects of water level alteration on carbon cycling in peatlands. *Ecosystem Health and Sustainability*, *6*(1), 1806113. https://doi.org/10.1080/20964129.2020.1806113